21806

National Library of Canada | Bibliothèque nationale du Canada

CANADIAN THESES ON MICROFICHE

THÈSES CANADIENNES SUR MICROFICHE

NAME OF AUTHOR/*NOM DE L'AUTEUR* Terry Edmond Eagles

TITLE OF THESIS/*TITRE DE LA THÈSE* Molecular Reorientation in Liquids and Gases

UNIVERSITY/*UNIVERSITÉ* Alberta

DEGREE FOR WHICH THESIS WAS PRESENTED/ *GRADE POUR LEQUEL CETTE THÈSE FUT PRÉSENTÉE* P.D

YEAR THIS DEGREE CONFERRED/*ANNÉE D'OBTENTION DE CE DEGRÉ* 1974

NAME OF SUPERVISOR/*NOM DU DIRECTEUR DE THÈSE* R. E. D. McClung

Permission is hereby granted to the NATIONAL LIBRARY OF CANADA to microfilm this thesis and to lend or sell copies of the film.

The author reserves other publication rights, and neither the thesis nor extensive extracts from it may be printed or otherwise reproduced without the author's written permission.

L'autorisation est, par la présente, accordée à la BIBLIOTHÈQUE NATIONALE DU CANADA de microfilmer cette thèse et de prêter ou de vendre des exemplaires du film.

L'auteur se réserve les autres droits de publication; ni la thèse ni de longs extraits de celle-ci ne doivent être imprimés ou autrement reproduits sans l'autorisation écrite de l'auteur.

DATED/*DATÉ* July 24, 1974 SIGNED/*SIGNÉ* Terry E Eagles

PERMANENT ADDRESS/*RÉSIDENCE FIXÉ*
Lower Five Islands
Colchester County
Nova Scotia.

NL-91 (11-73)

THE UNIVERSITY OF ALBERTA

MOLECULAR REORIENTATION IN LIQUIDS AND GASES

BY

© TERRY EDMOND EAGLES

A THESIS

SUBMITTED TO THE FACULTY OF GRADUATE STUDIES AND RESEARCH
IN PARTIAL FULFILMENT OF THE REQUIREMENTS FOR THE DEGREE

OF

DOCTOR OF PHILOSOPHY

DEPARTMENT OF CHEMISTRY

EDMONTON, ALBERTA

FALL, 1974

THE UNIVERSITY OF ALBERTA

FACULTY OF GRADUATE STUDIES AND RESEARCH

The undersigned certify that they have read, and recommend to the Faculty of Graduate Studies and Research for acceptance, a thesis entitled

"MOLECULAR REORIENTATION IN LIQUIDS AND GASES"

submitted by TERRY EDMOND EAGLES in partial fulfilment of the requirements for the degree of Doctor of Philosophy.

R E McClung
Supervisor

Robert. E. Jordan

John E. Bertie

George Kotowycz

D. G. Hughes

Lévi
External Examiner

Date July 22, 1974

TO PATRICIA

ABSTRACT

The interpretation of spectral band shapes in terms of the reorientational motion of the absorbing species has proven to be a powerful method for studying intermolecular interactions and reorientational motions of molecules in the liquid and the gaseous state. In this thesis the infrared band shapes of gaseous and liquid mixtures of methane and the ESR linewidths of vanadyl complexes are interpreted in terms of the reorientational motion of the absorbing molecules.

In Chapter II an extended rotational diffusion interpretation of Gordon's semiclassical band shape theory is developed and this modified theory is used to interpret the infrared band shape due to the ν_3 mode of methane. The angular momentum correlation times, τ_J, obtained from this analysis were in very close agreement with those obtained from an analysis using the classical model. This result indicates that the commonly used procedure of studying reorientational motion in terms of the Fourier cosine transform of the band shape is justified. This theory proves to be of limited applicability due to the details of the calculations.

In Chapter III a "true" semiclassical extended rotational diffusion theory is developed. The memory function approach is used to simplify the computation of reorientational correlation functions and spectral densities. This semiclassical theory is used to inter-

pret the infrared band shapes of methane due to ν_3 and ν_4. The angular momentum correlation times obtained from the two different infrared bands and those obtained from an independent nuclear magnetic resonance T_1 study on closely related systems show a similar density dependence indicating that the values of τ_J assigned by the extended rotational diffusion theories have physical significance and that τ_J is not a meaningless parameter.

The ESR spectra of a series of vanadyl complexes in various solvents were obtained. These spectra are interpreted in terms of the Kivelson linewidth theory. A procedure for fitting the M-dependent part of the linewidth using the Kivelson theory is introduced. This procedure is more representative of the Kivelson theory than the previous procedure of considering the M^2 contribution to the linewidth because each of the parameters of the Kivelson model are considered according to their contribution to the linewidth. It is demonstrated that the Kivelson theory gives better agreement with experiment if each spectrum is studied separately rather than if all the spectra for a given complex/solvent system are studied simultaneously and the Stokes-Einstein relation is used to relate the reorientational correlation time, τ_θ, to the temperature and viscosity of the solvent. This result indicates that possibly the Stokes-Einstein relation is the cause of the disagreement between predicted and experimental results.

ACKNOWLEDGEMENTS

I would like to express my sincere appreciation to Dr. R. E. D. McClung whose quidance and encouragement throughout the progress of this work has made this research a truly rewarding experience.

A special thanks is extended to Mrs. Mary Waters for the excellent preparation of this thesis.

Financial assistance from the National Research Council of Canada is gratefully acknowledged.

TABLE OF CONTENTS

Page

CHAPTER I

INTRODUCTION 1

CHAPTER II

SEMICLASSICAL BAND SHAPE THEORY 13

A INTRODUCTION. 13

B DEVELOPMENT OF SEMICLASSICAL BAND SHAPE THEORY. 17

1. The Gordon Semiclassical Theory 17

2. Extended Diffusion Interpretation of the Gordon Semiclassical Theory 22

C APPLICATION OF THE THEORY TO CH_4 BAND SHAPES 27

1. Calculations 27

2. Comparison with Experiment. 40

D DISCUSSION 49

1. Comparison of Semiclassical Results with Previous Treatments 49

2. Limitations of the Theory 55

CHAPTER III

SEMICLASSICAL EXTENDED ROTATIONAL DIFFUSION THEORY 60

A INTRODUCTION. 60

B THEORY 63

1. The Memory Function and Extended Rotational Diffusion 63

2. Quantum Mechanical Free Rotor Correlation Functions. 79

Page

3. Description of the Rotational Motion 81

4. Spectral Densities and Correlation Functions in the M- and J-diffusion Limits. 84

C NUMERICAL ANALYSIS PROCEDURES FOR IMPLEMENTATION OF THE MEMORY FUNCTION EQUATION 88

1. Calculation of $K_{FR}(t)$ from $G_{FR}(t)$ . . 89

2. Calculation of G(t) from K(t) 90

3. Investigation of the Stability of the Computation Procedures. 92

D APPLICATION TO ν_3 AND ν_4 BAND SHAPES OF CH_4 94

1. Calculation of Band Shapes of CH_4 . . 94

a. ν_3 Band 98

b. ν_4 Band 103

2. Comparison with Experiment. 112

E DISCUSSION. 127

CHAPTER IV

THE KIVELSON LINEWIDTH THEORY. 142

A INTRODUCTION. 142

B PREPARATION AND CHARACTERIZATION OF VANADYL COMPLEXES 153

1. Bis(3,5-heptanedionato)oxovanadium(IV) 153

2. Bis(2,2,6,6-tetramethyl-3,5-heptanedionato)oxovanadium(IV). 154

3. Bis(1-phenyl-1,3-butanedionato)oxovanadium(IV). 154

Page

4. Bis(1,3-phenyl-1,3-propanedionato)-oxovanadium(IV). 155

C SAMPLE PREPARATION 155

D INSTRUMENTATION AND MEASUREMENT TECHNIQUES 156

E ANALYSIS OF THE ESR SPECTRA OF VANADYL COMPLEXES. 157

F ANALYSIS OF ESR LINEWIDTHS 165

G DISCUSSION 182

CHAPTER V

CONCLUSION 194

REFERENCES. 205

APPENDIX I 213

APPENDIX II 222

APPENDIX III 238

LIST OF TABLES

Table		Page
1	Correlation Times Assigned Using Semi-Classical J-diffusion, Semiclassical M-diffusion, Classical J-diffusion and Classical M-diffusion.	46
2	Correlation Times Assigned Using the Semiclassical J-diffusion and Semi-classical M-diffusion Models	123
3	Comparison of Weights of the Exponential Terms in the Correlation Function in the Two Semiclassical Approaches to M-diffusion for the J=1 Lines in the ν_3 Band of CH_4	131
4	Magnetic Parameters of Vanadyl Complexes in Toluene	163
5	Values of κr^3 Obtained by Fitting the Kivelson Theory to Experimental β, γ and M-dependent part of Linewidth	168
6	Sources of Solvent Viscosities	179
7	Values of κ Assigned to Complex-Solvent System	181
8	The Effect of Randomly Assigned Line-width Error on the Linewidth Parameters	186
9	Experimental Linewidths for VODE Systems	239
10	Experimental Linewidths for VOPM Systems	241
11	Experimental Linewidths for VOTB Systems	243
12	Experimental Linewidths for VODP Systems	246

LIST OF FIGURES

Figure Page

1 Construction of average frequencies for the P(9) lines of CH_4 32

2 ν_3 band shapes of CH_4 computed from the semiclassical J-diffusion model 34

3 ν_3 band shapes of CH_4 computed with the semiclassical J-diffusion model at 295K 37

4 ν_3 bandshapes of CH_4 computed with the semiclassical M-diffusion model at 295K 39

5 Comparison of the observed ν_3 band shapes of CH_4 in dense gas mixtures at 295K with spectral band shapes calculated with the semiclassical J-diffusion model 45

6 Density dependence of τ_J determined by comparison of observed ν_3 band shapes with those computed using the semiclassical J-diffusion model 52

7 Comparison of the symmetric part of the ν_3 band shapes of methane calculated from the semiclassical J-diffusion model with the band shapes computed from the classical extended J-diffusion model 54

8 Comparison of the observed ν_3 band shape of methane gas at 0.1 amagats and 295K with the stick spectrum calculated from rigid rotor line amplitudes and Boltzmann factors 56

9 Free rotor correlation and memory functions for the ν_3 band of CH_4 at 295K 100

10 J-diffusion reorientational correlation functions of $G_J^{(1)}(t)$ for the ν_3 band of CH_4 at 295K for various values of τ_J 102

11 J-diffusion spectra band shapes $I_J(\omega)$ for the ν_3 band of CH_4 at 295K for various values of τ_J. 104

Figure		Page
12	M-diffusion spectral band shapes $I_M(\omega)$ for the ν_3 band of CH_4 at 295K for various values of τ_J	105
13	M-diffusion reorientational correlation functions $G_M^{(1)}(t)$ for the ν_3 band of CH_4 at 295K for various values of τ_J	107
14	J-diffusion spectral band shapes $I_J(\omega)$ for the ν_4 band at 297K	110
15	Free rotor correlation and memory functions for the ν_4 band of CH_4 at 297K	111
16	J-diffusion reorientational correlation functions $G_J^{(1)}$ for the ν_4 band of CH_4 at 297K for various values of τ_J	114
17	J-diffusion spectral band shapes $I_J(\omega)$ for the ν_4 band of CH_4 at 297K for various values of τ_J	115
18	M-diffusion spectral band shapes $I_M(\omega)$ for the ν_4 band of CH_4 at 297K for various values of τ_J	116
19	M-diffusion reorientational correlation functions of $G_M^{(1)}(t)$ for the ν_3 band of CH_4 at 297K for various values of τ_J	118
20	Comparison of observed band shapes for the ν_3 band of CH_4 in dense gas mixtures at 297K and band shapes computed with the J-diffusion model	120
21	Comparison of observed band shapes for the ν_4 band of CH_4 in dense gas mixtures at 297K and band shapes computed with the J-diffusion model	121
22	Density dependence of τ_J^{-1}	140
23	ESR spectrum of VOTB in toluene at T = 90°K	159
24	ESR spectrum of VOTB in toluene at T = 90°K in the region of the M = 3/2 x,y-transition	161

Figure Page

25 ESR spectrum of VOPM in toluene at T=90°K in the region of $M = 3/2$ x,y-transition 164

26 β and γ vs η/T for VODE/toluene 170

27 β and γ vs η/T for VODE/CS_2 171

28 β and γ vs η/T for VOPM/toluene 172

29 β and γ vs η/T for VOPM/CS_2 173

30 β and γ vs η/T for VOTB/toluene 174

31 β and γ vs η/T for VOTB/CS_2 175

32 β and γ vs η/T for VODP/toluene 176

33 β and γ vs η/T for VODP/CS_2 177

34 α'' vs η/T for toluene systems 184

35 α'' vs η/T for carbon disulfide systems 186

36 $\tau_\theta^{(2)}$ vs η/T for carbon disulfide systems 193

INTRODUCTION

CHAPTER I

The conventional spectroscopic method of studying a system is to assign the observed spectral frequencies to transitions between the various quantum states of the system. Because of its emphasis on energy levels, this approach might be referred to as the Schrödinger [1] picture of spectroscopy. The Schrödinger picture, with its emphasis on transition frequencies, yields information about the environment of the absorbing species. This information includes such things as bond lengths, bond strengths, electronic environment and chemical interactions with solvent species and can in general be described as dealing with the time-independent or time-averaged characteristics of the systems. If a time-dependent parameter of a system causes the absorption frequency of a given molecule to vary with a frequency ω_p between two values separated by $\Delta\omega$, then by time-independent we mean $\omega_p << \Delta\omega$, while by time averaged we mean $\omega_p >> \Delta\omega$. When $\omega_p << \Delta\omega$ the two lines will be resolved and the two values of the parameter can be calculated but when $\omega_p >> \Delta\omega$ only a single line is observed and an average value of the parameter can be determined. In the region when $\omega_p \cong \Delta\omega$ the spectral line will be very broad and little can be said about the parameter. In most liquids and dense gases, the

Schrödinger picture does not present the most effective description of the observed spectra because the individual spectral lines are blended together to form a continuous band. This broadening and coalescence of the spectral lines is due to time-dependent interactions within the system.[1,2]

The Heisenberg formulation of quantum mechanics [3] allows us to rephrase the Schrödinger expressions for spectral absorption so as to emphasize the time development of the system.[1,2] The Heisenberg formulation of quantum mechanics places the time dependence of the system into the operators and the wave functions are time independent. The Schrödinger formulation on the other hand uses time dependent wave functions and time independent operators. The Heisenberg picture of spectroscopy with its emphasis on the time development of the quantum states has proved to be a powerful tool in the interpretation of spectral band shapes in which the individual transition lines are not resolved.[4-10] In addition the Heisenberg approach to spectroscopy provides an easily visualized picture of how time dependent interactions influence observed band shapes.[2,4,6,8,9]

In the frequency region above 1000 cm^{-1}, where the influence of stimulated emission is negligible, the spectral band shape in the Schrödinger picture of spectroscopy is expressed by [2,11]

$$I(\omega) = \sum_{i,f} \rho_i \langle i|\hat{Y}|f\rangle\langle f|\hat{Y}|i\rangle\, \delta[(E_f - E_i)/\hbar - \omega], \qquad \text{(I-1)}$$

where the sum over i and f includes all relevant quantum states of the system, i indicating the initial and f the final state involved in the transition. ρ_i is the Boltzmann factor for the quantum state $|i\rangle$ and E_i is its energy; δ is the Dirac delta function and ω is the frequency of the applied radiation. The operator, $\hat{Y}$, represents the interaction being observed. For example, in infrared absorption spectroscopy, $\hat{Y}$ is $\vec{\varepsilon}.\vec{m}^{\nu}$ which represents the interaction of the electric field of the incident radiation, $\vec{\varepsilon}$, with the vibrational transition dipole moment of a molecule, $\vec{m}^{\nu}$. The Heisenberg equivalent of Eq. (I-1) can be obtained by replacing the Dirac delta function by the equivalent Fourier integral,

$$\delta(x) = \frac{1}{2\pi}\int_{-\infty}^{\infty} dt\; e^{ixt} \quad , \qquad \text{(I-2)}$$

where t is the Fourier variable and $i = \sqrt{-1}$. Making this substitution, we obtain

$$I(\omega) = \frac{1}{2\pi}\sum_{i,f} \rho_i\langle i|\hat{Y}|f\rangle\langle f|\hat{Y}|i\rangle \int_{-\infty}^{\infty} dt\, \exp[i((E_f - E_i)/\hbar-\omega)t] \qquad \text{(I-3)}$$

or in an equivalent form

$$I(\omega) = \frac{1}{2\pi}\int_{-\infty}^{\infty} dt\; e^{-i\omega t}\sum_{i,f} \rho_i\langle i|\hat{Y}|f\rangle\langle f| e^{\frac{i\hat{\mathcal{H}}t}{\hbar}}\,\hat{Y}\,e^{\frac{-i\hat{\mathcal{H}}t}{\hbar}}|i\rangle . \qquad \text{(I-4)}$$

The quantity, $e^{\frac{i\hat{\mathcal{H}}t}{\hbar}}\,\hat{Y}\,e^{\frac{-i\hat{\mathcal{H}}t}{\hbar}}$ is the Heisenberg time dependent operator which we will denote as Y(t). Then Eq. (I-4) becomes

$$I(\omega) = \frac{1}{2\pi}\int_{-\infty}^{\infty} dt\; e^{-i\omega t}\sum_{i,f} \rho_i\langle i|\hat{Y}(0)|f\rangle\langle f|\hat{Y}(t)|i\rangle \quad . \qquad \text{(I-5)}$$

Eq. (I-5) expreses the spectral density $I(\omega)$ in the form of the Fourier transform of a correlation function G(t) defined by

$$G(t) = \sum_{i,f} \rho_i\langle i|\hat{Y}(0)|f\rangle\langle f|\hat{Y}(t)|i\rangle = \sum_{i,f} \rho_i Y_{if}(0) Y_{if}^{*}(t) \quad , \qquad \text{(I-6)}$$

where the * indicates the complex conjugate and $Y_{if}(t)$ is the matrix element $\langle i|\hat{Y}(t)|f\rangle$.

The function, G(t), is the autocorrelation function for the quantity, Y, represented by the operator $\hat{Y}$. Let us consider the meaning of the correlation function. First of all we must note that the correlation function gives a description of the ensemble as a whole and not of an individual member of the ensemble. From Eq. (I-6) we see that the correlation function contains information about the ensemble average of the individual products of $Y_{if}^{*}(t)$ and $Y_{if}(0)$. Let us consider a hypothetical experiment in which all of the quantities Y_{if} are the same for every molecule at time zero. The correlation function would then simply describe the result of the dephasing as time progressed. The dephasing is due to the differing time dependence of the matrix elements, $Y_{if}(t)$, from molecule to molecule in the ensemble. In magnetic resonance spectroscopy, such an experiment can be performed. A pulse of incident radiation is used to give all transition magnetic dipoles of the ensemble the same phase at time zero. The magnetization vector, which is the sum of the transition magnetic dipoles, is detected. The magnetization decays in time and the decay curve is the correlation function for the transition magnetic dipole. The only purpose of the pulse in this experiment is to give all the transition magnetic dipoles the same phase at time zero (the time of the pulse) so as to produce a physically observable quantity. Discussion of correlation functions is still meaningful if the individual matrix elements, Y_{if}, are not in phase because the product considered does not depend on a phase which is universal to the system but depends only on the change in phase of Y_{if} relative to its phase at time zero.

The correlation function is the vehicle through which we can introduce the influence of molecular interactions to the band shape. In all systems studied in this thesis, the time dependence of the operator, $\hat{Y}(t)$, is due to the reorientational motion of the absorbing molecules. The correlation functions for Y in these systems will be referred to as reorientational correlation funct[illegible]

A reorientation correlation function is characterized by a reorientational correlation time, τ_θ, which is defined as

$$\tau_\theta = \text{Re}\left\{\int_0^\infty dt\ G(t)\right\} \quad . \tag{I-7}$$

τ_θ is a measure of the time over which the molecule "remembers" its orientation in space i.e. the time required for the molecule to reorient by ~1 radian. A second correlation time of importance in describing reorientational motion is the angular momentum correlation time, τ_J, which may be interpreted as the average time over which a molecule remains in the same rotational state. The two correlation times are related, but the exact details of this relationship depend on the nature of the reorientation process.

Reorientational motion affects various forms of spectroscopy in different ways. In magnetic resonance spectroscopy the energy levels of a spin system depend on the orientation of the molecule relative to the applied magnetic field. Reorientation of the molecule thus modulates these energy levels and the resulting fluctuating energy levels give rise to linewidth contributions. In vibrational-rotational spectroscopy reorientation of the molecule changes only the magnitude of the interaction between the incident radiation and the molecule, but does not alter the transition frequency. Rapid reorientation of the molecule causes the reorientational correlation function for the dipole-electric field interaction to decay rapidly. In terms of the band shape this means that the individual lines will be broadened.

In order to further explore the influence of reorientational motion on the band shape it is necessary to have a model to describe the reorientation of a molecule. There are two basic views on molecular reorientation in liquids. One view suggests that a liquid resembles a loosely structured solid in which the individual molecules are restricted from moving freely because of interactions between species. In this theory reorientation comes about because of very strong torques exerted on a molecule when it is involved in a collision. This approach has been developed by O'Reilly [12-15] but it has not been widely exploited. Similar approaches have been suggested by Brown _et al._[16], and by Kivelson _et al._[17,18], as possible solutions to problems dealing with hydrogen bonding solvents. The second view pictures a liquid to be very similar to a dense gas. Reorientation models based on this picture assume that reorientation takes place by rotational steps in the periods between collisions. These models are known as rotational diffusion models. The word collision here and in subsequent usage will be interpreted as an event in which the angular momentum of a molecule is altered. The models considered in this thesis are based on the dense gas picture for liquids.

The first rotational diffusion model was developed by Debye [19] to interpret dielectric relaxation experiments. In his model Debye assumed that reorientation took place by a series of short (<<1 radian) rotational steps. The requirement of short rotational steps has limited the application of the Debye theory to polar liquids.[20] Another reorientation model based on rotational steps is the perturbed free rotor model. In this model reorientation is assumed to take place by long (>>1 radian) rotational steps. Again the length of the rotational step has restricted the application of this model and it has been used only in studies of low pressure gases.[21]

Recently Gordon [5] has developed a theory of molecular reorientation which is not restricted by the length of the rotational steps. In this approach, which is referred to as the classical extended rotational diffusion theory, the classical motion of the molecules is followed in detail in the individual rotational diffusion steps and the reorientational correlation function is obtained by taking an ensemble average over these individual steps. Gordon's theory which was limited to linear molecules has been extended by McClung to the more complicated systems of spherical [6] and symmetric [8] top molecules. The classical extended rotational diffusion theories have been successfully used to interpret a considerable number of infrared [7,22-25], Raman [26-28] and NMR [28-33] band shapes.

A limitation of the classical extended rotational diffusion theory is that its application is limited to those systems which can be described by classical mechanics and thus the use of this theory to interpret asymmetric band shapes is often questionable or impossible. Gordon et al.[2,34,35] proposed a semiclassical theory to predict reorientational correlation functions. This theory makes use of semiclassical scattering theory to describe collisions and has been used to interpret the infrared spectra of CO/He mixtures [36] and HCl/Ar mixtures.[37]

In Chapter II we develop an extended diffusion interpretation of Gordon's semiclassical theory.[2,34,35] We have opted to pursue this approach rather than to use semiclassical scattering theory for several reasons.

(1) The Gordon approach using semiclassical scattering theory requires a good deal of preliminary mathematics in order to calculate the collision cross sections. These calculations are costly and in this sense make the theory of limited use.

(2) Semiclassical scattering theory requires the knowledge of an intermolecular potential. This in effect introduces another variable to the model.

(3) The semiclassical scattering calculations have been seriously questioned in the literature.[36]

(4) The success of the classical extended rotational diffusion theory [7,22-33] suggests this picture of a collision to be a reasonable approximation.

The band shapes predicted by this extended diffusion interpretation of Gordon's semiclassical theory are compared with the infrared band shape of CH_4 due to ν_3 in the pure liquid [38], in solutions of CH_4 in liquid inert gases [38] and in gaseous mixtures of CH_4/He and CH_4/N_2 at densities between 100 and 1000 amagats.[39]

Application of this semiclassical theory was restricted to band shapes which could be described by a small number of transition frequencies (<40). For this reason it was not possible to study the infrared band of CH_4 due to ν_4 because of the large Coriolis coupling constant, ζ_4, which splits each transition line into several components.[40]

In Chapter III we develop a "true" semiclassical version of the classical extended rotational diffusion model. In this model the number of transitions is not a limiting factor. The semiclassical extended rotational diffusion model is then used to interpret the infrared band shapes of CH_4 due to ν_4 in CH_4/He and CH_4/N_2 gas mixtures at densities between 100 and 800 amagats.[39] In addition, the gaseous systems studied in Chapter II are reanalyzed.

As pointed out above, reorientational motion of molecules in liquids can give rise to linewidth contributions in magnetic resonance spectra because the rotational modulation of anisotropic magnetic interactions gives rise to relaxation of the spin system. In Chapter IV, we describe the results of an experimental study of the ESR linewidths of several vanadyl-β-diketonate complexes in a variety of solvents. Kivelson et al. [41] have developed the theoretical relation between linewidths and the correlation times for molecular reorientation. Spin-rotational coupling also makes a contribution to T_1 and T_2. Kivelson et al.[42,43] have developed theoretical expressions for this contribution. Recent investigations at low temperatures [18] and in hydrogen bonding solvents [17,44,45] suggest that the expression for the spin-rotational contribution to T_2, and possibly, the entire Kivelson theory are not adequate. The study of vanadyl complexes described in Chapter IV was designed to further test the Kivelson theories in non-hydrogen bonding solvents.

SEMICLASSICAL BAND SHAPE THEORY

CHAPTER II

A. INTRODUCTION

The reorientational motion of molecules can be studied by analysis of the infrared and Raman band shapes.[2,4-6,8,9,46] In order to extract this information it is often necessary to make reference to a model for the molecular motion in the fluid. A number of theories [5,6,8,9,18,47-49], based on the hypothesis that a liquid resembles a dense gas, have proven quite successful in accounting for experimental results.[5,7,10,22-33] These models are generally referred to as rotational diffusion models. Rotational diffusion models consider reorientational motion to consist of a series of rotational steps which are terminated by "collisions". The reorientation during the rotational step is described by either free rotation of the molecule or by rotation executed under the influence of a retarding torque. The latter description has been employed by Debye [19] in his theory of dielectric relaxation. In the Debye model, the molecular reorientation is assumed to follow a rotational diffusion equation[50-52] and the rotational diffusion coefficient in this equation is related to the bulk shear viscosity of the liquid by a Stokes-Einstein hydrodynamic relationship.[53] The Debye theory is limited to systems in which the diffusive steps are very short (<<1 radian). This is a particularly restrictive condition for systems of spherical molecules where the experimental results suggest that rotational steps are often of the order of 1 radian.[54]

A perturbed free rotor model has been suggested for low pressure gaseous systems.[21] This approach, which assumes that the free rotation steps are long (>>1 radian), is a lifetime broadening interpretation of the band shape. This approximation neglects all but the first collision [6] and the theory has proved of limited applicability even in low pressure gases.[28]

Recently Gordon [5] has suggested a rotational diffusion model which is not restricted by the length of the rotational step. In this approach, which is referred to as the classical extended rotational diffusion theory, the classical motion of the molecule is followed in detail in the individual rotational steps and the reorientational correlation function is obtained by taking an ensemble average over all possible sequences of rotation steps. In this model, a "collision" is viewed as an instantaneous event in which the angular momentum of a molecule is changed. Two limiting cases are considered: M-diffusion and J-diffusion. In the J-diffusion model, the magnitude of the angular momentum vector is randomized onto a Boltzmann distribution and the orientation of the angular momentum vector is completely randomized at every collision. Each collision randomizes only the orientation of the angular momentum vector in the M-diffusion limit, and the magnitude of the angular momentum does not change. A more sophisticated approach [47] permits one to describe the reorientation by any desired combination of M- and J-diffusion processes. Gordon's theory which was limited to linear molecules has been extended to the more complicated systems of spherical [6] and symmetric [8,49] top molecules. The classical extended rotational diffusion theories have been successfully used to interpret a considerable number of infrared [7,22-25] and Raman [26-28] band shapes and nuclear relaxation times.[28-33]

A disadvantage of the classical extended rotational diffusion theory is that it is limited to those systems whose rotational motion can be described by classical mechanics. The classical approach predicts symmetrical band contours and the application of classical extended rotational diffusion theory is often questionable or impossible in systems with asymmetric band shapes. Gordon [2,34,35] has proposed a semiclassical theory to predict reorientational correlation functions. This theory, which in many ways parallels the modified Bloch equation treatment of chemical exchange used in magnetic resonance [55], makes use of semiclassical scattering theory [34,36] to describe collisions. Semiclassical scattering theory is a procedure which approximates quantum mechanical scattering theory by using classical scattering theory and the correspondence principle. In this procedure a particular intermolecular potential is adopted and classical scattering theory is used to predict the trajectories of particles before and after they have been involved in a collision. The classical angular momentum of the particle before and after the collision is determined and the semiclassical scattering cross section is calculated by rounding off the classical angular momenta to the nearest multiples of $\hbar$. Gordon et al.[36,37] have used this procedure to study reorientation in CO/He and HCl/Ar mixtures at low pressures.

In this chapter, we will develop an extended rotational diffusion interpretation of Gordon's semiclassical theory. In section II-B this semiclassical band shape theory will be developed, and in section II-C the theory will be applied to a study of the ν_3 infrared band of CH_4 in liquid and gaseous mixtures.[38,39] Section II-D will be devoted to a comparison of these results with those obtained by application of the classical theory [6] and with the results of an independent NMR-T_1 study [56] on CH_4 in the dense gas phase. In addition, the limitations of the theory will be discussed.

B. DEVELOPMENT OF SEMICLASSICAL BAND SHAPE THEORY

1. The Gordon Semiclassical Theory

The Fourier transform of the infrared absorption band shape is the dipole reorientational correlation function defined by [2],

$$G(t) = \sum_{i,f} \rho_i \langle i|\hat{\vec{m}}^{\nu}(0)|f\rangle\langle f|\hat{\vec{m}}^{\nu}(t)|i\rangle = \sum_{k} \rho_k d_k^{*}(0)\, d_k(t) \tag{II-1}$$

where ρ_i is the Boltzmann factor for the rotational state $|i\rangle$ and the sum over i and f is over the initial and final states respectively. The subscript k used here and in the following equations replaces the pair of subscripts i,f. The Heisenberg operator, $\hat{\vec{m}}^{\nu}(t)$, is the dipole operator at time t, and $d_k(t)$ is

$$d_k(t) = \langle f|\hat{\vec{m}}^{\nu}(t)|i\rangle \quad . \tag{II-2}$$

Equation (II-1) follows from Eq. (I-6) by replacing $\hat{Y}$ by the dipole operator, m^{ν}. In order to calculate this correlation function, it is necessary to know the time dependence of $d_k(t)$. If the molecule is not involved in collisions which cause changes in its angular momentum (and thus its reorientational motion) $d_k(t)$ is readily calculated. Replacing the Heisenberg operator $\hat{\vec{m}}^{\nu}(t)$ by the equivalent expression [3],

$e^{i\hat{\mathcal{H}}t/\hbar}\vec{m}^{\nu}(0)e^{-i\hat{\mathcal{H}}t/\hbar}$, Eq. (II-2) becomes

$$d_k(t) = \langle f|\vec{m}^{\nu}(0)|i\rangle e^{i\omega_k t} = d_k(0)e^{i\omega_k t} \qquad \text{(II-3)}$$

where ω_k is defined in terms of the rotational energies E_i and E_f by

$$\omega_k = (E_f - E_i)/\hbar \quad . \qquad \text{(II-4)}$$

In the absence of collisions the transition dipole moment $d_k(t)$ oscillates as $e^{i\omega_k t}$ with amplitude $d_k(0)$ and its time-derivative is given by

$$\frac{d[d_k(t)]}{dt} = i\omega_k d_k(t) \quad . \qquad \text{(II-5)}$$

Eqs. (II-3) and (II-5) are exact provided that the molecule is not involved in collisions. If the molecule is involved in collisions then the reorientational motion of the molecule in the other angular momentum states must also be included in the calculation of $d_k(t)$. One approach to this problem would be to follow the reorientational motion in each of the rotational states which the molecule samples between time 0 and t then $d_k(t)$ could be calculated as the statistical average of all possible sequences of sampled states. This is the procedure employed in extended rotational diffusion theory and will be considered in Chapter III. Gordon has suggested an alternative procedure which is similar to the "jumping spin" treatment of chemical exchange in magnetic resonance spectroscopy.[55] Gordon suggests that, instead of calculating the product in Eq. (II-1) for each individual transition dipole moment, the product be calculated at time t for the sum of the transition dipole moments of a particular form. He replaces Eq. (II-1) by

$$G(t) = \sum_k d_k^* d_k(t)_{Ave} \qquad \text{(II-6)}$$

where d_k, the intrinsic line amplitude, is the quantity $\langle f|\hat{m}^\nu|i\rangle$ and $d_k(t)_{Ave.}$ is the sum over all molecules, at time t, of the transition dipole moments of the form $\langle f|\hat{m}^\nu|i\rangle$. The subscript, Ave., has been introduced to emphasize the "averaged character" of $d_k(t)_{Ave.}$ and to distinguish it from $d_k(t)$ which refers to the transition dipole moment on a particular molecule. In order to clarify the wording in the development to follow, $d_k(t)_{Ave.}$ will be referred to as the line amplitude of the k-th spectral line.

Since, $d_k(t)_{Ave.}$ is simply the sum at time t of matrix elements of the form $\langle f|\hat{m}^\nu|i\rangle$ the time dependence of $d_k(t)_{Ave.}$ can readily be described simply by adding transfer terms to the equations of motion

[Eq. (II-5)]. These transfer terms would account for the collisional transfer of line amplitude from the k-th spectral line to all other lines and for the transfer of line amplitude to the k-th spectral line from all other lines. The time dependence of $d_k(t)_{\text{Ave.}}$ can then be expressed by,

$$\frac{d}{dt}[d_k(t)_{\text{Ave.}}] = i\omega_k d_k(t)_{\text{Ave.}} - \Pi_{kk} d_k(t)_{\text{Ave.}} + \sum_{l \neq k} - \Pi_{kl} d_l(t)_{\text{Ave.}} \qquad \text{(II-7)}$$

where the first term on the right represents the change in $d_k(t)_{\text{Ave.}}$ due to the free motion, while the second and third terms represent the transfer of line amplitude out of the k-th line and the transfer of line amplitude into the k-th line respectively. Thus Π_{kk} gives the rate at which a unit amplitude in line k would decrease due to collisions, while $-\Pi_{kl}$ gives the rate at which collisions would transfer unit amplitude in line l into line k. The set of simultaneous differential equations represented by Eq. (II-7) can be expressed in the matrix form

$$\frac{d}{dt}[\underset{\sim}{d}(t)_{\text{Ave.}}] = (i\underset{\sim}{\omega}_o - \underset{\sim}{\Pi})\underset{\sim}{d}(t)_{\text{Ave.}} \qquad \text{(II-8)}$$

where $\underset{\sim}{d}(t)_{\text{Ave.}}$ is a column matrix whose k-th element is $d_k(t)_{\text{Ave.}}$ and $\underset{\sim}{\omega}_o$ is a diagonal matrix with kk-th element ω_k. The matrix $\underset{\sim}{\Pi}$ is defined above.

Eq. (II-8) can be solved subject to the boundary condition that we start with an equilibrium distribution of line amplitudes, i.e. $d_k(0)_{\text{Ave.}} = d_k P_k$, where P_k is the equilibrium population factor for the k-th line and d_k is the intrinsic line amplitude defined earlier. Solving Eq. (II-8) subject to this initial condition, we obtain

$$\underset{\sim}{d}(t)_{\text{Ave.}} = (\exp\,[(i\underset{\sim}{\omega}_o - \underset{\sim}{\Pi})t]).\underset{\sim}{P}.\underset{\sim}{d} \qquad \text{(II-9)}$$

where $\underset{\sim}{P}$ is a diagonal matrix with kk-th element P_k and $\underset{\sim}{d}$ is a column matrix with k-th element d_k.

The reorientational correlation function defined in Eq. (II-6) can now be expressed by

$$\begin{aligned} G(t) = \sum_k d_k{}^* d_k(t)_{\text{Ave.}} &= \underset{\sim}{d}^+.\underset{\sim}{d}(t)_{\text{Ave.}} \\ &= \underset{\sim}{d}^+.\exp\,[(i\underset{\sim}{\omega}_o - \underset{\sim}{\Pi})t].\underset{\sim}{P}.\underset{\sim}{d} \end{aligned} \qquad \text{(II-10)}$$

where $\underset{\sim}{d}^+$ is the transpose of the matrix $\underset{\sim}{d}$. The corresponding expression for the spectral density is obtained by the Fourier transformation of Eq. (II-10):

$$I(\omega) = \mathrm{Im}\left\{\underset{\sim}{d}^{+}.(\omega\underset{\sim}{1} - \underset{\sim}{\omega}_{o} - i\underset{\sim}{\Pi})^{-1}.\underset{\sim}{P}.\underset{\sim}{d}\right\} \qquad \text{(II-11)}$$

where ω is the frequency of the incident radiation and $\underset{\sim}{1}$ is a unit matrix; Im{} implies the imaginary part of the quantity within the braces and $(\ )^{-1}$ implies the inverse of the matrix within the brackets.

2. Extended Diffusion Interpretation of the Gordon Semiclassical Theory

Gordon *et al.*[36,37] have determined the matrix, $\underset{\sim}{\Pi}$, for the CO/He and HCl/Ar systems using semiclassical scattering theory. Because semiclassical scattering theory calculations are very costly and possibly unreliable [36], and because they require a detailed knowledge of the intermolecular potentials in each particular system, we have opted to interpret $\underset{\sim}{\Pi}$ in terms of the classical extended rotational diffusion model.[5,6] This might appear to be an arbitrary decision, but we feel that it is justifiable in terms of the success achieved in the application of the classical extended rotational diffusion models.[7,22-33]

In the classical rotational diffusion models [5,6,8,49], in which the rotations of the molecules are treated using classical mechanics, collisional events are assumed to occur at an average rate τ_J^{-1}, where τ_J

is the mean time between events. Since each collisional event destroys all correlation in the angular momentum of the molecule, the angular momentum correlation time is τ_J. The "collisions" in the extended diffusion models are assumed to randomize the direction of the rotational angular momentum, and may randomize its magnitude as well. Analogous semiclassical rotational diffusion models may be constructed so that the discreteness of the rotational levels may be taken into account, but the basic intuitive simplicity of the diffusion picture is preserved.

The rotational states of a spherical or symmetric top molecule are described by three quantum numbers: the total angular momentum quantum number J and the projection quantum numbers on molecule-fixed and space-fixed directions, K and M respectively. The semiclassical analogs of the classical rotational diffusion models are models in which collisional events randomize the projection quantum numbers K and M in both M- and J-diffusion limits, and randomize the quantum number J onto a Boltzmann distribution in the limit of J-diffusion. Since the rotational states of a spherical top molecule within a J-manifold are degenerate, energy transfer can occur at the collisional events in J-diffusion only. In the semiclassical J-diffusion model, the probability that a molecule initially in the state $|J,K,M\rangle$ is put into the state $|J', K', M'\rangle$ by a collisional event depends only on the Boltzmann factor for the final state. In the semiclassical M-diffusion model, the quantum number J is not changed by collision, but the quantum numbers M and K are randomized.

The transfer matrix $\underset{\sim}{\Pi}$ does not describe the rate of transfer of molecules between rotational states, it describes the rate at which intensity amplitude (transition dipole moment) is transferred from one spectral line to another. One would expect, however, that the rates of these processes are related. A molecule in the rotation state $|J,K,M\rangle$ of the ground vibrational state can absorb infrared radiation at as many as three distinct frequencies, i.e. it may give rise to absorption lines in each of the P, Q and R branches of the spectrum. Consequently, the determination of the rate of transfer of line amplitude from one spectral line to another is somewhat more complicated than the determination of the rate of transfer of systems from one rotational level to another. In order to relate the rates of transfer of line amplitude between spectral lines to the rate of transfer of molecules between rotational levels, we make the argument that, although the individual molecules in the J-th rotational level are associated with more than one transition moment (i.e. can absorb at more than one frequency), we can divide the molecules in the J-th rotational level into groups associated with each of the possible transitions. This assumption implies that if one molecule is transferred out of the J-th rotational level, the P-, Q- and R-branch lines, which are derived from this rotational level, lose intensity amplitudes $d_{J(P)}/3, d_{J(Q)}/3$ and $d_{J(R)}/3$ respectively, where d_i is the intrinsic line amplitude of the i-th line in the spectrum. The intensity amplitude which is lost by the i-th line when one molecule is transferred out of that line is d_i, and the intensity amplitude gained by the j-th line to which transfer occurs is d_j. In general, d_i varies from line to line in the vibration-rotation spectrum. Since the fraction of collisional events which transfer a molecule from the J-th rotational level to the J'-th level, in the J-diffusion limit, is given by the Boltzmann factor, $\rho_{J'}$, for the J'-th level, the fraction which transfer line amplitude from the i-th spectral line, which is associated with the J-th level, to the i'-th spectral line, which is associated with the J'-th level, is $\rho_{J'}/3$. By analogy to the classical rotational diffusion models, we take the average rate of collisional events to be τ_J^{-1}. Then the transfer matrix, Π^J, which describes the rotational behaviour of molecules undergoing J-diffusion has elements

$$\Pi_{ij}^{J} = \begin{cases} (1-P_i)/\tau_J & i=j \\ -P_i(d_i/d_j)/\tau_J & i\neq j \end{cases} \qquad \text{(II-12)}$$

where P_i is equal to one-third of the Boltzmann factor for the rotational level with which the i-th transition is associated.

The prescription for the elements of the transfer matrix in the semiclassical M-diffusion model is somewhat different because the collisional events are assumed to randomize the direction of the angular momentum vector, but not change its magnitude. In this limit, line amplitude is transferred only between lines in the different branches of the spectrum which originate in the same J-level. In the absence of collisions, the equations of motion for the line amplitudes of the transitions originating in a common J-state are not coupled, so there is no reason to expect line amplitude transfer between these lines unless collisions occur. We therefore assume that the transition matrix, Π^M, in the M-diffusion model has elements

$$\Pi_{ij}^{M} = \begin{cases} \frac{2}{3}\tau_J^{-1} & i=j \\ -\frac{1}{3}(d_i/d_j)\tau_J^{-1} & i\neq j\text{, i and j associated with common J-levels} \\ 0 & i\neq j\text{, i and j associated with different J-levels.} \end{cases} \qquad \text{(II-13)}$$

where τ_J is the mean time between collisional events just as in the J-diffusion model.

A further subdivision of the molecules in an ensemble of spherical molecules like methane, which contain several equivalent nuclei with nuclear spins, is required because the molecules exist in different nuclear spin isomers, analogous to the ortho and para isomers of hydrogen.[40] Since the rate of interconversion of the nuclear spin isomers is several orders of magnitude slower than the rate of rotational energy transfer in methane [57], one must view the infrared spectrum of methane as a superposition of subspectra arising from ortho-CH_4 (symmetry F), para-CH_4 (symmetry E) and meta-CH_4 (symmetry A). The band shape of methane, therefore, should be calculated in three separate computations - one for each symmetry species - which allow transfer of line amplitude only between the lines of a single nuclear spin isomer.

C. APPLICATION OF THE THEORY TO CH_4 BAND SHAPES

1. Calculations

The vibration-rotation spectrum of the ν_3 mode of CH_4 in the low pressure gas phase is well resolved and exhibits some splitting of the lines arising from the rotational levels with high J, by Coriolis interactions.[58]

The observed absorption frequencies of CH_4 have been reported by Plyer *et al.*[59], and formulae for the intrinsic line amplitudes, d_i, have been given by Childs and Jahn.[60] The Boltzmann factors for the rotational levels of the various nuclear spin isomers of CH_4 were computed using the weights given by Wilson and Herzberg.[40,61]

The calculation of $I(\omega)$ and $G(t)$ for the ν_3 band of CH_4 with a given $\underset{\sim}{\Pi}$ matrix was accomplished using the diagonalization algorithm suggested by Gordon *et al.*[35,62] This algorithm improves the efficiency of the calculation of $I(\omega)$ because it takes advantage of the fact that the inverse of a diagonal matrix, $\underset{\sim}{C}$, is the diagonal matrix whose elements are the inverses of the elements of $\underset{\sim}{C}$. The $G(t)$ calculation is simplified by noting that the exponential of a diagonal matrix $\underset{\sim}{C}$ is a diagonal matrix whose kk-th element is $\exp[C_{kk}]$. Using these algorithms Eq. (II-10) and Eq. (II-11) become

$$G(t) = \underset{\sim}{d}^{+} \cdot \underset{\sim}{S} \cdot \exp[\underset{\sim}{\lambda} t] \cdot \underset{\sim}{S}^{-1} \cdot \underset{\sim}{P} \cdot \underset{\sim}{d} \qquad \text{(II-14)}$$

and

$$I(\omega) = \mathrm{Re}\left\{ \underset{\sim}{d}^{+} \cdot \underset{\sim}{S} \cdot (\underset{\sim}{\lambda} - i\omega \underset{\sim}{1})^{-1} \cdot \underset{\sim}{S}^{-1} \cdot \underset{\sim}{P} \cdot \underset{\sim}{d} \right\} \qquad \text{(II-15)}$$

where Re{} implies the real part of the quantity within the braces and the complex matrices $\underset{\sim}{S}$ and $\underset{\sim}{\lambda}$ are defined by

$$\underset{\sim}{S}^{-1} \cdot (i\underset{\sim}{\omega}_o - \underset{\sim}{\Pi}) \cdot \underset{\sim}{S} = \underset{\sim}{\lambda} \qquad \text{(II-16)}$$

where $\underset{\sim}{\lambda}$ is a diagonal matrix and $\underset{\sim}{S}^{-1}$ is the inverse of $\underset{\sim}{S}$. The calculations were performed on an IBM 360/67 digital computer using complex matrix inversion and diagonalization procedures throughout. A listing of the Fortran program is given in Appendix II-A. It was found to be more efficient to calculate G(t) by numerical Fourier transformation of I(ω) calculated from Eq. (II-15) then to calculate both G(t) and I(ω) independently from Eq. (II-14) and Eq. (II-15). This numerical Fourier transformation procedure was used throughout and employed trapezoidal rule integration.

In a set of preliminary calculations the band shape for the F-species was calculated in two different ways. In the first calculation, all 44 spectral lines associated with the rotational states in the range $0 \leq J \leq 7$ were included. In the second approach, the transition frequencies associated with a given J-state in a given branch were averaged and the averaged frequency was used in the band shape calculation. This method resulted in a band shape calculated from only 21 lines. The nature of the averaging process used is indicated in Fig. 1 (a)-(b). The resulting spectra for a τ_J of 9 x 10^{-13} sec, representative of a CH_4/He mixture at 100 amagats, were identical. Since the Coriolis splittings of the frequencies averaged in this latter calculations are representative of those encountered in the range $0 \leq J \leq 12$ and because the correlation time is representative of the least dense sample studied, it is apparent that neglect of Coriolis coupling is amply justified in these calculations.

In a second set of calculations the overall methane band shape was calculated by superposition of the component ortho-, para- and meta-CH_4 subspectra calculated from frequencies averaged over the Coriolis components of each as described above. In order to assess the importance of the separation into subspectra, a series of band shapes were computed by relaxing the restriction that line amplitude be transferred only between lines of the same nuclear spin isomer. In these latter calculations, the Boltzmann factors for the rotational levels were taken to be the sums of the Boltzmann factors for the nuclear spin isomers, and the absorption frequencies of the lines for each nuclear spin isomer were used to construct an average absorption frequency [see Fig. 1(b)-(c)]. Methane band shapes calculated using this procedure are given in Fig. 2 as the dashed curves. Also included in Fig. 2 are the corresponding band shapes for the individual nuclear

FIGURE 1

Construction of average frequencies for the P(9) lines of CH_4

(a) All multiplet lines in P(9).

(b) Average of Coriolis multiplets for each nuclear spin isomer.

(c) Average of nuclear spin isomer frequencies.

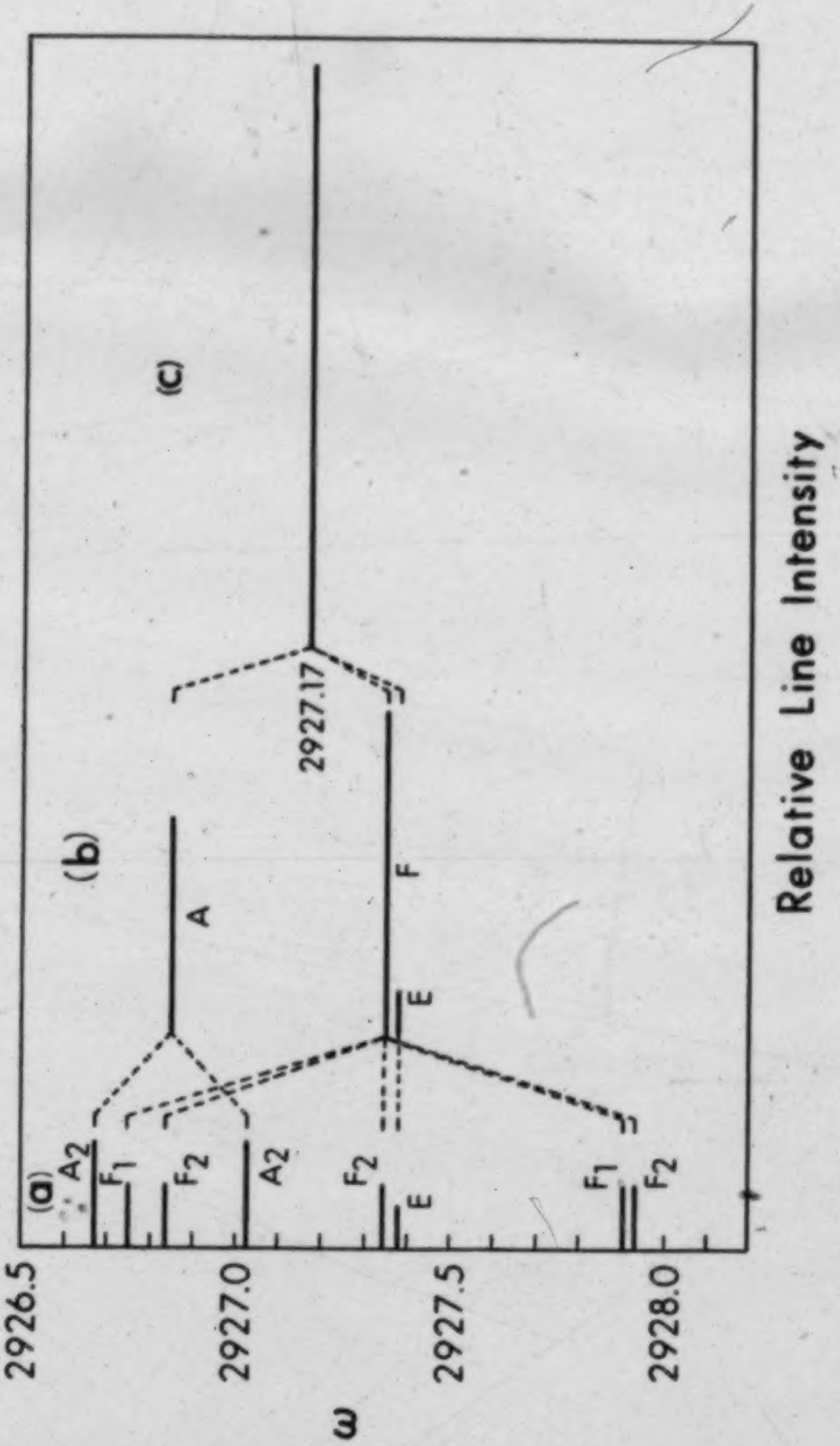
(a)
A_2
F_1
F_2
A_2
F_2
E
F_1
F_2
(b)
A
F
E
(c)
2927.17
2926.5
2927.0
2927.5
2928.0
ω
Relative Line Intensity

FIGURE 2

ν_3 band shapes of CH_4 computed from the semiclassical J-diffusion model

(a) $\tau_J = 9.0 \times 10^{-13}$ sec, T = 295K.

(b) $\tau_J = 1.5 \times 10^{-13}$ sec, T = 117K.

——— - Individual nuclear spin isomer spectra,

----- - spectra calculated using line frequencies obtained by averaging all Coriolis multiplets of all nuclear spin isomers. The vertical bars under the computed band contours indicate the positions and relative intensities of the line frequencies used in each calculation. The solid curves in the lowest section of the figure represent the normalized sum [(5A + 2E + 9F)/16] of the three nuclear spin isomer spectra.

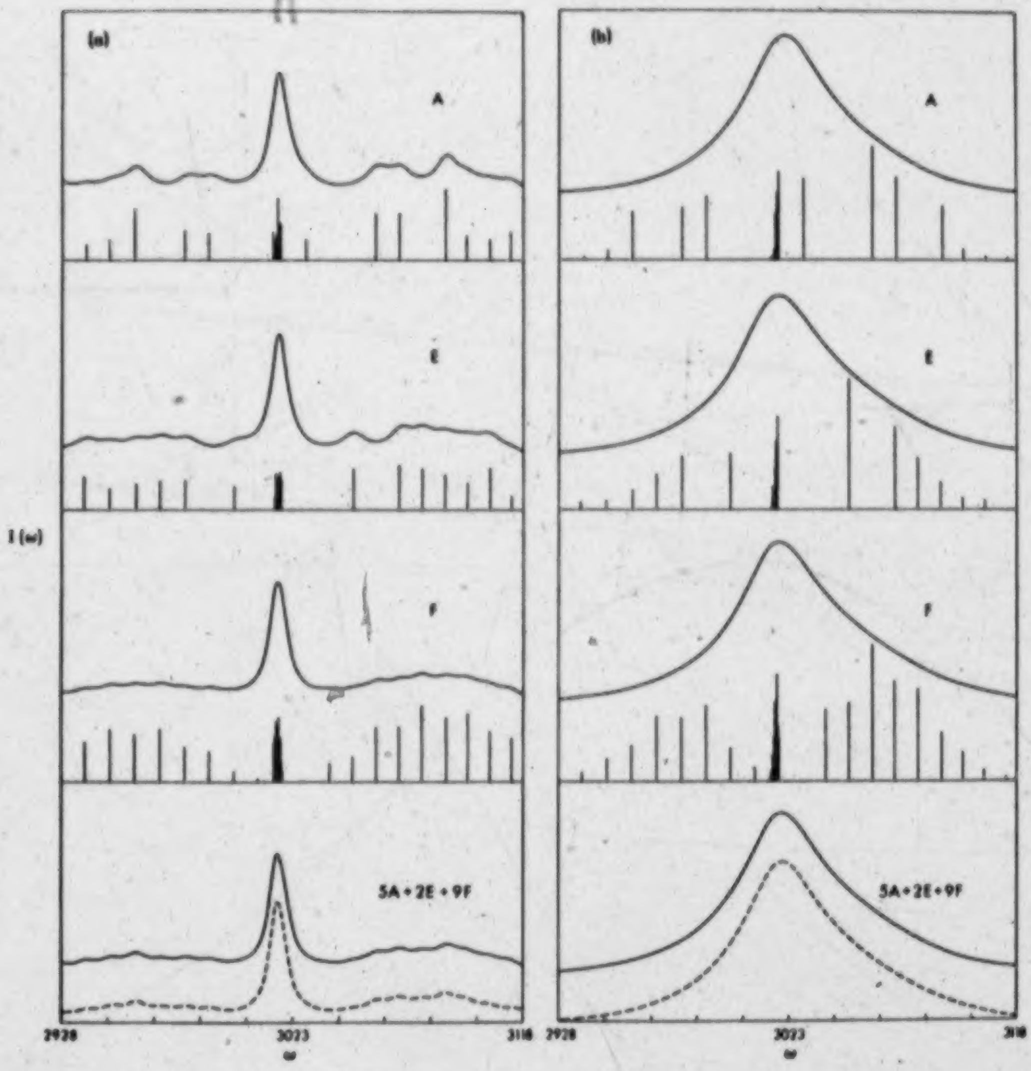
(a)
(b)
A
E
F
5A + 2E + 9F
I(ω)
2928
3023
3118
ω

spin isomers of methane and the band shape calculated by taking the weighted sum of these isomer band shapes. The band shapes in Fig. 2 (a) and (b) approximate the observed spectra of a CH_4/He mixture at 100 amagats and the observed spectra of liquid methane respectively. It is clear that the separation of the band shape computation into separate calculations for each nuclear spin isomer is unnecessary, in the range of τ_J of interest, since the differences in the spectra calculated by the two methods are insignificant. We have based subsequent calculations on a total methane picture which allows collisional transfer of intensity between lines belonging to different nuclear spin isomers, since this reduces computation time.

In Figs. 3 and 4, the band shapes calculated with the J- and M-diffusion limits of the semiclassical diffusion model are given for a range of values of τ_J. It is clear that the two limits of the diffusion model give similar results when τ_J is long, but give significantly different band shapes in the limit of motional narrowing where τ_J is short. Motional broadening of the individual vibration-rotation lines in the dilute gas limit, where τ_J is long, is more efficient in the J-diffusion model, for a given value of τ_J, than in the M-diffusion model. This observation is readily

FIGURE 3

ν_3 band shapes of CH_4 computed with the semiclassical J-diffusion model at 295K

The angular momentum correlation times, τ_J, are

(a) $11. \times 10^{-13}$ sec

(b) 7.0×10^{-13} sec

(c) 4.2×10^{-13} sec

(d) 2.0×10^{-13} sec

(e) 1.0×10^{-13} sec

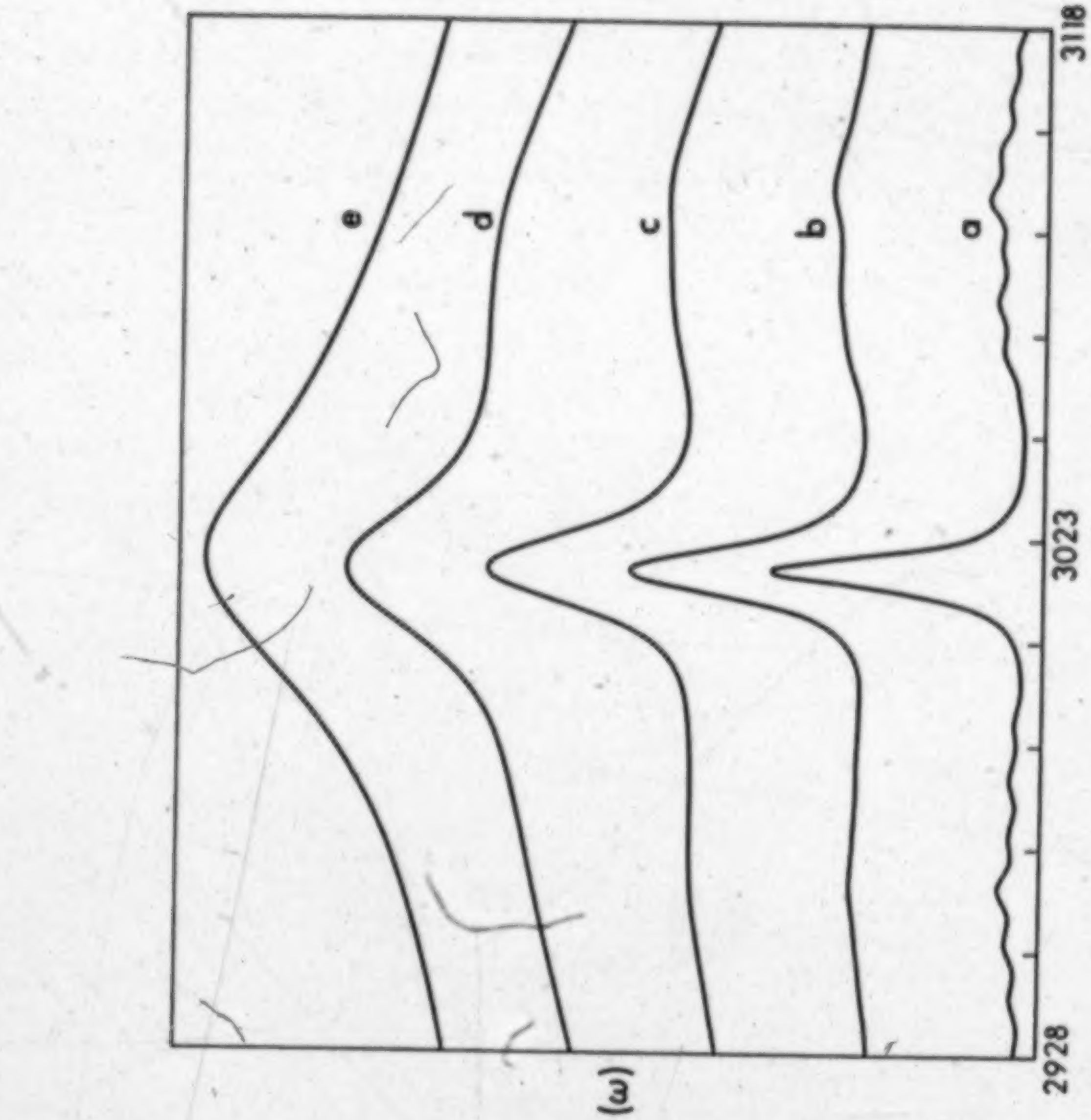
e
d
c
b
a
I(ω)
2928
3023
3118
ω

FIGURE 4

ν_3 band shapes of CH_4 computed with the semiclassical M-diffusion model at 295K

The angular momentum correlation times, τ_J, are

(a) $11. \times 10^{-13}$ sec

(b) 7.0×10^{-13} sec

(c) 4.2×10^{-13} sec

(d) 2.0×10^{-13} sec

(e) 1.0×10^{-13} sec

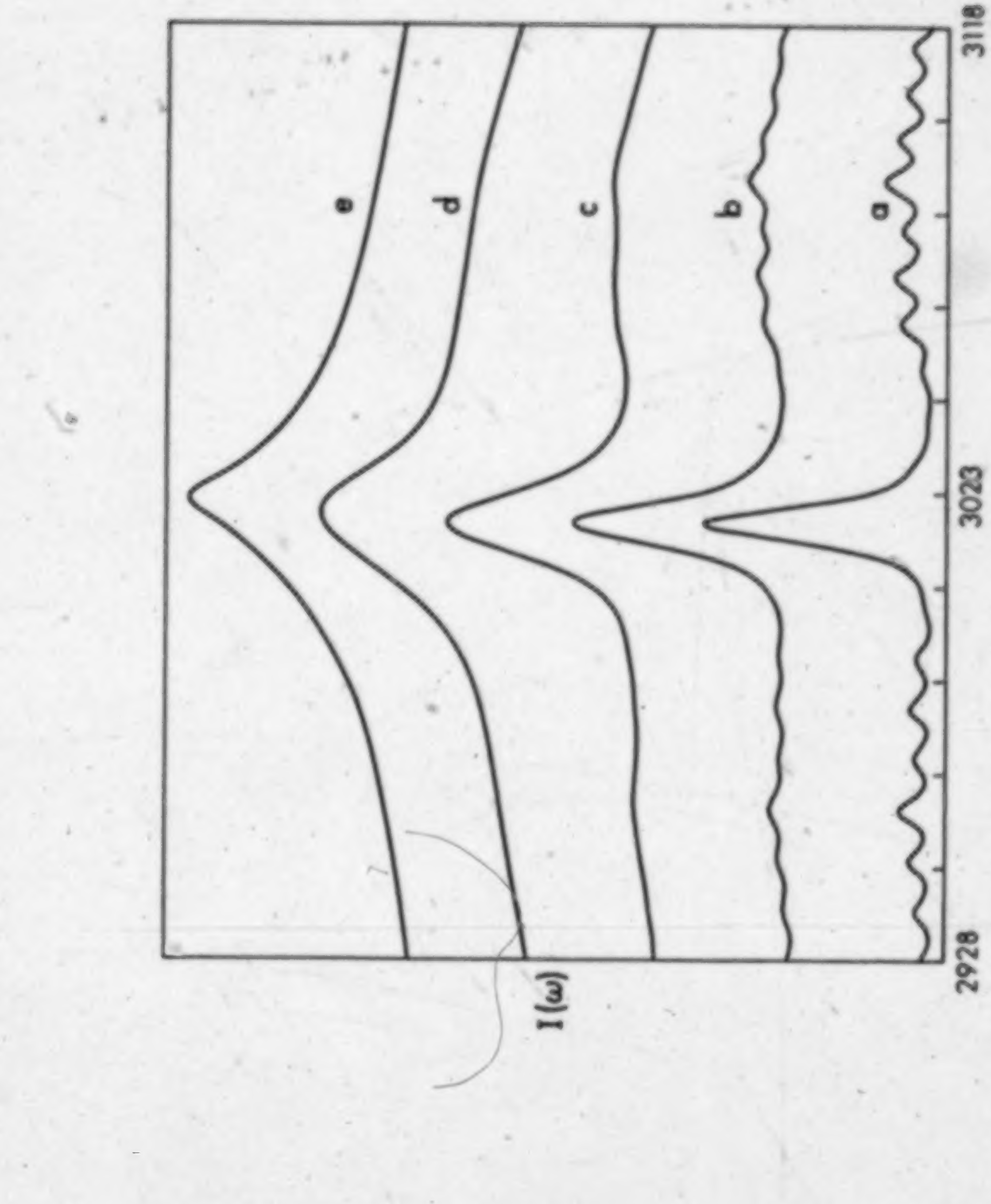
I(ω)
ω
2928
3023
3118
a
b
c
d
e

understood when one considers the lines between which intensity amplitude is transferred in the two models. In the J-diffusion model, line amplitude can be transferred between lines within a branch (spacings of 9 cm^{-1} to 11 cm^{-1}), while the M-diffusion model allows only those transfers which are between lines associated with the different transitions from a single rotational level (spacings of 8 cm^{-1} to 250 cm^{-1}). The amount of broadening of the lines is related to the spacing between them as well as the magnitude of the off-diagonal elements of $\underset{\sim}{\Pi}$ which connect them - the smaller the spacing and the larger the off-diagonal element, the broader the line.[55] In the limit of motional narrowing, the semiclassical M-diffusion model predicts a band shape with a sharp spike in the region of maximum absorption just as the classical extended M-diffusion model does.[6,8] The J-diffusion models (both classical and semiclassical versions) give a less rapidly varying spectral density in this region.

2. Comparison with Experiment

In comparing experimental results with those predicted by the semiclassical rotational diffusion models, one may choose to compare either the observed band contours with spectral densities computed from Eq. (II-15), or one may compare the reorientational correlation functions obtained by Fourier transformation of the band contours with theoretical correlation functions. We have found that the correlation functions obtained in our calculations were unreliable because we truncated the rotation-vibration spectrum at those lines arising from the J=12 rotational level. The neglect of the lines associated with J>12 was necessary to maintain computational efficiency by keeping the order of $\underset{\sim}{\Gamma}$ as small as possible. It did however lead to some unreliability in the spectral amplitudes in the wings of the spectral band and this unreliability is transmitted and amplified when the correlation function is obtained by Fourier transforming the computed band shape. We have chosen therefore to compare experimental and computed band shapes rather than their Fourier transforms.

Examination of Eq. (II-10) explains this dependence of G(t), at small t, on the wings of the spectral density. The contributions to the correlation function are determined by two factors: a damping term $\exp[-\underset{\sim}{\Gamma}t]$ and a term $\exp[i\underset{\sim}{\omega}_0 t]$ which oscillates with frequency $\underset{\sim}{\omega}_0$. At short times the oscillating terms are nearly in phase and the contributions to G(t) reinforce each other. As time progresses these terms get out of phase; the larger the difference in the frequencies of oscillation, the greater the dephasing. Therefore the contributions from the transitions in the wings (large ω) are dephased much faster than the contributions from the transitions near the center of the band (small ω). Because of this dephasing the contributions to G(t) from the wings of the spectral density soon cancel each other as time increases and their influence becomes negligible.

The fitting of observed band shapes with those calculated from the semiclassical rotational diffusion models involves comparing experimental spectra with a series of theoretical ones calculated with different values of τ_J in both J- and M-diffusion models. In preparing the calculated spectra for comparison with observed ones, one must choose a procedure for normalization of the spectral amplitudes. One can require the calculated and observed spectra to match at the point of maximum absorption (intensity normalization) or one can require them to be normalized such that the areas under the calculated and observed curves are equal (area normalization). Intensity normalization tends to weight the central section of the band very strongly, while area normalization allows a more realistic weighting over the whole spectral band and is the preferred method. As we have indicated above, the wings of our calculated spectra are not too reliable because we have not included all of the weak transitions which would contribute to the amplitude in the wings. We have chosen to take the spectral area in a 120 cm^{-1} region symmetrical about the frequency of maximum absorption as the area used in the normalization. The best fits of observed spectra with those calculated from the semiclassical diffusion models were judged by visual comparison.

The infrared data for methane in high pressure mixtures with inert gases were obtained from Armstrong[39], and those for liquid CH_4 and CH_4 in liquid noble gases were obtained from Cabana.[38] Equally satisfactory fits of the observed high pressure gas spectra were obtained using the M- or J-diffusion model. Representative examples of the agreement between calculated and observed band shapes are given in Fig. 5. The values of the angular momentum correlation time which were obtained from the comparisons of calculated and observed spectra are given in Table 1. It should be noted that the spectra were calculated using frequencies appropriate to the dilute gas phase and agreement between calculated spectra and those observed in the dense gas can only be achieved if the whole of the calculated spectrum is shifted by 3-10 cm^{-1} to higher frequencies for the gaseous systems and 5-13 cm^{-1} to lower frequencies for the liquid systems. This is not too unexpected because we have only considered the broadening effects of

FIGURE 5

Comparison of the observed ν_3 band shapes of CH_4 in dense gas mixtures at 295K with spectral band shapes calculated with the semiclassical J-diffusion model

The band shapes are area normalized over a 120 cm^{-1} region about the center of the band. The intensity scale numbers are for comparison purposes only and are relevant only within the figure. Observed - ———, calculated - -----.

(a) CH_4/He, 96 amagats; $\tau_J = 12. \times 10^{-13}$ sec
(b) CH_4/N_2, 186 amagats; $\tau_J = 4.2 \times 10^{-13}$ sec
(c) CH_4/He, 543 amagats; $\tau_J = 2.9 \times 10^{-13}$ sec
(d) CH_4/N_2 463 amagats; $\tau_J = 1.8 \times 10^{-13}$ sec

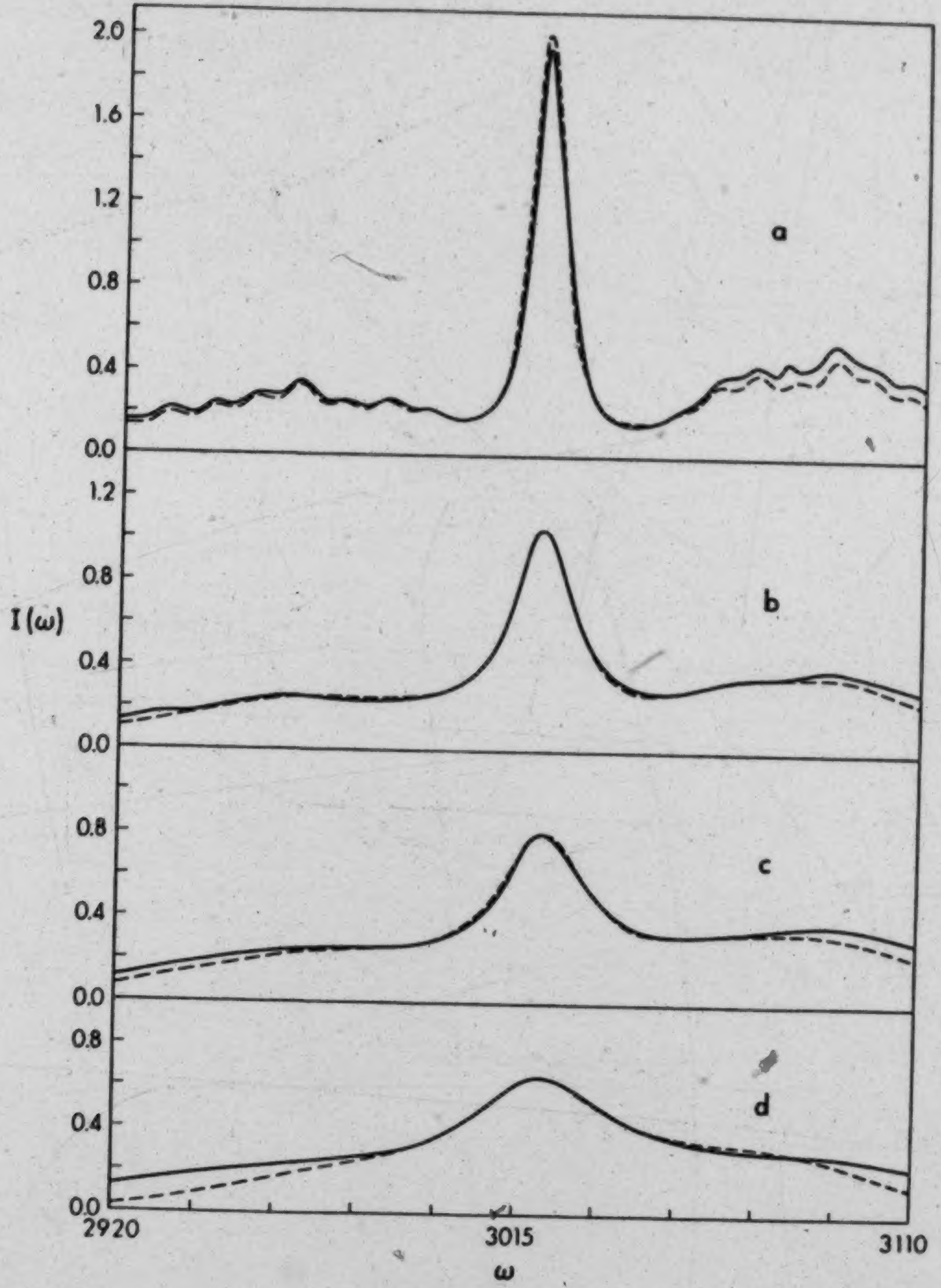
2.0
1.6
1.2
0.8
0.4
0.0
a
1.2
0.8
0.4
0.0
b
I(ω)
0.8
0.4
0.0
c
0.8
0.4
0.0
d
2920
3015
3110
ω

TABLE 1

Correlation Times Assigned Using Semiclassical J-diffusion (SCJ), Semiclassical M-diffusion (SCM), Classical J-diffusion (CJ) and Classical M-diffusion (CM)

System	Temperature (°K)	Density (amagats)	$\tau_J \times 10^{13}$ sec (SCJ)	$\tau_J \times 10^{13}$ sec SCM)	$\tau_J \times 10^{13}$ sec (CJ)	$\tau_J \times 10^{13}$ sec (CM)
CH_4/He	295	96	12.	11.	-	-
CH_4/He	295	437	3.6	3.5	3.0	3.9
CH_4/He	295	544	2.9	2.9	2.4	3.3
CH_4/He	295	745	1.9	-	1.9	2.5
CH_4/He	295	1096	-	-	1.4	-
CH_4/N_2	295	186	4.2	4.0	3.6	4.0
CH_4/N_2	295	243	3.5	3.3	2.9	3.4
CH_4/N_2	295	308	2.7	2.6	2.2	2.9
CH_4/N_2	295	463	1.8	1.5	1.6	2.3
CH_4/N_2	295	620	1.5	-	1.3	1.7
CH_4	117	liquid	1.5	-	1.5	-
CH_4/Ar	111	liquid	-	1.5	-	1.5
CH_4/Kr	135	liquid	-	1.3	-	1.2
CH_4/Xe	163	liquid	-	1.3	-	1.2

molecular collisions. Frequency shifts can also be produced by intermolecular interactions ^{63}, but we have made no attempt to include them. Our neglect of these frequency shifts may account for the poorer quality of the fits of the highest pressure gas spectra.

The spectra of CH_4 in the liquid phase and in dilute solutions in liquid rare gases were compared with calculated spectra, and it was concluded that the best agreement was obtained with the J-diffusion model for the neat liquid, and with the M-diffusion model for the liquid rare gas solutions. This is in accord with the conclusions drawn in an earlier analysis of these spectra using the classical extended diffusion models.[7] Moreover, the estimates of the angular momentum correlation times τ_J which give best agreement between the observed spectra and those calculated from the semiclassical diffusion models are in close agreement with the correlation times required to obtain a satisfactory fit of the symmetrical part of the observed band shape with the spectral densities obtained from the classical extended diffusion models.

The calculated band shapes discussed above have been compared to experimental spectra assuming that the experiments were performed under conditions in which instrumental broadening of the bands was insignificant.

Since the exact nature of the slit function of the spectrometer was not known, the effects of convoluting theoretical absorbance spectra with a triangular slit function of width 4.5 cm^{-1} were studied. The band shapes computed in this way were compared with observed spectra, and with the exception of the low density methane-helium band shape, the slit function had very little effect on the band shape, and had no effect on the assessment of the angular momentum correlation times obtained in these comparisons. For the spectrum of CH_4 in helium at 96 amagats, the slit function had a significant effect on the shape of the band, and the value of τ_J which yielded best agreement between theory and experiment was 12×10^{-13} sec, in contrast to the value of 9.0×10^{-13} sec obtained neglecting instrumental broadening. Because the effects of the slit function on the band shape are of the same order of magnitude as the effects of collisional broadening in this low density gas mixture, the angular momentum correlation time obtained in our analysis is subject to large uncertainties.

The analysis of the gas phase spectra did not give a clear cut distinction between M- and J-diffusion limits. The reason for this is the similarity between M- and J-diffusion spectra in the range of interest. The semi-classical correlation times of the angular momentum from this analysis are given in Table 1 for both the M- and J-diffusion limits. Except in the cases of the very high pressure samples we see that the values are essentially identical. In the high pressure samples M-diffusion exhibited motional narrowing effects which were inconsistent with the experimental band shapes.

D. DISCUSSION

1. Comparison of Semiclassical Results with Previous Treatments

The magnitudes of the angular momentum correlation times obtained by fitting the observed spectral band shapes with band shapes calculated from the semiclassical rotational diffusion models can be compared with those obtained from the analysis of proton magnetic relaxation times which are dominated by spin-rotational interactions. Since the only relevant experimental data in the literature consists of proton relaxation rates for methane gas at densities up to 550 amagats [56], the angular momentum correlation times obtained from the relaxation data are not strictly comparable to those obtained in this work because the conditions were not identical. However, it is of interest to ascertain the reasonability of our estimates of τ_J. Trappeniers *et al.*[56] used a perturbed free rotor model [21] of reorientation to analyse their data. As noted above, this implies that the effects of only the first "collision" are included and the anisotropic spin-rotation contributions to the NMR relaxation times are treated in an approximate fashion. We have reanalysed their data using the classical extended rotational diffusion theory.[6] The values of τ_J obtained in this way are shown in Fig. 6 together with the present τ_J values for CH_4 in dense gas mixtures. Although, as mentioned earlier, the numbers are not directly comparable because of the difference in the perturbing species, we see that the angular momentum correlation times obtained by the different methods are very similar.

Since the general conclusions of the analysis of the ν_3 band of methane both in liquid and high pressure gas systems by the classical extended diffusion and semiclassical diffusion models are the same, it is of interest to compare the band shape computed from the classical extended diffusion model [6,7] with the symmetric portion of the band shape computed using the semiclassical rotational diffusion model. Several representative examples are shown in Fig. 7 for the J-diffusion limit. It is clear that, with the exception of the rotational fine structure which appears in the semiclassical spectra at long τ_J, the two models give similar results for correlation times

FIGURE 6

Density dependence of τ_J determined by comparison of observed ν_3 band shapes with those computed using the semiclassical J-diffusion model.

O - CH_4/He, Δ-CH_4/N_2, □-determined from proton relaxation times in methane gas (ref. 56).

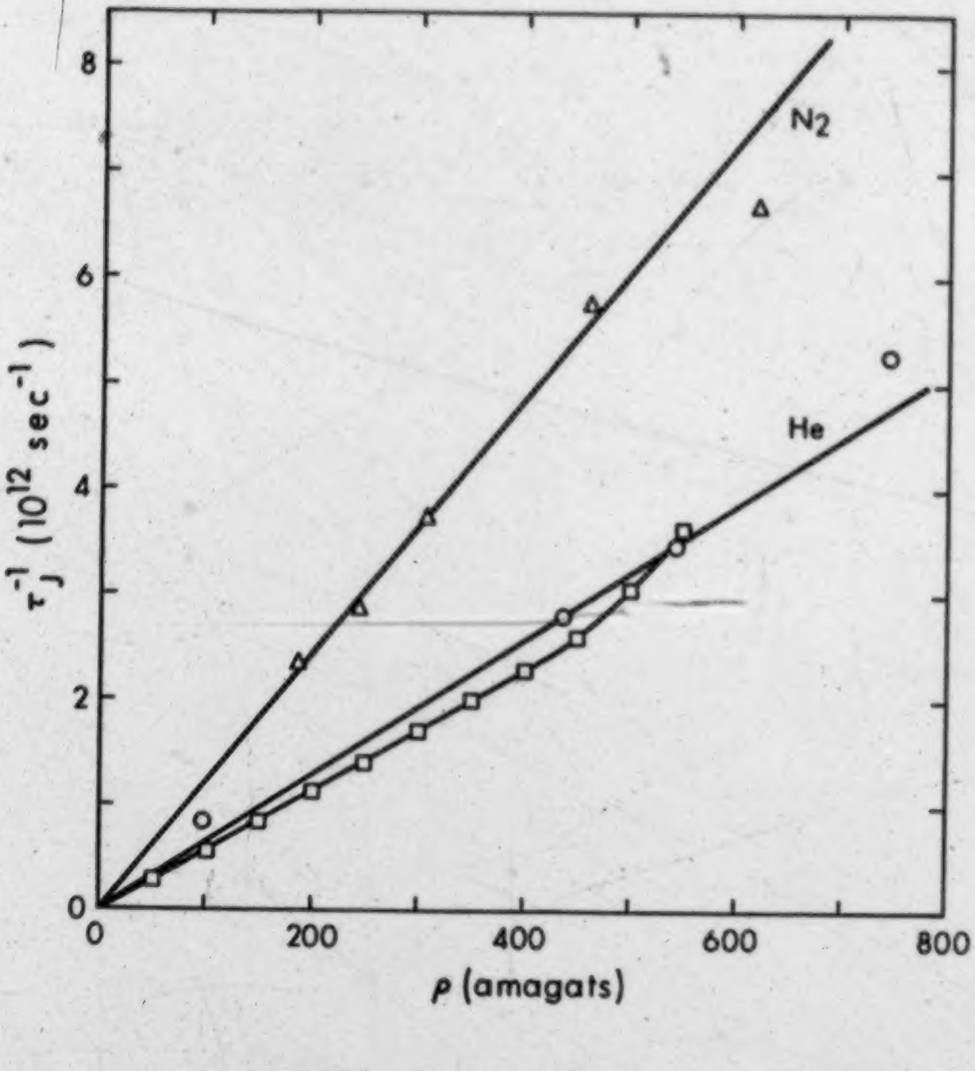
τ_J^{-1} (10^{12} sec^{-1})
0
2
4
6
8
0
200
400
600
800
ρ (amagats)
N2
He

FIGURE 7.

Comparison of the symmetrical part of the ν_3 band shapes of methane calculated from the semiclassical J-diffusion model with the band shapes calculated from the classical extended J-diffusion model

Semiclassical J-diffusion - ———, classical J-diffusion ----. The angular momentum correlation times, τ_J, are (a) 11. x 10^{-13}, (b) 7.0 x 10^{-13}, (c) 2.9 x 10^{-13}, and (d) 1.0 x 10^{-13} sec. The frequency scale is in reduced units of $2\pi c\,\bar{\nu}\,(I/kT)^{1/2}$ where I is the moment of inertia of CH_4 and c is the speed of light. The band shapes are area normalized as in Fig. 5.

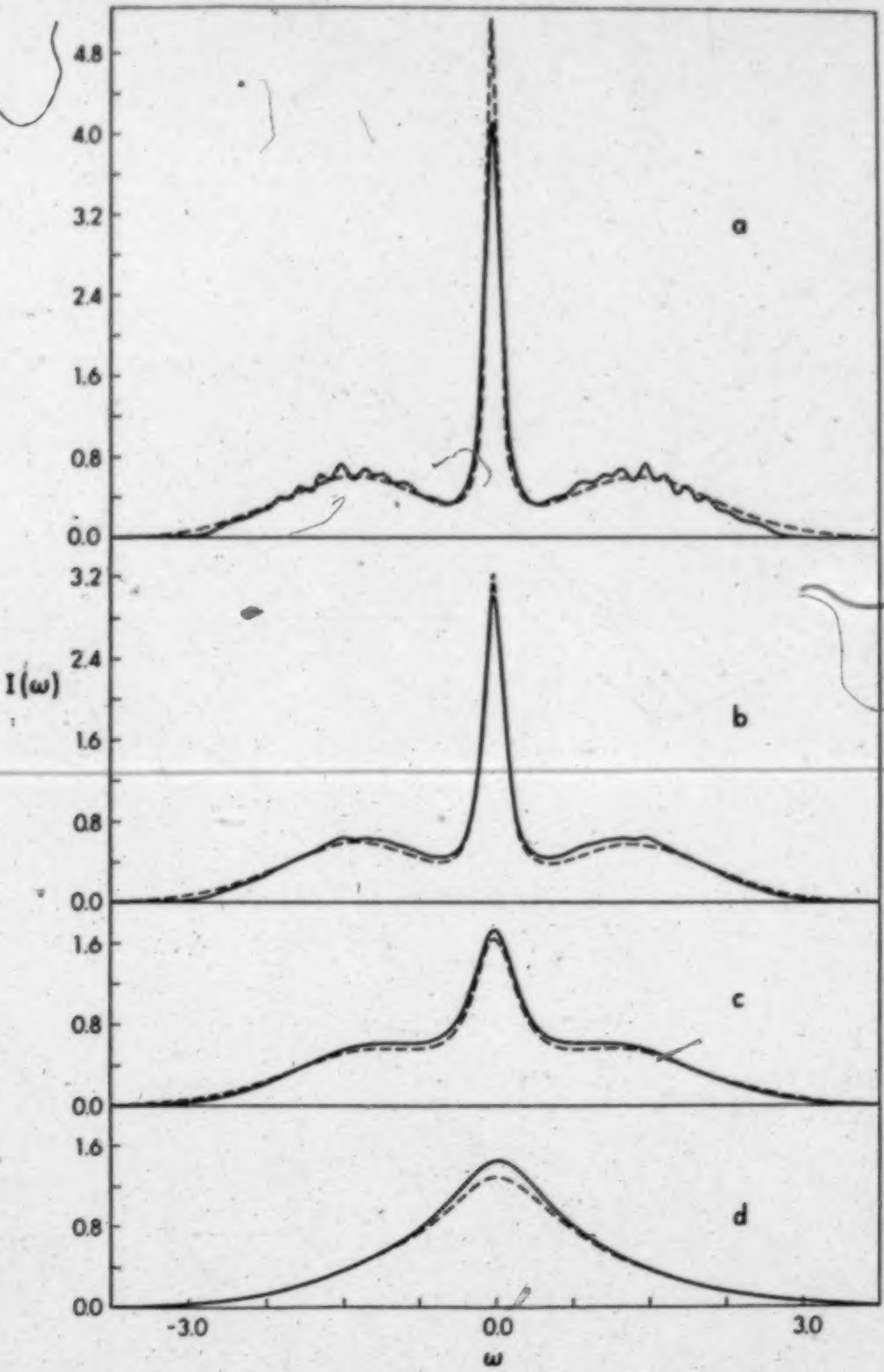
4.8
4.0
3.2
2.4
1.6
0.8
0.0
a
3.2
2.4
1.6
0.8
0.0
b
1.6
0.8
0.0
c
1.6
0.8
0.0
d
I(ω)
-3.0
0.0
3.0
ω

greater than 2×10^{-13} sec. For correlation times less than 2×10^{-13} sec the semiclassical spectra begin to narrow more rapidly than the classical spectra. It is interesting to note that the classical model produces the "better" fit for high pressure samples. One must conclude therefore that the asymmetry of the spectral band is due to quantum mechanical effects, but that the symmetric part of the band contains enough information about the reorientation of the molecules to permit study using the simple cosine Fourier transform of the band shape. This procedure has been applied by a number of workers [4,6,38,39,46] with little justification and the results presented here establish its validity.

2. Limitations of the Theory

In our semiclassical calculations we have used intrinsic line amplitudes appropriate to a rigid spherical rotor.[60] Since vibrational-rotational coupling is important in methane [40,58,60] this rigid rotor approximation requires some justification. In Fig. 8 we have compared the ν_3 infrared spectra of CH_4 determined at a density of 0.1 amagat, with the stick spectra calculated using the rigid rotor approximation. We see that although the rigid rotor approximation predicts the R-branch to be more intense than the P-branch the reverse is true in the experimental spectrum. This

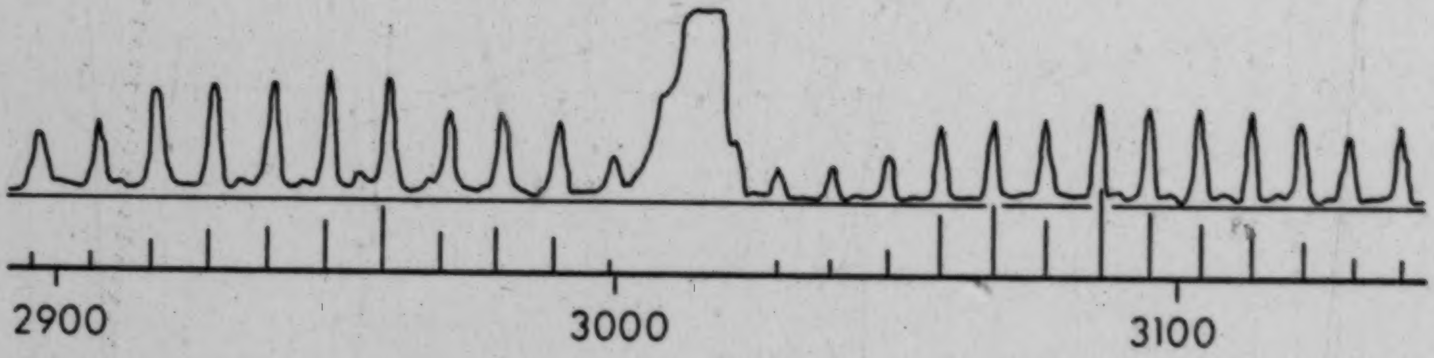

Figure 8. Comparison of the observed ν_3 band shape of methane gas at 0.1 amagats and 295K with the stick spectrum calculated from rigid rotor line amplitudes and Boltzmann factors.

observation has been reported previously by Welsh, Pashler and Dunn.[64] However, the intensities of the R-branch lines are greater than those of the P-branch at higher densities (see Fig. 5), which is more compatible with the rigid rotor line strengths. There is, therefore, little justification in using intrinsic line amplitudes other than those of the rigid spherical rotor unless a more exact treatment of the vibrational-rotational interaction is to be attempted. Because of this failing in the calculated intrinsic line amplitudes, the application of this theory to the band shapes of CH_4 in low density mixtures may be of questionable significance.

We have used the extended rotational diffusion picture of a collision to define the collisional transfer matrix, $\underset{\sim}{\Pi}$, rather than semiclassical scattering theory because it drastically reduced the computation time required to calculate a band shape and thus makes the theory practical for "every day" use. In addition, we felt that the application of scattering theory with an ill-defined intermolecular potential merely served to obscure any information that could be realized from the experiment. Gordon et al.[36] have fitted the infrared band shapes of the carbon monoxide molecule using the semiclassical[2,34] approach. They found that the widths of the vibrational-rotational lines predicted by their calculation were 23% larger than the observed widths of low density gas mixtures. This discrepancy was attributed to either inadequacies in the intermolecular potential used in their collisional cross section calculations or to possible errors in their trajectory calculation routines. At higher densities, the agreement between their calculated and observed band shapes was no better than ours. Clearly, from the success of our simple theory relative to the success of the more sophisticated treatment of Gordon, we must conclude that until more accurate intermolecular potentials become available, the simple theory is adequate for the interpretation of band shapes in terms of intermolecular interactions.

The semiclassical theory developed in section II-B is restricted to band shapes which can be described by a limited number (<40) of transitions. This restriction is due to the need to diagonalize a complex matrix whose order is the number of transitions included in the calculation. For the ν_3 band shape calculations we included all transitions arising from rotational states with total rotational angular momentum quantum number $J \leq 12$. Although this included approximately 96% of the CH_4 molecules in the system, the predicted band shapes were still inadequate in the wings of the spectrum. Coriolis coupling is much more important in the ν_4 mode than the ν_3 mode of CH_4.[40] The larger Coriolis splitting in the ν_4 mode invalidates the averaging of the frequencies of the lines within a branch arising from each J-manifold which we have used to simplify the ν_3 calculations. Therefore, in order to include the same number of ground rotational states as in the ν_3 study, approximately 200 transition lines would have to be considered. This is far too great a number to handle efficiently by the present procedure and still maintain reasonable computation time. Similarly the application of the theory to more massive molecules would be impractical because larger numbers of rotational states are populated.

In chapter III we will develop a "true" semi-classical version of the extended rotational diffusion theory. This theory will not be so severely restricted to a limited number of rotational states and will be used to study the ν_4 band shape.

SEMICLASSICAL EXTENDED ROTATIONAL DIFFUSION THEORY

CHAPTER III

A. INTRODUCTION

In Chapter II, we have developed a semiclassical extended rotational diffusion interpretation of Gordon's [2,34] semiclassical band shape theory. This approach adequately described the infrared absorption band shapes of the ν_3 mode of methane in gaseous and liquid mixtures, however the application of the theory was restricted to band shapes which could be described by a limited number of transitions (<40). For this reason the ν_4 mode of methane, in which Coriolis coupling is important, could not be treated by this procedure nor could band shapes of larger molecules in which a greater number of rotational states have significant populations. This restriction to a minimal set of transition lines also resulted in very poor agreement between predicted and experimental results in the wings of the band shapes of the ν_3 mode of CH_4 and made the predicted correlation functions meaningless at short times. Because the classical theories cannot be used to interpret band shapes in which Coriolis coupling is significant and the previous semiclassical theory cannot be used to treat systems in which there are a large number of transitions, there is a need for a semiclassical model which is not severely restricted by the number of distinct transitions included in the calculation.

The classical extended rotational diffusion theory [5,6,8,49] has been widely used to interpret spectral band shapes and magnetic resonance linewidths in terms of molecular reorientation.[22-33] The versatility of this theory lies in the fact that the individual steps in the molecular reorientation processes are followed in detail. Thus the theory is not restricted by the length of the rotational diffusion step as is the case for the Debye [54] and perturbed free rotor models.[6,21,28] Because of the versatility of the extended rotational diffusion model one would expect that a semiclassical interpretation of this model would prove quite effective in treating band shapes in which Coriolis effects are important.

Recently Bliot et al.[65,66] have recognized the potential of a memory function approach to the extended rotational diffusion model. Berne and Harp [67] have shown that the reorientational correlation function G(t) and its associated memory function K(t) satisfy the Volterra equation

$$\dot{G}(t) = -\int_0^t du K(u) G(t-u) , \qquad \text{(III-1)}$$

where $\dot{G}(t)$ is the time derivative of G(t). Bliot et al.[65,66] were able to show that, in the J-diffusion limit of the extended rotational diffusion model, the memory function $K(t)$ was related to $K_{FR}(t)$, the memory function for molecules undergoing free rotation, by

$$K(t) = K_{FR}(t)\exp(-t/\tau_J) \quad , \qquad \text{(III-2)}$$

where τ_J is the angular momentum correlation time. If the free rotation correlation function $G_{FR}(t)$ and its time derivative $\dot{G}_{FR}(t)$ are known then $K_{FR}(t)$ can be calculated using Eq. (III-1). Then Eq. (III-2) can be used to calculate $K(t)$, the memory function for a system of molecules undergoing rotational diffusion. Once $K(t)$ is known, $G(t)$ can be readily calculated from Eq. (III-1). Therefore, using Eqs. (III-1) and (III-2), and the functions $G_{FR}(t)$ and $\dot{G}_{FR}(t)$, the reorientational correlation function $G(t)$ can be calculated. All details of the free rotational steps are included in $G_{FR}(t)$ and $\dot{G}_{FR}(t)$ and therefore all that is necessary to define a semiclassical version of the extended rotational diffusion model is to calculate the semiclassical free rotor correlation function and its time derivative.

In section B of this chapter, Eq. (III-2) will be derived and the necessary relationships required for the application of the memory function approach will be developed. In section C the numerical analysis procedures used in the application of the theory are presented, while in section D the model will be applied to the calculation of the ν_3 and ν_4 band shapes of high pressure methane/inert gas mixtures.[39] Finally, in section E, the τ_J's obtained from this analysis are discussed and the present model is compared to the model presented in Chapter II.

B. THEORY

1. The Memory Function and Extended Rotational Diffusion

The infrared absorption band shape can be expressed by [2]

$$I(\omega) = \mathrm{Re}\int_0^{\infty} dt\, \exp[-i\omega t] \sum_{i,f} \rho_i \left\langle i \middle| \vec{p}.\vec{E}(0) \middle| f \right\rangle \quad \left\langle f \middle| \vec{p}.\vec{E}(t) \middle| i \right\rangle \tag{III-3}$$

where $\vec{p}$ is the transition dipole moment vector and $\vec{E}(t)$ is the electric field of the applied radiation, $|i\rangle$ and $|f\rangle$ are the initial and final states of a vibrational-rotational transition, ρ_i is the Boltzmann factor for state $|i\rangle$ and ω is the frequency of the incident radiation. In Eq. (III-3), both $\vec{p}$ and $\vec{E}(t)$ are defined in a molecular coordinate system. The time dependence of $\vec{E}(t)$ arises from the reorientational motion of the molecule since the direction of $\vec{E}$ is fixed in the laboratory.

The electric field E(t), defined in the molecular coordinate system, can be related to the electric field, $\vec{E}^{lab}$, of the laboratory coordinate system using the Wigner rotation matrix, $\mathcal{D}^{(1)}$.[68] The properties of the $\mathcal{D}$ matrices are discussed in Appendix I. Using the $\mathcal{D}$ matrix

$$E_k(t) = \sum_m E_m^{\ lab}\, \mathcal{D}_{mk}^{(1)}[\Omega(t)] \qquad \text{(III-4)}$$

where $E_k(t)$ is the k-th spherical tensor component of the first order spherical tensor (a vector), $\vec{E}(t)$, defined in the molecular coordinate system and $E_m^{\ lab}$ is the m-th spherical tensor component of the spherical tensor, $\vec{E}^{lab}$, defined in the laboratory coordinate system. $\Omega(t)$ represents the set of Euler angles describing the transformation from the laboratory to the molecular coordinate system. Introducing Eq. (III-4) to Eq. (III-3), we obtain

$$I(\omega) = \mathrm{Re}\int_0^\infty dt\ \exp[-i\omega t] \sum_{i,f} \rho i \sum_{\substack{k,k' \\ m,m'}} P_{-k}^{\ *} P_{-k'}(-1)^{k'+k} E_{m'}^{lab} E_m^{lab^*}$$

$$\times \langle i|\mathcal{D}_{m'k'}^{(1)}[\Omega(0)]|f\rangle \quad \langle f|\mathcal{D}_{m,k}^{(1)*}[\Omega(t)]|i\rangle \qquad \text{(III-5)}$$

where P_{-k} are the spherical tensor components of the transition dipole moment defined in the principal axis coordinate system (the coordinate system in which the inertia tensor of the molecule is diagonal). For a spherical top, the inertia tensor is diagonal in all coordinate systems and the spherical tensor components of the transition dipole moment can be taken to be the transition moments of the degenerate vibrational modes of the molecules all of which are of equal magnitude. It should be noted that in expressing $I(\omega)$ in the form of Eq. (III-5) we have assumed that the transition dipole moment is independent of the vibrational-rotational state of the molecule. In Appendix I, ~~it~~ is demonstrated that the space average over the product of rotational matrices in Eq. (III-5) vanishes except when $m' = m$ and $k' = k$. Thus Eq. (III-5) becomes

$$I(\omega) = \mathrm{Re}\int_0^\infty dt\, \exp[-i\omega t] \sum_{i,f} \rho_i \sum_{k,m} |p_{-k}|^2 |E_m^{lab}|^2$$

$$\times \left\langle i \middle| \mathcal{D}_{mk}^{(1)}[\Omega(0)] \middle| f \right\rangle \left\langle f \middle| \mathcal{D}_{mk}^{(1)*}[\Omega(t)] \middle| i \right\rangle . \qquad \text{(III-6)}$$

The orientation of $\vec{E}^{lab}$ is arbitrary so we average over all possible orientations to obtain

$$|E_m^{lab}|^2 = \frac{1}{3}\mathcal{E}^2 \qquad \text{(III-7)}$$

where $\mathcal{E}$ is the magnitude of $\vec{E}^{lab}$. Substituting Eq. (III-7) into Eq. (III-6) and omitting all constant multiplicative factors

$$I(\omega) = \mathrm{Re}\int_0^\infty dt\, \exp[-i\omega t]\sum_{k,m}\left\langle \mathcal{D}_{mk}^{(1)}[\Omega(0)]\mathcal{D}_{mk}^{(1)*}[\Omega(t)]\right\rangle \tag{III-8}$$

and the associated correlation function is given by

$$G^{(1)}(t) = \sum_{k,m}\left\langle \mathcal{D}_{mk}^{(1)}[\Omega(0)]\,\mathcal{D}_{mk}^{(1)*}[\Omega(t)]\right\rangle . \tag{III-9}$$

In going from Eq. (III-6) to Eq. (III-8) the sum over the projection operator, $|f\rangle\langle f|$, has been carried out and the statistical average indicated by the weighted sum over the expectation values $\langle i| \quad |i\rangle$ has been indicated by the angular brackets.

In the remainder of this section, a classical description of reorientational motion will be used to predict the reorientational correlation function defined by Eq. (III-9), and the relationship between this correlation function and its associated memory function will be examined in order to derive the relationship of Bliot et al.^{65,66} [Eq. (III-2)]. The development of the classical extended diffusion model has been chosen here, rather than a semiclassical approach, because the physics of the model is most clearly conveyed in classical terms. Because we are only concerned with the memory function as a vehicle for simplifying the mathematical apparatus used to derive the expressions for the reorientational correlation functions and spectral densities, not as a statistical mechanical function in its own right, we will develop the theory using the classical description of reorientation and show that the memory function formalism leads to the same results as the detailed geometric approach does. The development of the semiclassical model will then be made using the memory function approach.

The extended rotational diffusion model describes the reorientational motion of a molecule as a series of rotational steps which are terminated by "collisions". Two limiting types of "collisions" are considered: the M-diffusion and J-diffusion limits.[5,6,8] In the J-diffusion limit, the orientation of the angular momentum vector and its magnitude are randomized onto a Boltzmann distribution, while in the M-diffusion limit, only the orientation of the angular momentum vector is randomized by "collisions". In both cases, the reorientational motion will be changed by the collision.

If we divide the ensemble into groups of molecules which are in their n-th diffusive step at time t (i.e. have experienced exactly n-1 collisions at time t) then the correlation function of the ensemble can be expressed as

$$G^{(1)}(t) = \sum_{n=1}^{\infty} p(n,t) G^{(1)}(n,t) \quad , \qquad \text{(III-10)}$$

where $G^{(1)}(n,t)$ is the correlation function for those molecules which are in their n-th diffusive step at time t, p(n,t) is given by the Poisson distribution

$$p(n,t) = \frac{(t/\tau_J)^{n-1} \exp[-t/\tau_J]}{(n-1)!} \quad , \qquad \text{(III-11)}$$

and τ_J is the angular momentum correlation time which is the average time between "collisions". From Eq. (III-9), it is clear that the partial correlation function $G^{(1)}(n,t)$ is given by

$$G^{(1)}(n,t) = \sum_{km} \left\langle \mathcal{D}_{mk}^{(1)}[\Omega(0)] \, \mathcal{D}_{mk}^{(1)*}[\Omega_n(t)] \right\rangle \qquad \text{(III-12)}$$

where $\Omega_n(t)$ describes the orientation of the molecular coordinate system of a molecule in its n-th diffusive step at time t relative to a lab-fixed coordinate system.

We will now consider the classical reorientational motion of a spherical molecule undergoing changes in its angular momentum due to collisions. It will be assumed that the collisions have occurred at times t_1, t_2, ..., t_{n-1} and that the molecule rotates freely about the direction of the angular momentum vector, $\vec{J}$, with angular frequency, $\vec{\omega}$, given by

$$\vec{\omega} = \vec{J}/I \qquad \text{(III-13)}$$

where I is its moment of inertia. The matrix $\underset{\sim}{\mathcal{D}}^{(1)}[\Omega_1(t)]$ describing the transformation from the laboratory coordinate system to the molecular coordinate system of the molecule in its first diffusive step at time t can be expressed as a product of $\underset{\sim}{\mathcal{D}}$ matrices in the following way

$$\begin{aligned} \underset{\sim}{\mathcal{D}}^{(1)}[\Omega_1(t)] &= \underset{\sim}{\mathcal{D}}^{(1)}[\Omega_o]\, \underset{\sim}{\mathcal{D}}^{(1)}[\alpha_1,\beta_1,0] \\ &\quad \times \underset{\sim}{\mathcal{D}}^{(1)}[\omega_1 t,0,0]\, \underset{\sim}{\mathcal{D}}^{(1)}[\alpha_1,\beta_1,0]^{-1} \end{aligned} \qquad \text{(III-14)}$$

where $\underset{\sim}{\mathcal{D}}^{(1)}[\Omega_o]$ describes the transformation from the laboratory to the molecular coordinate system at time zero, $\underset{\sim}{\mathcal{D}}^{(1)}[\alpha_1,\beta_1,0]$ describes the transformation from the molecular coordinate system, at time zero, to a coordinate system in which the z-axis lies along the direction of the angular momentum vector, $\underset{\sim}{\mathcal{D}}^{(1)}[\omega_1 t_1,0,0]$ describes the rotation of the molecule about this z-axis through an angle $\omega_1 t$, and $\underset{\sim}{\mathcal{D}}^{(1)}[\alpha_1,\beta_1,0]^{-1}$ describes the transformation back to the molecular coordinate system defined at time zero.

Equation (III-14) defines the transformation of a first rank spherical tensor from the laboratory coordinate system to the molecular coordinate system of a molecule which is in its first diffusive step at time t. This transformation for a molecule which is in its second diffusive step at time t is given by

$$\begin{aligned}\underset{\sim}{\mathcal{D}}^{(1)}[\Omega_2(t)] &= \underset{\sim}{\mathcal{D}}^{(1)}[\Omega_1(t_1)]\ \underset{\sim}{\mathcal{D}}^{(1)}[\alpha_2,\beta_2,0] \\ &\quad \times\ \underset{\sim}{\mathcal{D}}^{(1)}[\omega_2(t-t_1),0,0]\,\underset{\sim}{\mathcal{D}}^{(1)}[\alpha_2,\beta_2,0]^{-1} \\ &= \underset{\sim}{\mathcal{D}}^{(1)}[\Omega_0]\ \underset{\sim}{\mathcal{D}}^{(1)}[\alpha_1,\beta_1,0]\,\underset{\sim}{\mathcal{D}}^{(1)}[\omega_1 t_1,0,0] \\ &\quad \times\ \underset{\sim}{\mathcal{D}}^{(1)}[\alpha_1,\beta_1,0]^{-1}\ \underset{\sim}{\mathcal{D}}^{(1)}[\alpha_2,\beta_2,0] \\ &\quad \times\ \underset{\sim}{\mathcal{D}}^{(1)}[\omega_2(t-t_1),0,0]\,\underset{\sim}{\mathcal{D}}^{(1)}[\alpha_2,\beta_2,0]^{-1}.\end{aligned} \tag{III-15}$$

where $\underset{\sim}{\mathcal{D}}^{(1)}[\Omega_1(t_1)]$ describes the transformation from the laboratory to the molecular coordinate systems at time t_1, the time of the first collision, and $\underset{\sim}{\mathcal{D}}^{(1)}[\alpha_2,\beta_2,0]\ \underset{\sim}{\mathcal{D}}^{(1)}[\omega_2(t-t_1),0,0]\,\underset{\sim}{\mathcal{D}}^{(1)}[\alpha_2,\beta_2,0]^{-1}$ describes the reorientational motion during the second diffusive step in the period $(t-t_1)$. Similarly, for a molecule which is in its n-th diffusive step at time t,

$$\underset{\sim}{\mathcal{D}}^{(1)}[\Omega_n(t)] = \underset{\sim}{\mathcal{D}}^{(1)}[\Omega_o] \prod_{i=1}^{n} \left\{ \underset{\sim}{\mathcal{D}}^{(1)}[\alpha_i,\beta_i,0] \right.$$

$$\left. \times \underset{\sim}{\mathcal{D}}^{(1)}[\omega_i(t_i-t_{i-1}),0,0] \; \underset{\sim}{\mathcal{D}}^{(1)}[\alpha_i,\beta_i,0]^{-1} \right\}$$

(III-16)

where $\prod_{i=1}^{n}$ indicates an ordered running product from left to right in ascending order of i, and t_i is the time at which the i-th diffusive step terminated. The angular momentum vector, $\vec{J}_i$, during the i-th diffusive step has an orientation $(\alpha_i,\beta_i,0)$ with respect to the molecular coordinate system at time t_{i-1} and ω_i, the angular frequency of rotation about the direction of $\vec{J}_i$, is given by Eq. (III-13). In Eq. (III-16) t_o and t_n are associated with 0 and t respectively.

Equation (III-16) describes the transformation from the laboratory to the molecular coordinate system for a molecule which has undergone a particular series of n diffusive steps. The partial reorientational correlation function $G^{(1)}(n,t)$ can then be written as

$$G^{(1)}(n,t) = \sum_{k,m} \Big\langle \mathcal{D}^{(1)}_{mk}[\Omega_o] \, \mathcal{D}^{(1)*}_{ma}[\Omega_o]$$

$$\times \mathcal{D}^{(1)*}_{ab}[\alpha_1,\beta_1,0] \exp[ib\omega_1 t_1] \, \mathcal{D}^{(1)}_{db}[\alpha_1,\beta_1,0]$$

$$\times\ \mathcal{D}^{(1)*}_{de}[\alpha_2,\beta_2,0]\exp[ie\omega_2(t_2-t_1)]\ \mathcal{D}^{(1)}_{ge}[\alpha_2,\beta_2,0] \times \text{-----}$$

$$\times\ \mathcal{D}^{(1)*}_{uv}[\alpha_{n-1},\beta_{n-1},0]\exp[iv\omega_{n-1}(t_{n-1}-t_{n-2})]$$

$$\times\ \mathcal{D}^{(1)}_{xv}[\alpha_{n-1},\beta_{n-1},0]\ \mathcal{D}^{(1)*}_{xy}[\alpha_n,\beta_n,0]\exp[iy\omega_n(t-t_{n-1})]$$

$$\times\ \mathcal{D}_{ky}[\alpha_n,\beta_n,0]\Big\rangle \qquad \text{(III-17)}$$

in which advantage was taken of the relationship [68]

$$\mathcal{D}^{(1)}_{ab}[\phi,0,0] = \exp[-ia\phi]\ \delta_{a,b} \qquad \text{(III-18)}$$

and

$$\mathcal{D}^{(1)}_{ab}[\alpha,\beta,0]^{-1} = \mathcal{D}^{(1)*}_{ba}[\alpha,\beta,0]\ . \qquad \text{(III-19)}$$

In Eq. (III-17) and subsequent equations the Einstein convention of implied summation over repeated indices is used.

The ensemble average over the initial orientations Ω_o is independent of all other averages and in the absence of a strong applied field all orientations are of equal probability so that [68]

$$\Big\langle \mathcal{D}^{(1)}_{mk}[\Omega_o]\ \mathcal{D}^{(1)*}_{ma}[\Omega_o] \Big\rangle_{\Omega_o} = \frac{1}{3}\,\delta_{k,a} \qquad \text{(III-20)}$$

The angles $\alpha_1, \ldots, \alpha_n$; $\beta_1, \ldots, \beta_n$, which define the orientation of the angular momentum vector in the molecular coordinate system at the beginning of each rotational diffusion step, are randomized at each collision, thus statistical averages can be independently taken over each set of these angles. This statistical average is given by [68]

$$(4\pi)^{-1}\int_0^{2\pi} d\alpha \int_0^{\pi} d\beta \sin\beta \, \mathcal{D}^{(1)}_{m_1,m}[\alpha,\beta,0] \, \mathcal{D}^{(1)*}_{m_2,m}[\alpha,\beta,0]$$

$$= \frac{1}{3} \delta_{m_1,m_2} \; . \qquad \text{(III-21)}$$

Applying these relationships to Eq. (III-17) we obtain

$$G^{(1)}(n,t) = \left\langle \prod_{i=1}^{n} \left\{ \frac{1}{3} \sum_a \exp[i a \omega_i (t_i - t_{i-1})] \right\} \right\rangle_{\substack{t_1 \ldots t_n \\ \omega_1 \ldots \omega_n}} \qquad \text{(III-22)}$$

where the angular brackets imply a statistical average over $t_1, \ldots t_{n-1}$ and $\omega_1 \ldots \omega_n$.

In the extended rotational diffusion model the times between collisions are assumed to be independent of the angular momentum state of the molecule, thus the averages over the collision times $t_1, \ldots, t_{n-1}$ can be taken independently of the average over the angular frequencies, $\omega_1, \ldots, \omega_n$. It will be assumed that the probability that a molecule has experienced exactly n-1 collisions in the periods t_1, $t_1 + dt_1$; t_2, $t_2 + dt_2$; ....; t_{n-1}, $t_{n-1} + dt_{n-1}$ is given by [5] $(n-1)!\, dt_1 dt_2 \ldots dt_{n-1}/t^{n-1}$. Taking the statistical average over the collision times, we obtain

$$G^{(1)}(n,t) = \frac{(n-1)!}{t^{n-1}} \int_0^t dt_{n-1} \int_0^{t_{n-1}} dt_{n-2} \cdots \int_0^{t_2} dt_1$$
$$\times \left\langle \prod_{i=1}^{n} \left\{ \frac{1}{3} \sum_a \exp[i a \omega_i (t_i - t_{i-1})] \right\} \right\rangle_{\omega_1 \ldots \omega_n} \tag{III-23}$$

In order to perform the statistical average over $\omega_1, \ldots, \omega_n$ it is necessary to specify either M- or J-diffusion. In the M-diffusion limit, the magnitude of the angular momentum vector is not changed in a collision therefore $\omega_1 = \omega_2 = \ldots\ldots = \omega_n \equiv \omega$ and Eq. (III-23) becomes

$$G_M^{(1)}(n,t) = \left\langle \frac{(n-1)!}{t^{n-1}} \int_0^t dt_{n-1} \cdots \int_0^{t_2} dt_1 \prod_{i=1}^{n} \left\{ G_{FR}^{(1)}[t_i - t_{i-1}, \omega] \right\} \right\rangle_\omega \tag{III-24}$$

where the angular brackets indicate the statistical average over ω and the free rotor correlation function $G_{FR}^{(1)}[t,\omega]$ is given by

$$G_{FR}^{(1)}[t,\omega] = \frac{1}{3}\sum_{a}\exp[i a\omega t] \ . \tag{III-25}$$

In the J-diffusion limit, the magnitude of the angular momentum is randomized onto a Boltzmann distribution at each collision and the statistical average over ω must therefore be performed independently for each diffusive step. Therefore in the J-diffusion limit, Eq. (III-23) becomes

$$G_J^{(1)}(n,t) = \frac{(n-1)!}{t^{n-1}}\int_0^t dt_{n-1}\cdots\int_0^{t_2} dt_1 \prod_{i=1}^{n}\left\{G_{J:FR}^{(1)}[t_i-t_{i-1}]\right\} \tag{III-26}$$

where the free rotor correlation function $G_{J:FR}^{(1)}(t)$ is given by

$$G_{J:FR}^{(1)}(t) = \left\langle \frac{1}{3}\sum_{a} \exp[i a\omega t] \right\rangle_{\omega} \ . \tag{III-27}$$

The reorientational correlation functions are then obtained by substituting Eq. (III-24) or (III-26) into Eq. (III-10) and applying Eq. (III-11). Thus

$$G_M^{(1)}(t) = \left\langle \exp[-t/\tau_J]\sum_{n=1}^{\infty}\tau_J^{-n+1}\int_0^t dt_{n-1} \ \cdots\cdot \right.$$

$$\times \int_{0}^{t_2} dt_1 \prod_{i=1}^{n} \left\{ G_{FR}^{(1)}[t_i - t_{i-1}, \omega] \right\} \Big\rangle_{\omega} \qquad \text{(III-28)}$$

and

$$G_J^{(1)}(t) = \exp[-t/\tau_J] \sum_{n=1}^{\infty} \tau_J^{-n+1} \int_{0}^{t} dt_{n-1} \cdots\cdots$$

$$\times \int_{0}^{t_2} dt_1 \prod_{i=1}^{n} \left\{ G_{J:FR}^{(1)} [t_i - t_{i-1}] \right\} . \qquad \text{(III-29)}$$

The memory function K(t) can be conveniently expressed in terms of the correlation function using Laplace transforms. By taking the Laplace transform of Eq. (III-1) and applying the convolution theorem [69] of Laplace transform theory we obtain

$$\bar{K}(s) = \frac{1 - s\bar{G}(s)}{\bar{G}(s)} \qquad \text{(III-30)}$$

where $\bar{K}(s)$ and $\bar{G}(s)$ are the Laplace transforms of K(t) and G(t) respectively and s is the Laplace variable. Using the extended rotational diffusion expression for G(t) and Eq. (III-30) we can obtain expressions for $\bar{K}(s)$ in the extended rotational diffusion model. First consider the J-diffusion limit. Taking the Laplace transform of Eq. (III-29) we obtain

$$\bar{G}_J^{(1)}(s) = \sum_{n=1}^{\infty} \tau_J^{-n+1} \left\{ \bar{G}_{J:FR}^{(1)}(s + \tau_J^{-1}) \right\}^n$$

$$= \frac{\tau_J \bar{G}_{J:FR}^{(1)}(s + \tau_J^{-1})}{\tau_J - \bar{G}_{J:FR}^{(1)}(s + \tau_J^{-1})} \qquad \text{(III-31)}$$

where $\bar{G}_J^{(1)}(s)$ is the Laplace transform of $G_J^{(1)}(t)$ and $\bar{G}_{J:FR}^{(1)}(s + \tau_J^{-1})$ is the Laplace transform of $\exp(-t/\tau_J)G_{J:FR}^{(1)}(t)$. The convolution theorem of Laplace transform theory was used in deriving Eq. (III-31) and the infinite sum rule for geometric progressions was used to obtain the second expression on the right hand side. Substituting Eq. (III-31) into Eq. (III-30) we obtain upon rearrangement

$$\bar{K}_J^{(1)}(s) = \frac{1 - (s + \tau_J^{-1})\bar{G}_{J:FR}^{(1)}(s + \tau_J^{-1})}{\bar{G}(s + \tau_J^{-1})} \qquad \text{(III-32)}$$

where $\bar{K}_J^{(1)}(s)$ is the Laplace transform of $K_J^{(1)}(t)$, the memory function in the J-diffusion limit. Using Eq. (III-30) the memory function associated with $G_{J:FR}^{(1)}(t)$ is given by

$$\bar{K}_{J:FR}^{(1)}(s') = \frac{1 - s'\bar{G}_{J:FR}^{(1)}(s')}{\bar{G}_{J:FR}^{(1)}(s')} . \qquad \text{(III-33)}$$

Comparison of Eqs. (III-32) and (III-33) we see that if we associate s' with $s + \tau_J^{-1}$ and thus $K_J^{(1)}(t)$ with $K_{J:FR}^{(1)}(t)\exp[-t/\tau_J]$ then the equations are the same. This is the relationship given in Eq. (III-2). Bliot et al.[65,66] obtained this relationship [Eq. (III-2)] using statistical mechanical arguments and they demonstrated that it defined the extended J-diffusion model.

In the M-diffusion limit the treatment is more involved because only the orientation of the angular momentum vector and not its magnitude is changed in a "collision". Thus molecules with different angular frequencies are treated as separate species and there will be a separate memory function equation for each species. The development in the M-diffusion limit is analogous to the J-diffusion limit except $G_{FR}^{(1)}(t,\omega)$ is used instead of $G_{J:FR}^{(1)}(t)$ and $K_M^{(1)}(t,\omega)$ is obtained. In order to calculate the ensemble function $G_M^{(1)}(t)$ or $K_M^{(1)}(t)$, an ensemble average over ω must be performed.

From the above development it is clear that all that is required to calculate the classical reorientational correlation function for the extended rotational diffusion model is the free rotor correlation function $G_{J:FR}^{(1)}(t)$ or $G_{FR}^{(1)}(t,\omega)$ and the memory function relationships given in Eqs. (III-1) and (III-2). The relationship between $K_J(t)$ and $K_{J:FR}(t)$ has been derived for the classical extended diffusion theory, however the expressions are determined by the description of the collision process and not by the description of the free rotation step. Therefore the theory can be modified to yield a semiclassical model simply by replacing the classical free rotor correlation functions $G_{J:FR}^{(1)}(t)$ and $G_{FR}^{(1)}(t,\omega)$ by the corresponding quantum mechanical functions. In the next section, quantum mechanical free rotor correlation functions will be considered and in later sections these functions and their time derivatives will be used to calculate spectral densities and reorientational correlation functions for a semiclassical extended rotational diffusion model.

2. Quantum Mechanical Free Rotor Correlation Functions

The relationships developed in the previous section indicate that a semiclassical extended rotational diffusion model is readily developed provided one can calculate a quantum mechanical free rotor reorientational correlation function and its first time derivative. In this section, these functions will be considered.

From Eq. (III-9) we see that the quantum mechanical free rotor correlation function is given by

$$G_{FR}^{(1)}(t) = \sum_{i,f} \rho_i \sum_{k,m} \langle i|\mathcal{D}_{mk}^{(1)}[\Omega(o)]|f\rangle \langle f|\mathcal{D}_{mk}^{(1)^*}[\Omega(t)_{FR}]|i\rangle \qquad \text{(III-34)}$$

where ρ_i is the Boltzmann factor for the state $|i\rangle$, $\Omega(t)_{FR}$ represents the set of Euler angles describing the transformation from the laboratory to the molecular coordinate system [68] of a freely rotating molecule at time t. The sums over i and f are over the initial and final transition states of the molecule and the sum over k is over the degenerate vibrational modes of the vibrational transition of interest while the sum over m is over arbitrary directions in the laboratory coordinate system and can be ignored since it results simply in multiplication by a constant factor.

The time dependence of $\underset{\sim}{\mathcal{D}}^{(1)}[\Omega(t)_{FR}]$ is determined by the motion of the free non-interacting molecule. Since $\underset{\sim}{\mathcal{D}}^{(1)}[\Omega(t)_{FR}]$ is a Heisenberg operator, its explicit time dependence is given by

$$\underset{\sim}{\mathcal{D}}^{(1)}[\Omega(t)_{FR}] = \exp[\frac{i\hat{\mathcal{H}}t}{\hbar}]\,\underset{\sim}{\mathcal{D}}^{(1)}[\Omega(0)]\exp[\frac{-i\hat{\mathcal{H}}t}{\hbar}] \qquad \text{(III-35)}$$

where $\hat{\mathcal{H}}$ is the Hamiltonian of the system. In the case of a rigid rotor, $\hat{\mathcal{H}}$ is the rotational Hamiltonian. The free rotor correlation function can therefore be written in the form

$$G^{(1)}_{FR}(t) = \sum_i \rho_i \sum_f \sum_{m,k} |\langle i|\mathcal{D}^{(1)}_{mk}[\Omega(0)]|f\rangle|^2 \exp i\omega_{if}t, \qquad \text{(III-36)}$$

where ω_{if} is the frequency of the transition i → f.

It is clear from Eq. (III-36) that one requires only a knowledge of the ground vibration-rotation state Boltzmann factor ρ_i, the transition moments $\langle i|\mathcal{D}^{(1)}_{mk}[\Omega(0)]|f\rangle$ and the transition frequencies ω_{if} of the molecule in order to determine the quantum mechanical free rotor correlation function from which $I(\omega)$ and $G(t)$ can be determined using the methods suggested in the previous section and which will be discussed in detail in the following sections. In the next section a brief description of the rotational states of molecules is presented and the semiclassical extended rotational diffusion model is discussed.

3. Description of the Rotational Motion

In a classical rotor, the angular momentum vector can take on any one of an infinite number of orientations with respect to a molecule-fixed coordinate system and with respect to a space-fixed coordinate system. The magnitude of the angular momentum vector can vary continuously from 0 to ∞, with the probability of a given magnitude and orientation following a Boltzmann distribution.[8] In the quantum mechanical description of rotating molecules, the orientation and magnitude of the angular momentum vector are no longer continuous variables as they are in a classical top. There exist distinct rotational states, which we shall denote

$|J\ K\ M\rangle$. The magnitude of the angular momentum vector for a molecule in the state $|J\ K\ M\rangle$ is $\sqrt{J(J+1)}\hbar$, while the projections of this vector onto the space-fixed z-axis and onto the molecular symmetry axis are $M\hbar$ and $K\hbar$ respectively. The quantum number J is a non-negative integer and the quantum numbers M and K can take on integral values from +J to -J. It is clear that K and M define the spatial orientation of the angular momentum vector and J determines its magnitude. The equilibrium populations of the rotational states follow a Boltzmann distribution just as the orientation and magnitude of the angular momentum vector in the classical top does.

In the absence of electric and magnetic fields, all rotational states with the same J and K, but different M, are degenerate. In linear molecules, the angular momentum vector is perpendicular to the molecular axis so that $K \equiv 0$. For a symmetric top molecule, the rotational states with different values of $|K|$ are non-degenerate, and their energy differences depend on the relative magnitudes of the moments of inertia about the symmetry axis and about axes perpendicular to it. The rotation states of a spherical top molecule, with the same value of J but different K values are degenerate, because of the inertial isotropy of the molecule.

In the simplest version of the classical extended rotational diffusion theory [5,6,8,49] a "collision" was interpreted as an event during which the angular momentum vector of a molecule was changed. In the J-diffusion limit, both the orientation and magnitude of the angular momentum vector are randomized onto a Boltzmann distribution at every collisional event. In M-diffusion, the magnitude of the angular momentum vector is unchanged by collisions, and only its orientation is randomized. By analogy to this classical extended rotational diffusion picture, we suggest that, in a semiclassical version of this model, "collisions" be considered as events wherein molecules undergo transitions from one rotational state to another due to perturbations from neighboring molecules. In the semiclassical J-diffusion model, "collisions" will be assumed to randomize all three quantum numbers J, K and M onto a Boltzmann distribution of rotational states, i.e. the probability of a transition to a state $|J\ K\ M\rangle$ brought about by a "collision" will be determined by the Boltzmann factor for that state and will be independent of the initial rotational state. Only transfers between levels with the same value of J will be allowed in the M-diffusion limit, where the quantum numbers K and M will be randomized by collisions. It is clear that in the M-diffusion limit, the molecules in the ensemble are subdivided according to their total angular momentum quantum numbers J and remain within such a subdivision throughout the diffusion process. The molecules within a given J-manifold will therefore be characterized in the M-diffusion limit by a unique reorientational correlation function and spectral band shape. The ensemble correlation function and band shape will, of course, be weighted sums of these components.

4. Spectral Densities and Correlation Functions in the M- and J-Diffusion Limits.

The Fourier relationship [Eqs. (I-5) and (I-6)] between the spectral density $I(\omega)$ and the correlation function $G(t)$ is conveniently expressed using Laplace transforms as

$$I(\omega) = \mathrm{Re}\left\{\overline{G}(i\omega)\right\} , \qquad \text{(III-37)}$$

where $\overline{G}(i\omega)$ is the Laplace transform of $G(t)$ and $i\omega$ is the Laplace variable. Equation (III-37) takes advantage of the time symmetry of $G(t)$, i.e. $G(t)^* = G(-t)$. Equation (III-37) will prove a convenient means of calculating $I(\omega)$.

The computation of spectral densities and reorientational correlation functions in the two limiting cases of the extended rotational diffusion model differ only in the manner in which the ensemble average over the rotational states of the molecule is performed. In the J-diffusion limit, where collisional events effect transfer of molecules between all possible rotational states, the appropriate free rotor correlation function, $G_{J:FR}^{(1)}(t)$, is given by Eq. (III-36) in which the sum over i encompasses all rotational states, $|\Lambda:JKM\rangle$ of the lower vibrational level. The Laplace transform of $G_{J:FR}^{(1)}(t)$ is given by

$$\bar{G}_{J:FR}^{(1)}(i\omega + \tau_J^{-1}) = \sum_{JKM} \rho_{JKM} \sum_{f} \sum_{m,k} |\langle\Lambda:JKM| \mathcal{D}_{mk}^{(1)}[\Omega(0)]|f\rangle|^2$$

$$\times \quad \tau_J/[1 + i(\omega - \omega_{JK,f})\tau_J] \,, \qquad \text{(III-38)}$$

where ρ_{JKM} is the Boltzmann factor for the state $|\Lambda:JKM\rangle$, $\omega_{JK,f}$ is the transition frequency of the transition $|\Lambda:JKM\rangle \longrightarrow |f\rangle$ and Λ is a vibrational quantum number. The band shape in the J-diffusion limit [see Eqs. (III-31) and (III-37)] is

$$I_J(\omega) = \text{Re}\left\{\tau_J A_J(\omega)/[1-A_J(\omega)]\right\} \quad , \qquad \text{(III-39)}$$

where

$$A_J(\omega) = \tau_J^{-1}\bar{G}_{J:FR}(i\omega + \tau_J^{-1}) \,. \qquad \text{(III-40)}$$

The reorientational correlation function in the J-diffusion limit, $G_J^{(1)}(t)$, can be obtained from $G_{J:FR}^{(1)}(t)$

by the memory function procedures to be described in the next section.

In the M-diffusion limit, as indicated in the previous section, all molecules with a common total angular momentum quantum number J are characterized by a unique reorientational correlation function $G^{(1)}(t;J)$ and a unique spectral density $I(\omega;J)$. The M-diffusion correlation function, $G_M^{(1)}(t)$, and spectral density $I_M(\omega)$ are related to these J-manifold functions by

$$G_M^{(1)}(t) = \sum_J \rho_J \, G^{(1)}(t;J) \quad , \tag{III-41}$$

and

$$I_M^{(1)}(\omega) = \sum_J \rho_J \, I^{(1)}(\omega;J) \quad , \tag{III-42}$$

where

$$\rho_J = \sum_{K,M} \rho_{JKM} \quad . \tag{III-43}$$

The free rotor correlation function appropriate for molecules in the J rotational manifold, $G_{FR}^{(1)}(t;J)$ is

$$G^{(1)}_{FR}(t;J) = \sum_{K,M} \rho^{J}_{KM} \sum_{f} \sum_{m,k} \left|\langle \Lambda;JKM| \mathcal{D}^{(1)}_{mk} [\Omega(0)] |f \rangle\right|^{2} \times \exp(i\omega_{JK,f}t) \quad ,$$

(III-44)

where

$$\rho^{J}_{KM} = \rho_{JKM}/\rho_{J} \quad .$$

(III-45)

The Laplace transform of $G_{FR}^{(1)}(t;J)$ is

$$\bar{G}^{(1)}_{FR}(i\omega + \tau_J^{-1};J) = \sum_{K,M} \rho^{J}_{KM} \sum_{f} \sum_{m,k} \left|\langle \Lambda;JKM| \mathcal{D}^{(1)}_{mk} [\Omega(0)] |f \rangle\right|^{2} \times \tau_J/[1 + i(\omega - \omega_{JK,f})\tau_J] \quad ,$$

(III-46)

and the M-diffusion spectral density, $I_M(\omega)$, is given by

$$I_M(\omega) = \sum_{J} \rho_J \tau_J \mathrm{Re}\left\{ B_J(\omega)/[1 - B_J(\omega)] \right\} \quad ,$$

(III-47)

where

$$B_J(\omega) = \tau_J^{-1} \bar{G}^{(1)}_{FR}(i\omega + \tau_J^{-1};J) \quad .$$

(III-48)

One could calculate the M-diffusion correlation function from the free rotor correlation functions $G_{FR}^{(1)}(t;J)$ via the corresponding free rotor memory functions $K_{FR}^{(1)}(t;J)$ for each J-manifold, but this would be rather impractical if the number of J-manifolds were large. On the other hand, one can compute $I_M(\omega)$ from Eq. (III-47) with little difficulty, even for a large number of J-manifolds, and the correlation function can be computed by Fourier transformation:

$$G_M^{(1)}(t) = \int_{-\infty}^{\infty} I_M(\omega) \exp(-i\omega t)\, d\omega \;. \tag{III-49}$$

C. NUMERICAL ANALYSIS PROCEDURES FOR IMPLEMENTATION OF THE MEMORY FUNCTION EQUATION

The computation of a reorientational correlation function using the Memory Function approach consists of two steps: calculation of $K_{FR}(t)$ from $G_{FR}(t)$ and $\dot{G}_{FR}(t)$; and calculation of G(t) from K(t). The first calculation is carried out using Eq. (III-1). Once $K_{FR}(t)$ is known, K(t) can be calculated for a given τ_J using Eq. (III-2). Equation (III-1) can then be used to calculate G(t) from K(t). In this section the numerical analysis procedures used to perform these calculations are described. Throughout this section, no distinction will be made between M- and J-diffusion since they differ only in the definition of $G_{FR}(t)$. In the M-diffusion limit the G(t) of the ensemble can be calculated using Eq. (III-41).

1. Calculation of $K_{FR}(t)$ from $G_{FR}(t)$

$G_{FR}(t)$ and $\dot{G}_{FR}(t)$ can be readily calculated from Eq. (III-36) or Eq. (III-44) depending on which limit is desired. The numerical procedure [70] for generating $K_{FR}(t)$ for t = 0, Δ,---,nΔ,-----, is based on a trapezoidal approximation to the integral in Eq. (III-1) and uses the relations

$$K_{FR}[0] = -\ddot{G}_{FR}[0] \quad , \qquad \text{(III-50)}$$

$$K_{FR}[\Delta] = \frac{-2}{\Delta}\dot{G}_{FR}[\Delta] - K_{FR}[0]G_{FR}[\Delta] \; , \qquad \text{(III-51)}$$

and

$$K_{FR}[n\Delta] = \frac{-2}{\Delta}\dot{G}_{FR}[n\Delta] - K_{FR}[0]G_{FR}[n\Delta] - 2\sum_{\ell=1}^{n-1} K_{FR}[\ell\Delta]G_{FR}[(n-\ell)\Delta] . \qquad \text{(III-52)}$$

K(t) is obtained from $K_{FR}(t)$ by multiplying by $\exp(-t/\tau_J)$.

2. Calculation of G(t) from K(t)

The procedure for computing G(t) at $t = 0, \Delta, 2\Delta, \text{---} \text{---} n\Delta, \text{-----}$, given K(t) at these values of t, is based on trapezoidal approximations for the integrations in Eq. (III-1) given by,

$$\dot{G}[n\Delta] = -\Delta\left\{\frac{K[0]G[n\Delta]}{2} + K[\Delta]G[(n-1)\Delta] + \text{---} + K[(n-1)\Delta]G[\Delta] + \frac{K[n\Delta]G[0]}{2}\right\} \tag{III-53}$$

and in the equation

$$G[n\Delta] = G[(n-1)\Delta] + \int_{(n-1)\Delta}^{n\Delta} du\, \dot{G}(u)$$

$$\cong G[(n-1)\Delta] + \frac{\Delta}{2}\left\{\dot{G}[n\Delta] + \dot{G}[(n-1)\Delta]\right\} \quad . \tag{III-54}$$

In addition, the conditions

$$G[0] = 1 \quad , \tag{III-55}$$

and

$$\dot{G}[0] = 0 \tag{III-56}$$

are required. The first is just a normalization condition, while the second determines the phase of G(t) and is required by the theory [see Eq. (III-1)].

Substituting Eq. (III-53) into Eq. (III-54) and imposing conditions (III-55) and (III-56) we obtain

$$G[\Delta] = \left\{1 - \frac{\Delta^2}{4}K[\Delta]\right\} \Big/ \left\{1 + \frac{\Delta^2}{4}K[0]\right\} , \qquad \text{(III-57)}$$

and from Eq. (III-54) we obtain

$$\dot{G}[(n-1)\Delta] = -\dot{G}[(n-2)\Delta] + \frac{2}{\Delta}(G[(n-1)\Delta] - G[(n-2)\Delta]) \qquad \text{(III-58)}$$

Substituting Eq. (III-53) into Eq. (III-54) and solving for G[nΔ] we obtain,

$$G[n\Delta] = \left\{G[(n-1)\Delta] + \frac{\Delta}{2}\dot{G}[(n-1)\Delta] - \frac{\Delta^2}{4}K[n\Delta] - \frac{\Delta^2}{2}\sum_{\ell=1}^{n-1} K[(n-\ell)\Delta]G[\ell\Delta]\right\} \Big/ \left\{1 + \frac{\Delta^2}{4}K[0]\right\} \qquad \text{(III-59)}$$

Therefore given the functions $G_{FR}(t)$ and $\dot{G}_{FR}(t)$, $G(t)$ can be calculated by simple numerical procedures involving the intermediate memory functions $K_{FR}(t)$ and $K(t)$. It should be pointed out that $K_{FR}(t)$ need be calculated only once and can be employed to compute $K(t)$ and $G(t)$ for the required values of τ_J in later calculations. A listing of the Fortran programs used to calculate $K_{FR}(t)$ from $G_{FR}(t)$ and $G(t)$ from $K_{FR}(t)$ are given in Appendix IIB and IIC respectively.

3. Investigation of the Stability of the Computation Procedures.

We have employed the trapezoidal approximation in the numerical solutions to Eq. (III-1), rather than a more sophisticated numerical integration formula. In test calculations using Simpson's rule formulae and higher order Newton-Cotes approximations, it was found that the calculated correlation functions and memory functions were much less stable than in calculations performed with Eqs. (III-50) - (III-59) above. This numerical integration procedure is also much more versatile than the power series expansion procedures used previously.[65,66] This procedure consisted of expanding K(t) and G(t) as power series in t and relating the coefficients in these series using the Laplace transform relationships. This procedure broke down at times greater than $4\sqrt{I/kT}$ seconds even when 100 or more terms were included in the expansion. The present procedure is stable at times as large as $20\sqrt{I/kT}$ seconds and, if longer times are required, it is necessary to reduce only the size of Δ, the time increment to increase the range of stability. In our calculations, we were interested in times in the range 0 to $10\sqrt{I/kT}$. For this range of times, we found that a time increment of $0.02\sqrt{I/kT}$ was more than adequate to assure numerical precision and accuracy.

The stability of the numerical methods were evaluated using the following procedures. The memory function calculated from the free rotor correlation function using the methods developed in section III-C-1 was compared to that calculated using the power series expansion technique [65,66] (which is exact for small t). This test indicated that the trapezoidal procedure is accurate over the range in which the power series approach is reliable. The generation of $K_{FR}(t)$ from $G_{FR}(t)$ was also tested by applying the numerical procedure to the "correlation function" defined by $(1 + t/2)\exp(-t/2)$ whose associated "memory function" is defined by $.25\exp(-t)$. The values of K(t) calculated from this G(t) agree with those calculated from the closed expression $.25[\exp(-t)]$ to four significant figures at $t = 20\sqrt{I/kT}$.

The numerical procedure for calculating G(t) from K(t) was tested by calculating G(t) using the methods of section III-C-2 when, $\tau_J = \infty$. The agreement between the function calculated in this way and $G_{FR}(t)$ indicated that this procedure is very accurate over the range $0 \leq t \leq 20\sqrt{I/kT}$.

D. APPLICATION TO ν_3 AND ν_4 BAND SHAPES OF CH_4

1. Calculation of Band Shapes of CH_4

In section III-B-3, we described the properties of the rotational states of molecules, pertinent to considerations in the rotational diffusion model, and developed these ideas in section III-B-4 into formulae for the spectral densities and reorientational correlation functions for molecules whose rotational behaviour was approximated by the J- and M-diffusion models. For spherical top molecules like CH_4, certain complicating features arise which affect the populations of the rotational levels and the vibration-rotation coupling in the upper vibrational state, and these factors must be taken into account. The first complication arises because the nuclear spin wavefunctions of the equivalent nuclei (e.g. the protons in CH_4) combine with the rotational wavefunctions in only certain ways, in order that the total molecular wavefunction satisfies the Pauli principle. Molecules which have rotational wavefunctions which combine with a given set of symmetry-adapted nuclear spin wavefunctions are often designated nuclear spin isomers. In the case of CH_4, where the four protons each have nuclear spin $\frac{1}{2}$; there are three nuclear spin isomers: ortho-CH_4 (rotational and nuclear spin wavefunctions of symmetry F), para-CH_4 (symmetry E) and meta-CH_4 (symmetry A), which correspond to nuclear spin triplet, singlet and quintet states respectively. The expected 2J + 1-fold degeneracy of the J-manifolds in the spherical top due to the 2J + 1 allowed values of K must be modified since a different number of nuclear spin wavefunctions can be combined with the various K-states within the J-manifold. The resulting degeneracy varies with symmetry type and has been calculated by Wilson [61] using group theoretic methods. The symmetry-adapted rotational wavefunctions $|J\Gamma_s M\rangle$, where Γ designates the irreducible representation and s is a serial index to distinguish linearly independent functions belonging to the same irreducible representation, are linear combinations of the functions $|JKM\rangle$ with different values of K, but with the same values of the quantum numbers J and M.

Since the rate of interconversion of nuclear spin isomers is believed to be slow compared to the molecular reorientation process [57], the spectral band shape is really a superposition of the contours for each nuclear spin species. This implies that calculations for each of the isomers must be performed separately and the results combined at the end to produce the composite correlation function.

If one neglects very small effects due to centrifugal distortion, all rotational states $|J\Gamma_s M\rangle$ in a J-manifold of a spherical molecule in its ground vibration state will be degenerate, but in an excited vibrational state in which one or more degenerate vibrational modes are excited, the degeneracies are lifted by the interaction between rotational and vibrational angular momenta.[58] This Coriolis interaction causes the degeneracy of the states with different quantum numbers Γ_s but identical quantum numbers J and M to be removed, and each of these rotational wavefunctions combine with each of the vibrational wavefunctions to produce as many distinct vibration-rotation states with a common symmetry label Γ_s as there are components of the degenerate vibration. The magnitude of the Coriolis coupling therefore varies with both rotational and vibrational quantum numbers. If all rotational transitions, $\Delta J = 0, \pm 1$ accompanying vibrational excitation were allowed, we would expect several lines to arise from each ground state molecule with rotational wavefunction $|J\Gamma_s M\rangle$. However, a detailed analysis of the selection rules[40,71] indicates that only one transition is allowed in each of the P, Q and R branches of the infrared spectrum of a tetrahedral top with ground state rotational wavefunction $|J\Gamma_s M\rangle$, and the magnitudes of the transition moments of the transitions in each branch arising from states within a given J-manifold are equal. The transition moments are given by Childs and Jahn.[60]

In section III-B-3 and III-B-4, we have expressed the free-rotor correlation functions and their Laplace transforms in terms of the transition moments $\sum_{m,k} | \langle \Lambda;JKM| \mathcal{D}^{(1)}_{mk}[\Omega(0)]|f\rangle|^2$. From the above discussion, we conclude that all transitions arising from states $|\Lambda;JKM\rangle$, or more correctly $|\Lambda;J\Gamma_s M\rangle$, within a single J-manifold have transition moments [60] which depend only on the value of ΔJ for that transition. For $\Delta J = +1$ (R-branch)

$$\sum_{m,k} |\langle \Lambda;J\Gamma_s M| \mathcal{D}^{(1)}_{mk} [\Omega(0)]|f\rangle|^2 = (2J + 3)/(2J + 1) \tag{III-60}$$

for $\Delta J = 0$ (Q-branch)

$$\sum_{m,k} |\langle \Lambda;J\Gamma_s M| \mathcal{D}^{(1)}_{mk} [\Omega(0)]|f\rangle|^2 = 1 \quad , \tag{III-61}$$

and for $\Delta J = -1$ (P-branch)

$$\sum_{m,k} |\langle \Lambda;J\Gamma_s M| \mathcal{D}^{(1)}_{mk} [\Omega(0)]|f\rangle|^2 = (2J -1)/(2J + 1) \quad . \tag{III-62}$$

With these transition moments and the observed [59,78] and calculated[71,73] transition frequencies in each vibration-rotation band, one can compute theoretical reorientational correlation functions and spectral band shapes which can be compared to those obtained from experimental measurements.[39]

a. ν_3 Band

The transitions in the ν_3 band of CH_4 are not strongly influenced by Coriolis effects because the Coriolis' coupling constant is very small [40] so that the transitions within a branch of the spectrum which arise from states within a given J-manifold are not widely separated in frequency (<2 cm^{-1}). The frequencies of the lines originating in states in the $J = 0$ through $J = 16$ manifolds were obtained from the experimental results of Plyler _et_ _al_. [59], and it was found that calculated correlation functions and spectral densities based on frequencies calculated from theoretical formulae [40] which do not include splitting of the lines from $|J\Gamma_s M\rangle$ for different Γ_s were essentially identical to those based on the exact experimental frequencies. Since the experimental frequencies were known only to $J = 16$, we have used calculated frequencies for lines originating in the $J = 17$ through $J = 25$ rotational levels. As we found in Chapter II (see Fig. 2) the spectral band shapes and reorientational correlation functions computed as superpositions of the functions for A, E and F nuclear spin isomers, were virtually indistinguishable from the band shapes and correlation functions calculated by allowing "collisions" to bring about nuclear spin isomerization as well as rotational state transitions. The results for ν_3 reported below are from calculations in which the transition frequencies involving the rotational states of all symmetry species are included in a single computation, rather than separate calculations, each including only the transitions arising from rotation levels of a single symmetry.

The free rotor memory function for the ν_3 band of CH_4 is shown in Fig. 9. It is to be noted that this free rotor memory function is complex because the transition frequencies and intensities are not symmetrically disposed about the frequency of the band center and that the real part of the memory function closely resembles the classical free rotor memory function for a spherical rotor.[74] The zero of frequency for the transition frequencies $\omega_{J\Gamma_s,f}$ was chosen so that the free rotor correlation function at t = 0, $G_{J:FR}^{(1)}(0)$, was real and equal to unity as required by Eq. (III-1). The free rotor correlation function, $G_{J:FR}^{(1)}(t)$, which is also complex, is also shown in Fig. 9.

The J-diffusion reorientational correlation functions $G_J^{(1)}(t)$ at 295K for various values of the angular momentum correlation time, τ_J, shown in Fig. 10 were calculated from $K_{FR}(t)$ using Eqs. (III-53) - (III-59).

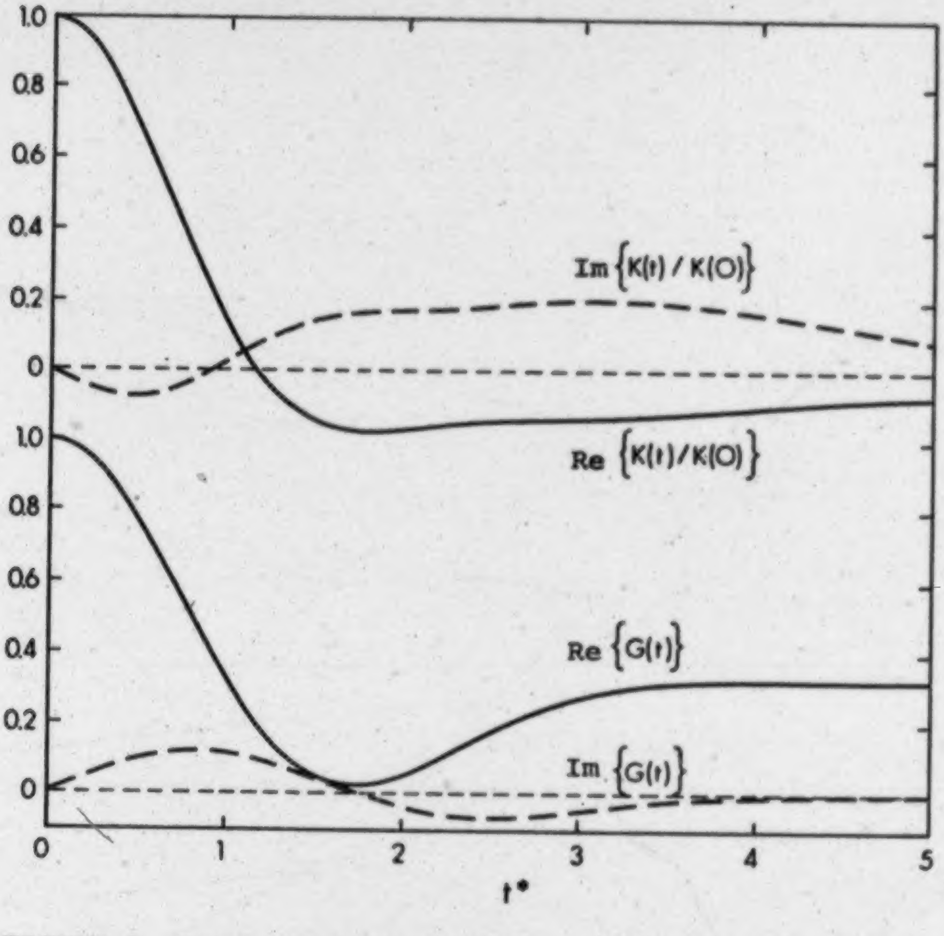

FIGURE 9. Free rotor correlation and memory functions for the ν_3 band of CH_4 at 295K. Time scale is in reduced units of $t(kT/I)^{\frac{1}{2}} = 8.7 \times 10^{12}t$. $K(0) = 1.95$.

FIGURE 10

J-Diffusion reorientational correlation functions $G_J^{(1)}(t)$ for the ν_3 band of CH_4 at 295K for various values of τ_J.

—— $-\mathrm{Re}\{G_J^{(1)}(t)\}$, -----$\mathrm{Im}\{G_J^{(1)}(t)\}$. For clarity, successive correlation functions have been displayed vertically by 0.2 units. Time is in reduced units as in Fig. 9.

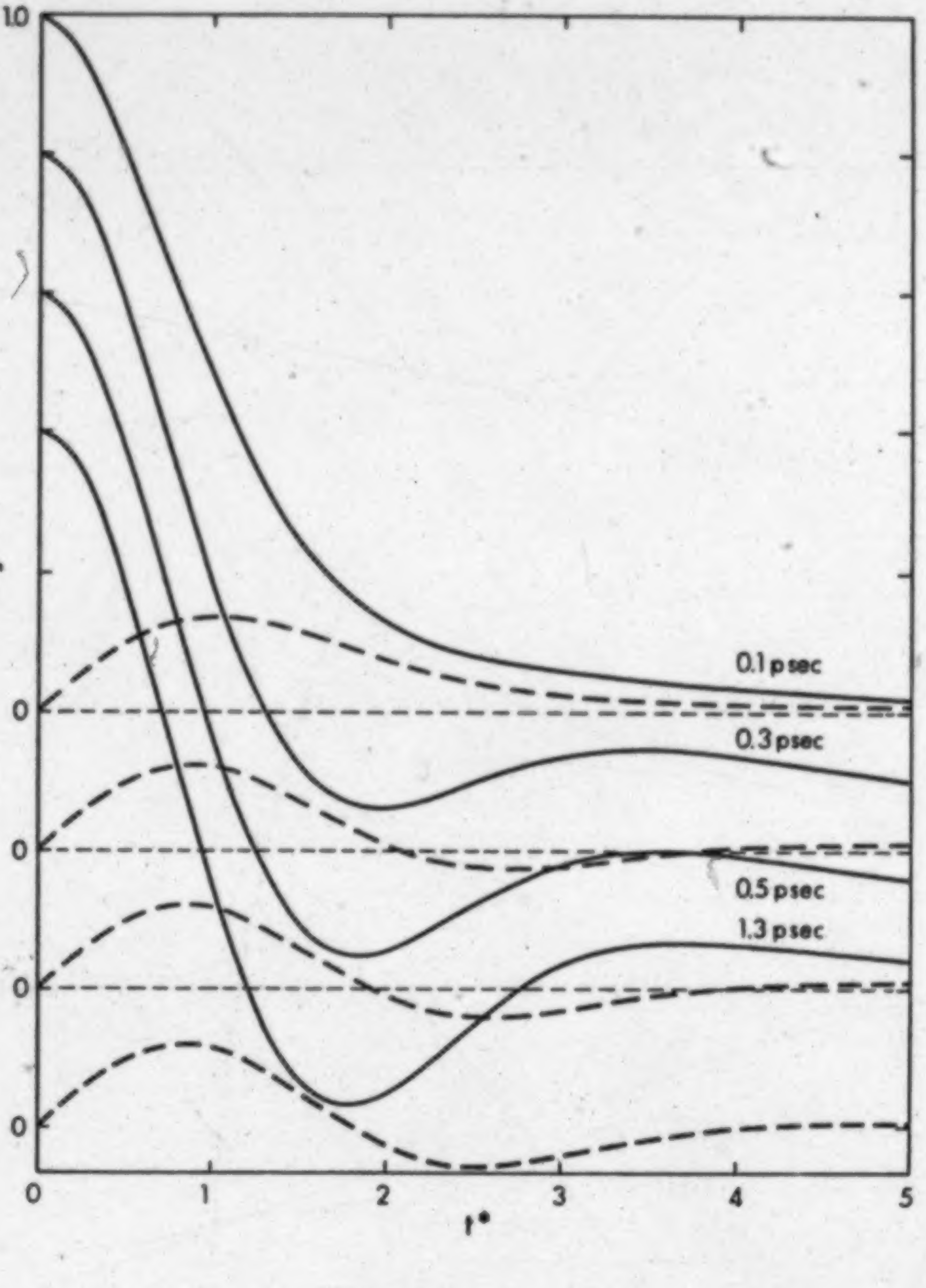
1.0
0
0
0
0
$G_J^{(1)}(t^*)$
0.1 psec
0.3 psec
0.5 psec
1.3 psec
0
1
2
3
4
5
t*

The spectral densities $I_J(\omega)$ at 295K for the same values of τ_J are shown in Fig. 11.

The spectral densities $I_M(\omega)$ at 295K, for various values of the angular momentum correlation time τ_J, in the M-diffusion limit were calculated using Eqs. (III-46) - (III-48) and are shown in Fig. 12. The corresponding reorientational correlation functions $G_M^{(1)}(t)$ were obtained by Fourier transformation of the spectral densities and are given in Fig. 13.

b. ν_4 Band

Coriolis coupling is very significant in the ν_4 band of methane, and the splitting of the lines within a given branch arising from molecules with ground rotational states $|J\Gamma_s M\rangle$ within a given J-manifold is very large, often large enough that the lines from different J-manifolds are interspersed.[72] The frequencies of the lines in the ν_4 branch were calculated from the formulas given by Moret-Bailly [71,73,75], although the off-diagonal elements of the vibration-rotation coupling were neglected. The frequencies calculated in this way compare well with the observed frequencies.[73] In the calculations reported below, all transitions arising from the rotational levels with J = 0 to J = 21 have been included. In calculations of the ν_4 spectral densities or reorientational correlation functions, we calculated the function for each of

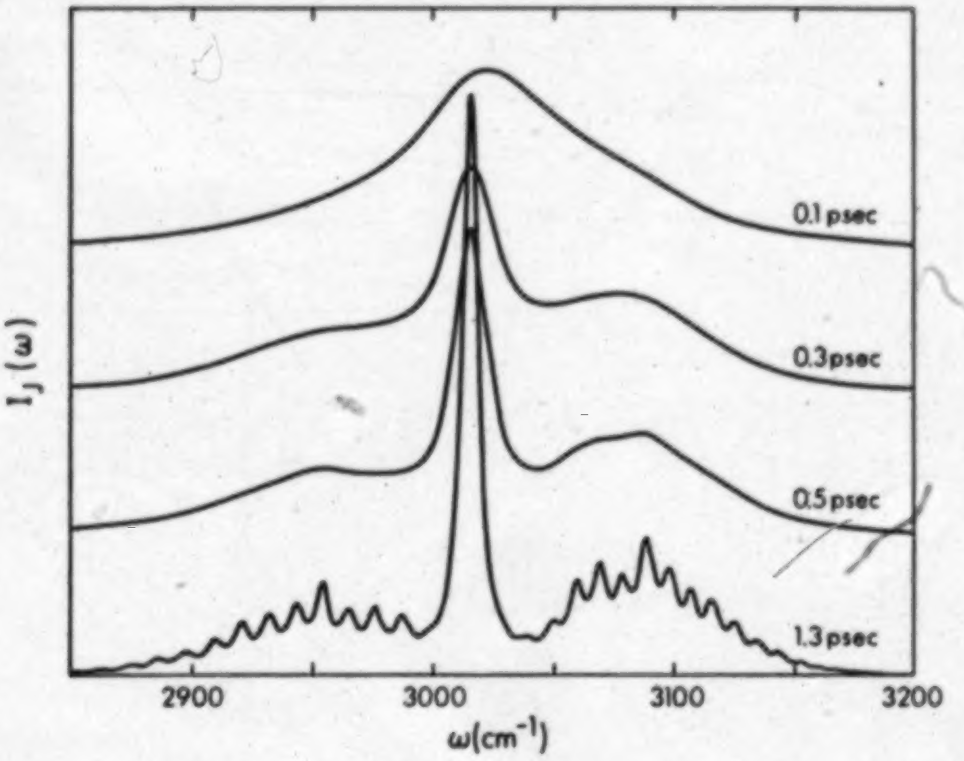

FIGURE 11. J-Diffusion spectral band shapes $I_J(\omega)$ for the ν_3 band of CH_4 at 295K for various values of τ_J. Intensities are normalized so that the integrated intensity is constant for all values of τ_J.

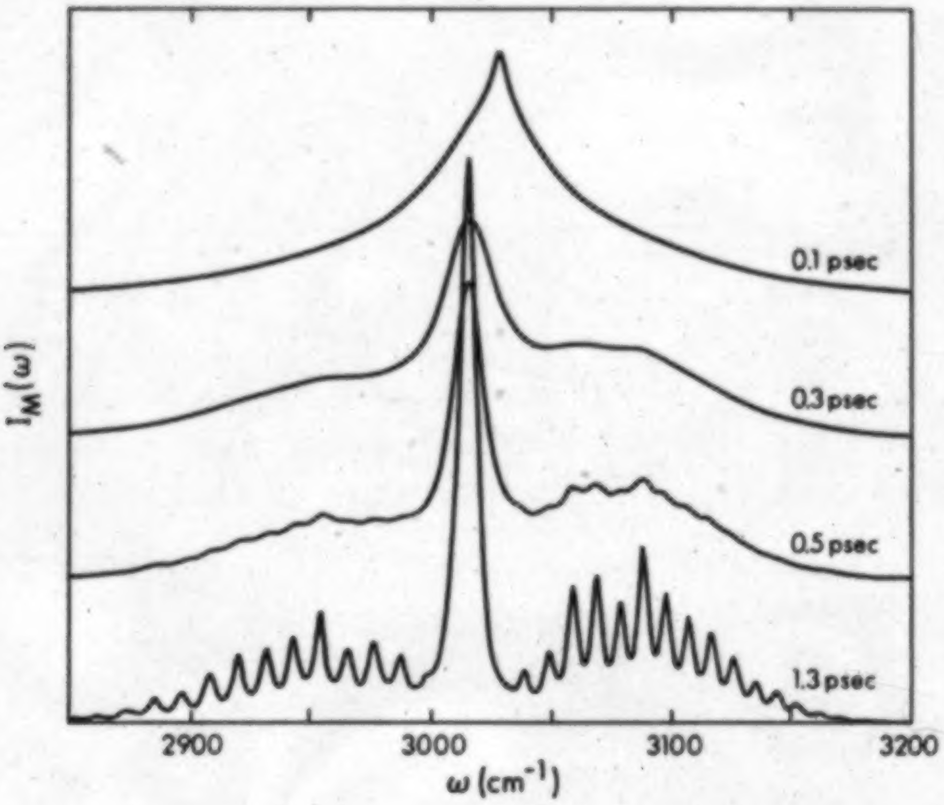

FIGURE 12. M-Diffusion spectral band shapes $I_M(\omega)$ for the ν_3 band of CH_4 at 295K for various values of τ_J. Intensities are normalized so that the integrated intensity is constant for all values of τ_J.

FIGURE 13

M-Diffusion reorientational correlation functions $G_M^{(1)}(t)$ for the ν_3 band of CH_4 at 295K for various values of τ_J.

—— $-\mathrm{Re}\{G_M^{(1)}(t)\}$, ----- $-\mathrm{Im}\{G_M^{(1)}(t)\}$. For clarity, successive correlation functions have been displayed vertically by 0.2 units. Time is in reduced units as in Fig. 9.

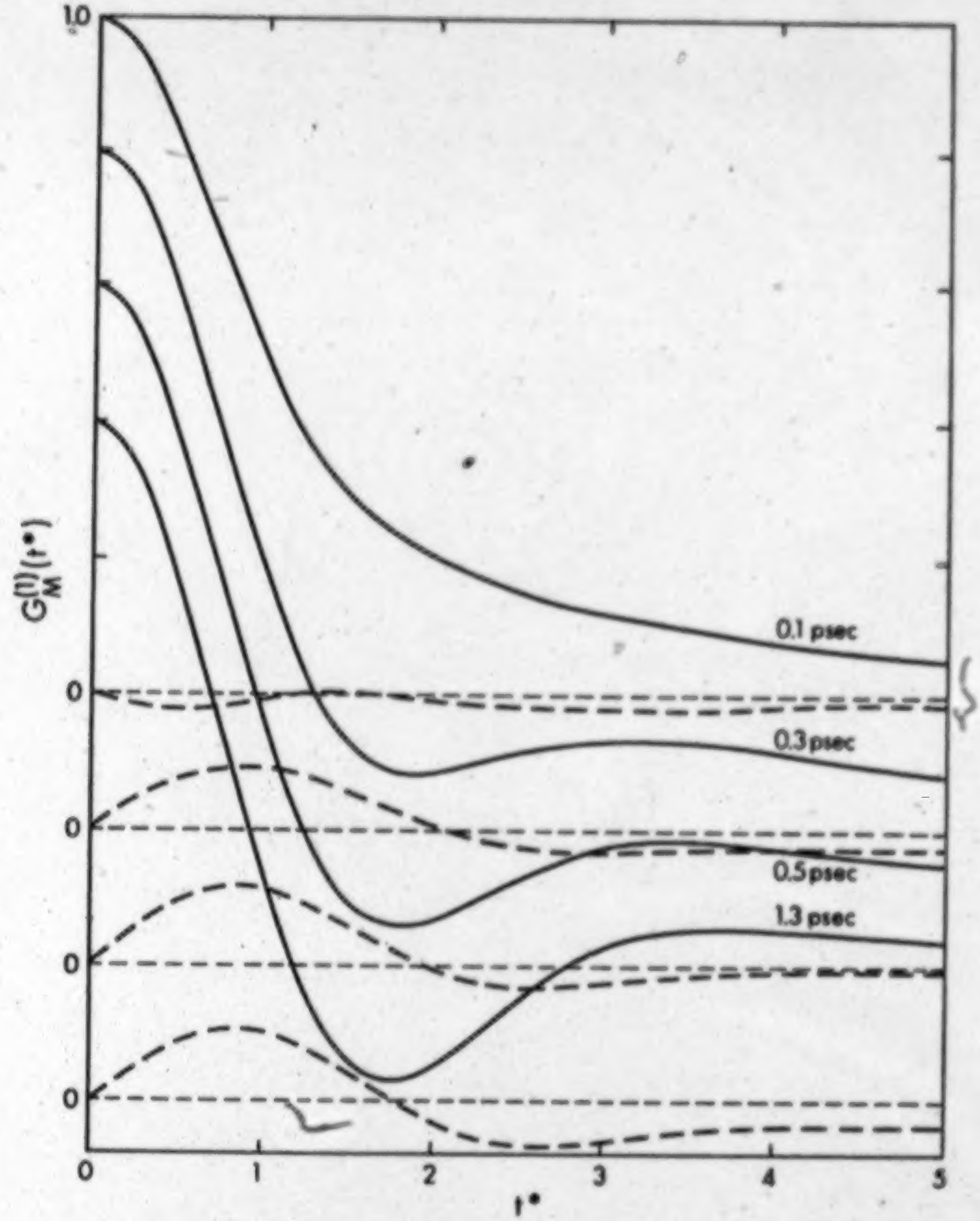
1.0
0
0
0
0
$G_M^{(1)}(t^*)$
0.1 psec
0.3 psec
0.5 psec
1.3 psec
0
1
2
3
4
5
t^*

the nuclear spin isomers and computed the composite function as a weighted average with weightings A:E:T = 5:2:9. Calculations of ν_4 spectral densities and correlation functions based on average transition frequencies (the method employed in section III-D-1-a and in section II-C-2 for the ν_3 band) gave results which were significantly different from those obtained in calculations based on all of the accurately known transition frequencies for each nuclear spin isomer as described above. These spectral densities are compared in Fig. 14 for τ_J = 0.3, 0.5 and 1.3 picoseconds.

The free rotor correlation function and memory function for the ν_4 band of meta-CH_4 (A symmetry) at 295K are shown in Fig. 15. The corresponding functions for ortho- and para-CH_4 closely resemble those for meta-CH_4 at short times, but differ significantly at long times. This is not too surprising since the wings of the spectra for the three nuclear spin isomers are very similar, but the spectral intensities near the band centers of each isomer are quite different. Since the time-dependence of the correlation function at short times reflects the intensity in the wings of the spectrum, and the long-time behaviour reflects the intensities near the band center, one would expect significant differences in the free rotor correlation and memory functions of the different nuclear spin

FIGURE 14

J-Diffusion spectral band shape $I_J(\omega)$ for the ν_4 band of CH_4 at 297K.

All transition frequencies considered———; average transition frequencies considered -----; τ_J as indicated.

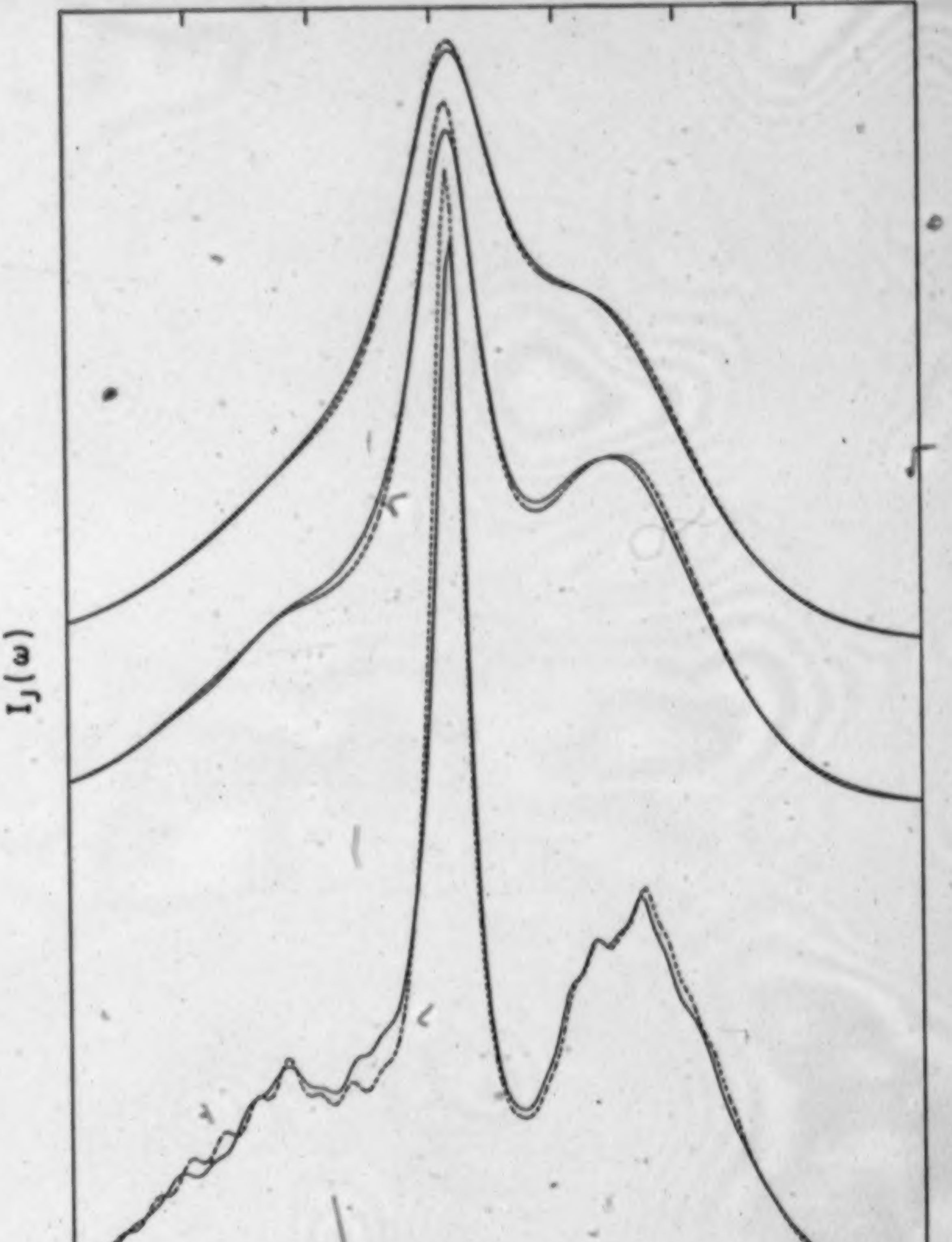

$I_J(\omega)$
1225
1300
1400
$\omega(cm^{-1})$

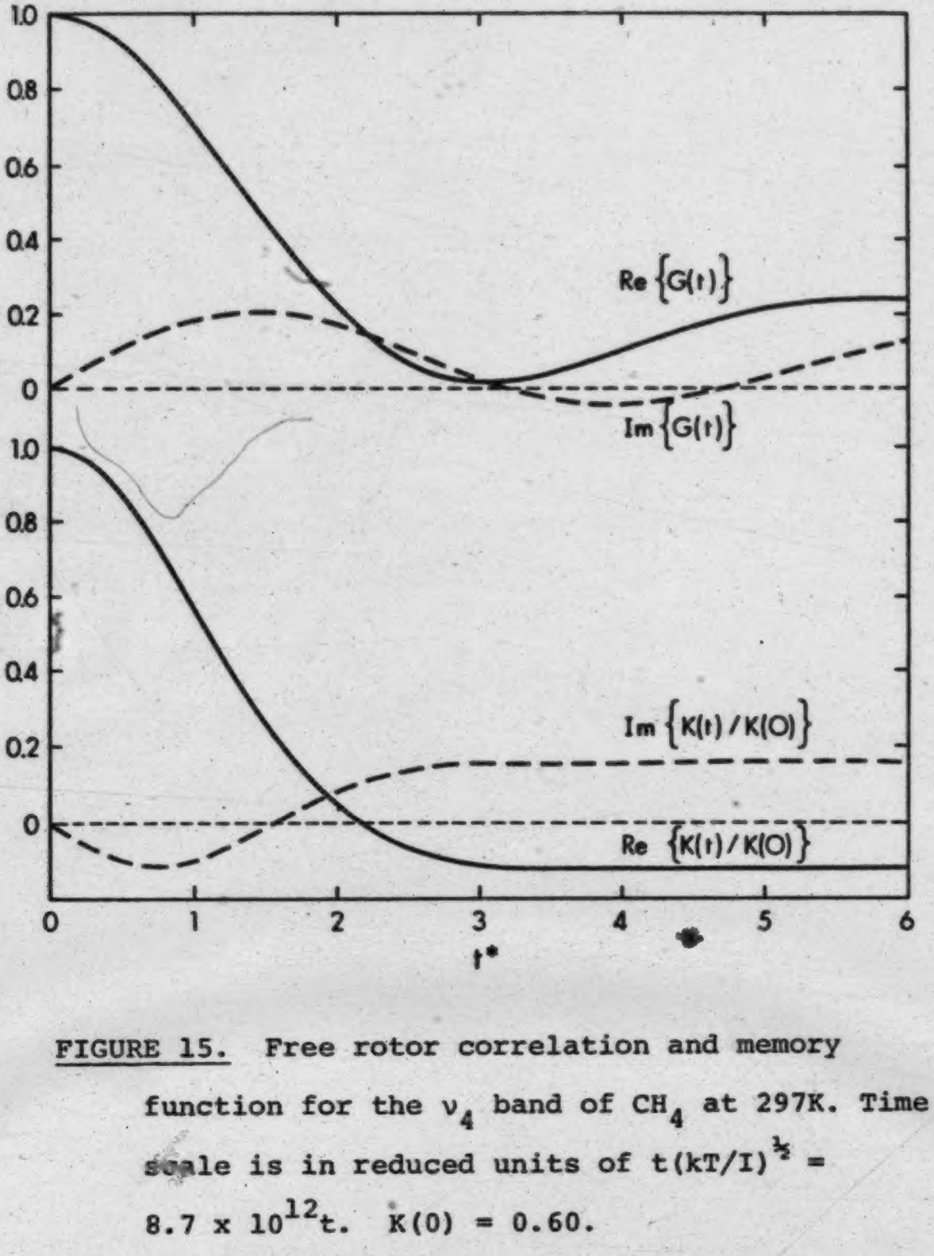

FIGURE 15. Free rotor correlation and memory function for the ν_4 band of CH_4 at 297K. Time scale is in reduced units of $t(kT/I)^{\frac{1}{2}}$ = $8.7 \times 10^{12}t$. $K(0) = 0.60$.

isomers only at long times.

The J-diffusion reorientational correlation functions $G_J^{(1)}(t)$ at 297K, for various values of the angular momentum correlation time τ_J shown in Fig. 16 were calculated from the correlation functions for each of the nuclear spin isomers, which were in turn calculated from the corresponding memory functions. The spectral densities $I_J(\omega)$, at 295K, for the same values of τ_J are shown in Fig. 17.

The spectral densities, $I_M(\omega)$, in the M-diffusion limit, for various values of the angular momentum correlation time τ_J were calculated from the spectral densities for each nuclear spin isomer, which were calculated using Eqs. (III-46) - (III-48) and are shown in Fig. 18. The corresponding reorientational correlation functions, $G_M^{(1)}(t)$, were obtained by Fourier transformation of the spectral densities and are shown in Fig. 19.

2. Comparison with Experiment

In order to fit observed band contours of CH_4 in dense gas solutions [39] with those calculated from the semiclassical M- and J-diffusion models, we have normalized observed and calculated spectra so that they have the same integrated intensity (area normalization). The value of the single variable parameter of the models, τ_J, was varied until the agreement between the

FIGURE 16

J-Diffusion reorientational correlation functions $G_J^{(1)}(t)$ for the ν_4 band of CH_4 at 297K for various values of τ_J.

——— $-\mathrm{Re}\{G_J^{(1)}(t)\}$, ----- $-\mathrm{Im}\{G_J^{(1)}(t)\}$. For clarity, successive correlation functions have been displaced vertically by 0.2 units. Time is in reduced units as in Fig. 15.

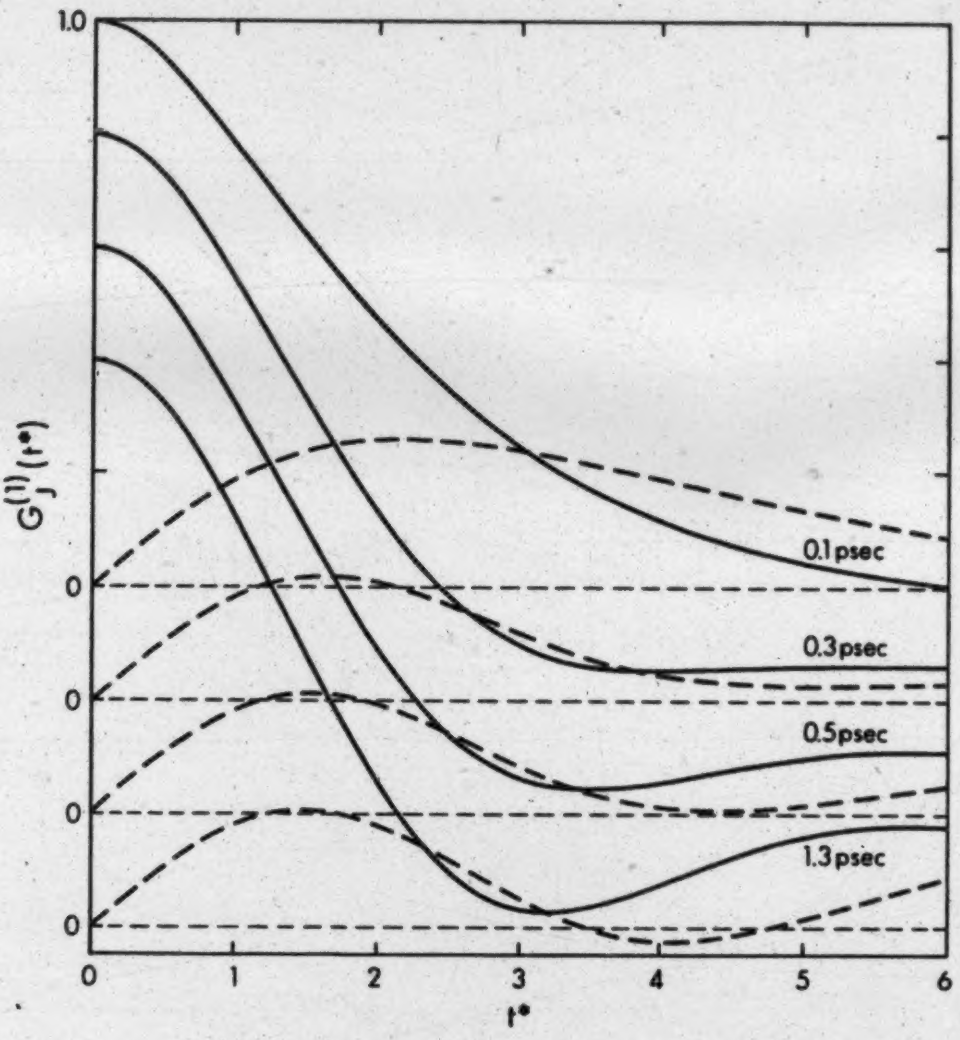
1.0
0
0
0
0
$G_J^{(1)}(t^*)$
0.1psec
0.3psec
0.5psec
1.3psec
0
1
2
3
4
5
6
t^*

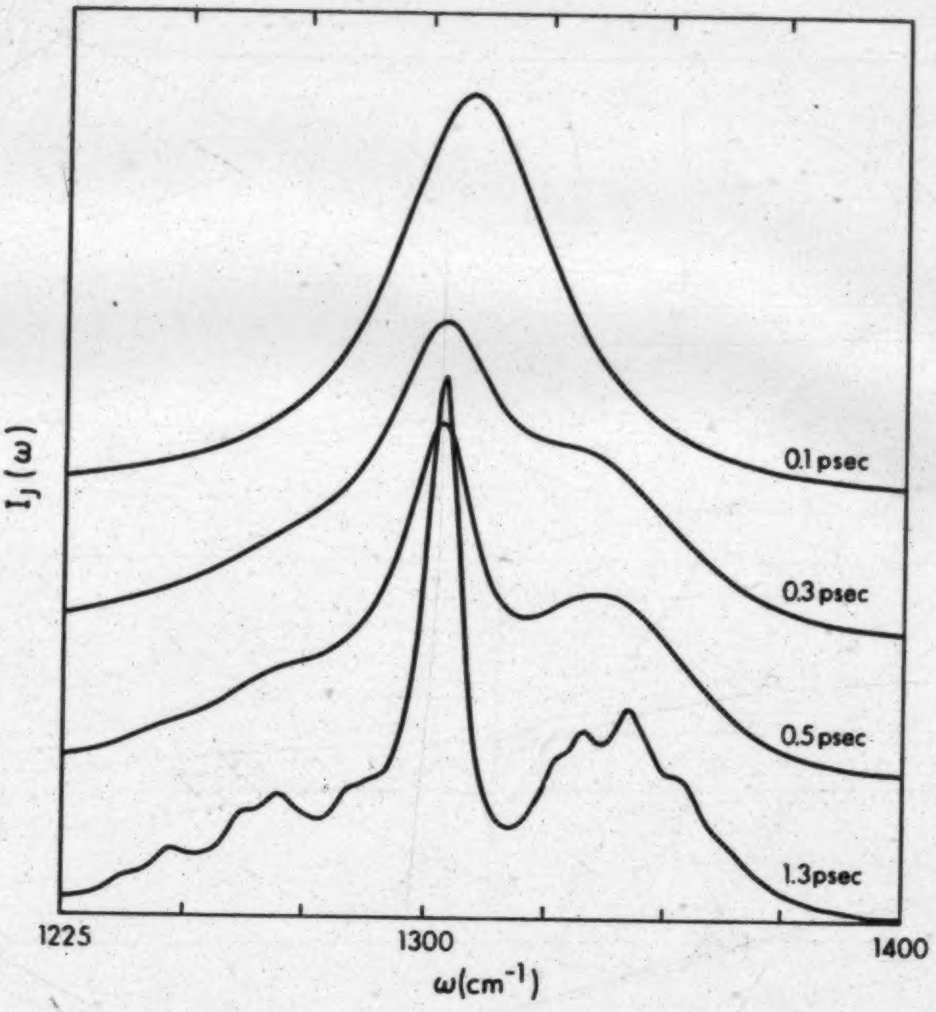

FIGURE 17. J-Diffusion spectral band shapes $I_J(\omega)$ for the ν_4 band of CH_4 at 297K for various values of τ_J. Intensities are normalized so that the integrated intensity is constant for all values of τ_J.

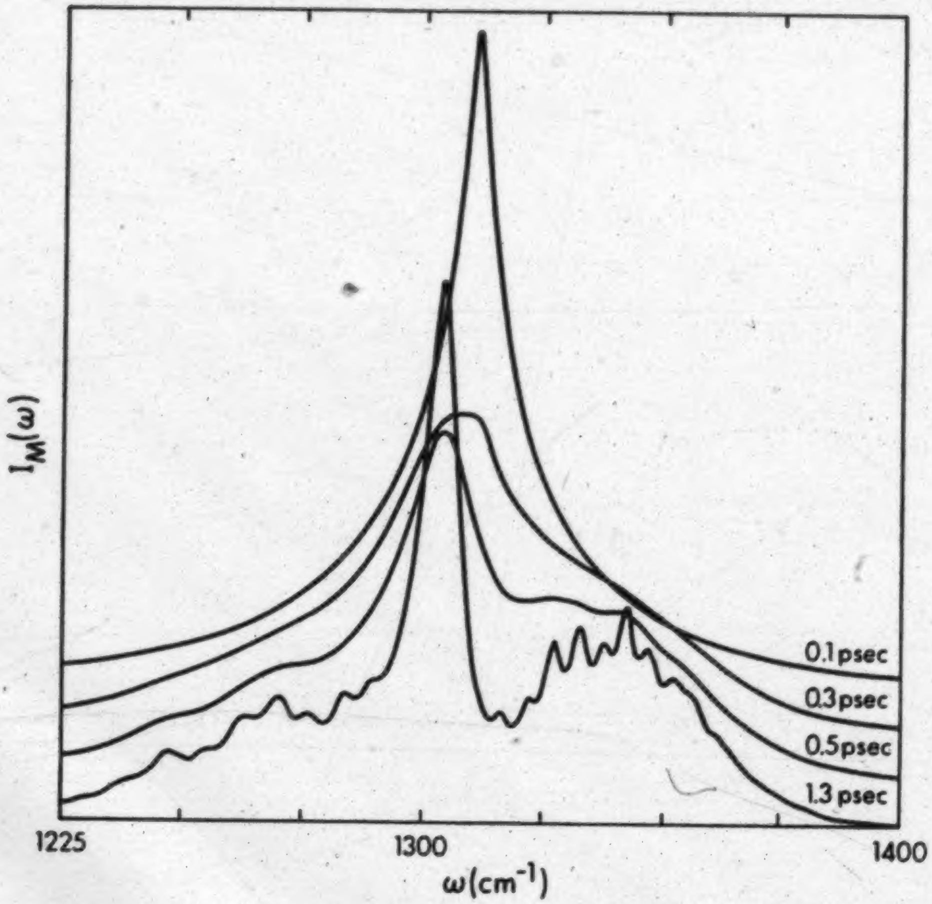

FIGURE 18. M-Diffusion spectral band shapes $I_M(\omega)$ for the ν_4 band of CH_4 at 297K for various values of τ_J. Intensities are normalized so that the integrated intensity is constant for all values of τ_J.

FIGURE 19

M-Diffusion reorientational correlation functions $G_M^{(1)}(t)$ for the ν_3 band of CH_4 at 297K for various values of τ_J.

——— - $\mathrm{Re}\{G_M^{(1)}(t)\}$, ----- $-\mathrm{Im}\{G_M^{(1)}(t)\}$. For clarity, successive correlation functions have been displaced vertically by 0.2 units. Time is in reduced units as in Fig. 15.

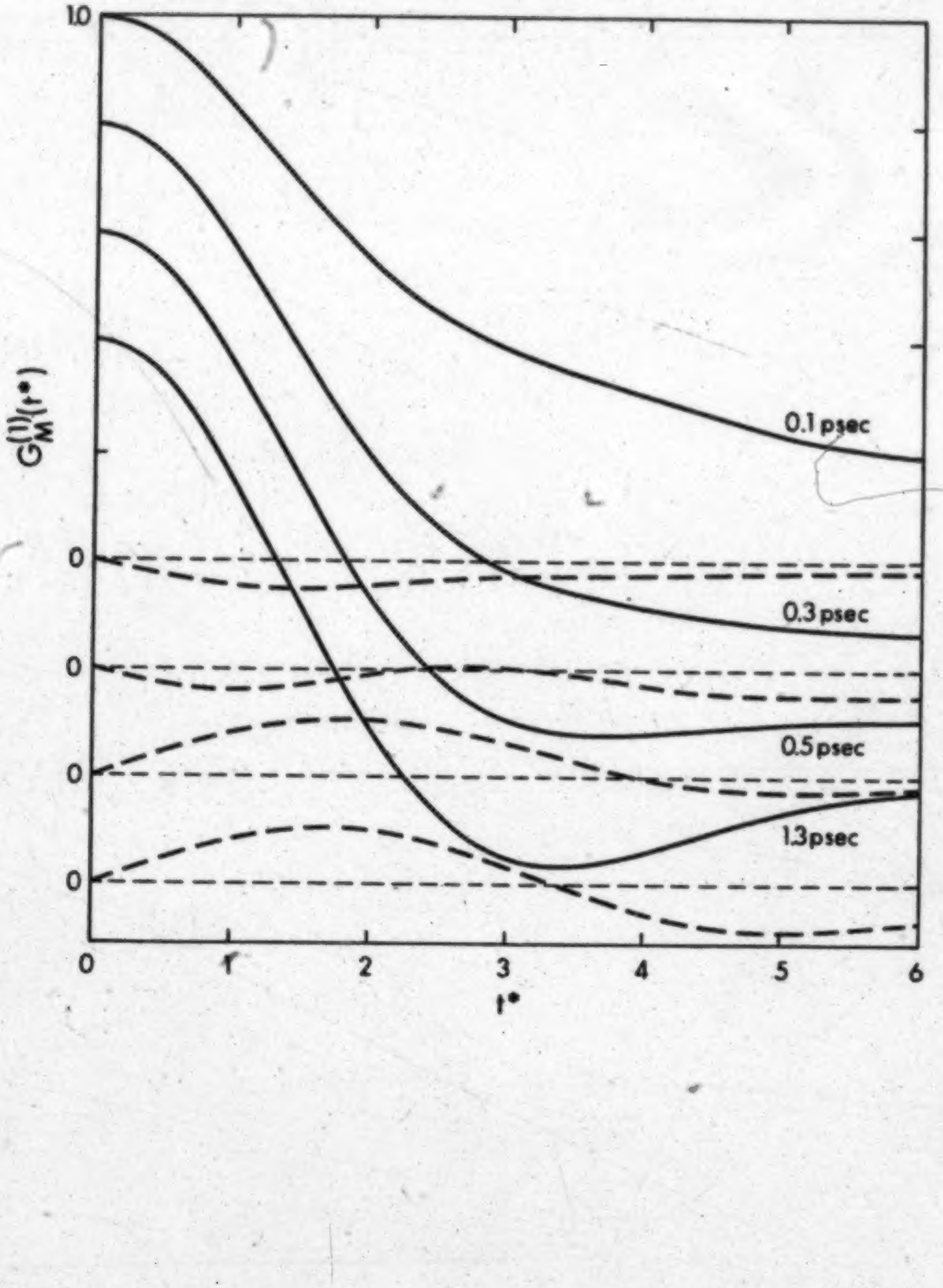
1.0
0
0
0
0
G_M^(1)(t*)
0.1 psec
0.3 psec
0.5 psec
1.3 psec
0
1
2
3
4
5
6
t*

calculated and observed spectral densities was satisfactory as judged by visual comparison. Representative comparisons of calculated and observed ν_3 band contours are shown in Fig. 20, while representative comparisons for the ν_4 band contours are given in Fig. 21. The band shapes calculated with the M-diffusion model were incompatible with those observed in the low pressure CH_4/He mixtures because the intensity of the Q-branch was too low (relative to the P- and R-branches) in the calculated spectra for values of τ_J where the broadening of the rotational structure in the P- and R-branches of calculated and observed spectra were comparable. At higher pressures, however, the band shapes calculated with the M-diffusion model, with suitable values of τ_J, agreed with the observed band contours as well as the band shapes calculated with the J-diffusion model did. The spectra shown in Figs. 20 and 21 are compared with band shapes calculated with the J-diffusion model, since this model appears to be more compatible with the observed spectra over the complete range of pressures.

The calculated band shapes discussed above have been compared to experimental spectra assuming that the experiments were performed under conditions in which instrumental effects on the band shapes were insignificant. As pointed out in Chapter II, the convolution of a 4.5 cm^{-1} triangular slit function with

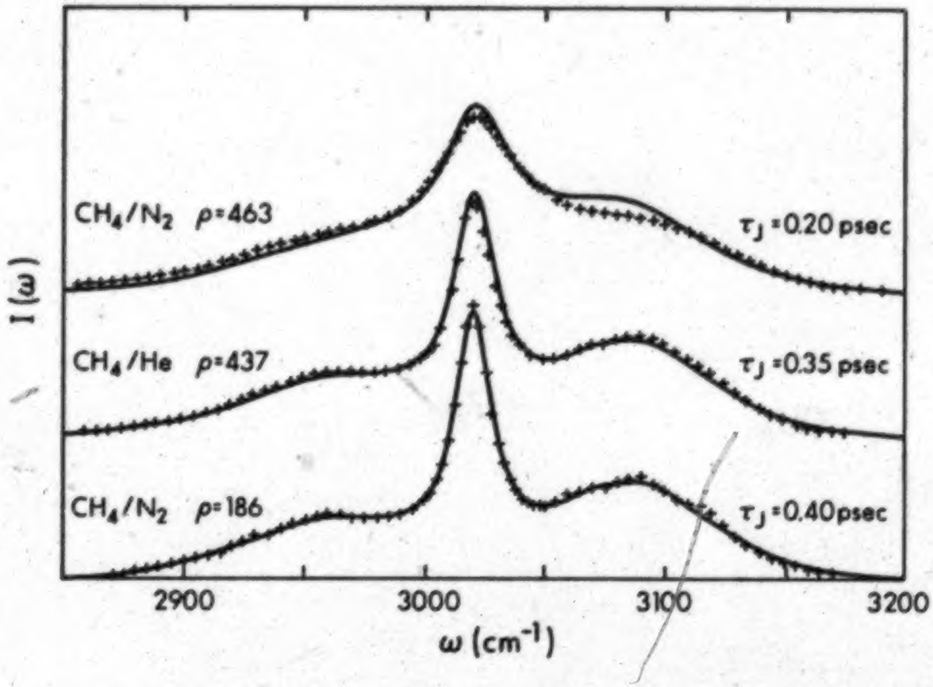

FIGURE 20. Comparison of observed band shapes for the ν_3 band of CH_4 in dense gas mixtures at 295K and band shapes computed with the J-diffusion model. The intensities are normalized as in Fig. 18 and the indicated densities, ρ, are in amagats. ——— calculated, +++++ observed.

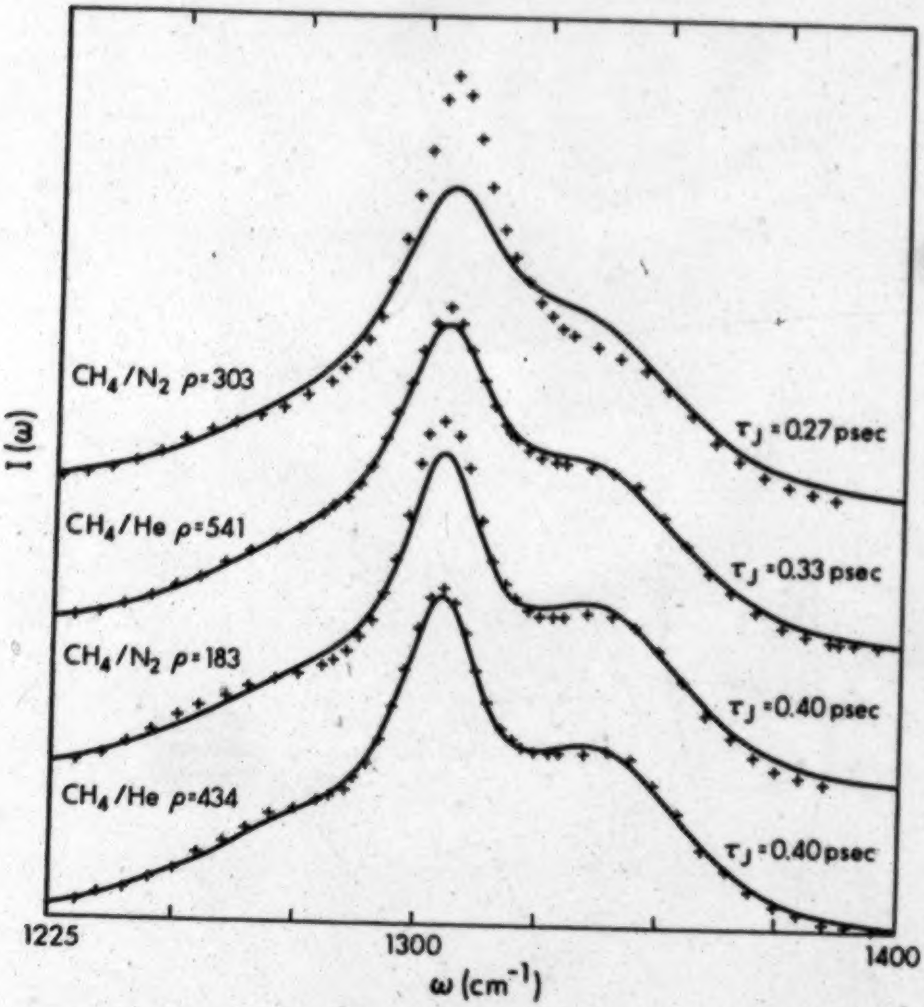

FIGURE 21. Comparison of observed band shapes for the ν_4 band of CH_4 in dense gas mixtures at 297K and band shapes computed with the J-diffusion model. The densities are in amagats and the band shapes are area normalized as in Fig. 18.

——— calculated, +++++ observed.

calculated band shapes produced significant effects on the band contours for the low pressure mixtures only. It may be that the apparent incompatibility of the M-diffusion model with low pressure CH_4/He mixtures is due only to our neglect of instrumental contributions to the band shapes. Because the effects of the slit function on the band shape are of the same order of magnitude as the effects of collisional broadening in this low pressure region, and because the exact nature of the slit function is not known, the angular momentum correlation time obtained in our J-diffusion analysis of these cases has a large uncertainty.

The values of τ_J which gave the best agreement between observed[39] and calculated spectral densities and reorientational correlation functions for the ν_3 and ν_4 bands of CH_4 in a large number of fluid media are given in Table 2. Since the quality of the fits of observed spectra with those calculated with the M-diffusion and with the J-diffusion model was not significantly different except at low pressures, we have included the values of τ_J which gave the best fits in each model. The values of τ_J obtained by fitting the ν_3 data are not significantly different from those obtained in Chapter II.

It should be noted that the agreement between the calculated and observed ν_3 band contours of CH_4, parti-

TABLE 2

Correlation Times Assigned Using the Semiclassical J-diffusion (SCF) and Semiclassical M-diffusion (SCM) Models.[a]

System	Band	Temperature (°K)	Density (amagats)	τ_J psec (SCF)	τ_J psec (SCM)
CH_4/He	ν_3	295	96	1.3	b
			437	0.35	0.35
			544	0.30	0.30
			745	0.20	0.20
	ν_4	297	110	1.1	b
			134	1.0	b
			156	0.90	0.80
			178	0.80	0.80
			200	0.78	0.80
			208	0.70	0.75
			222	0.73	0.78
			242	0.65	0.75
			250	0.60	0.65
			290	0.55	0.60
			328	0.50	0.58
			365	0.48	0.53
			434	0.40	0.48
			491	0.35	0.45
			541	0.33	0.43
			588	0.30	0.38
			682	0.25	0.35
			687	0.28	0.35
			747	0.23	0.33
CH_4/N_2	ν_3	295	186	0.40	0.45
			243	0.33	0.35

(continued....)

TABLE 2 (continued)

System	Band	Temperature (°K)	Density (amagats)	τ_J psec (SCF)	τ_J psec (SCM)
CH_4/N_2	ν_3	295	308	0.28	0.28
			463	0.28	0.23
	ν_4	297	82	0.65	0.70
			93	0.65	0.70
			104	0.60	0.65
			114	0.58	0.65
			138	0.50	0.58
			161	0.45	0.53
			183	0.40	0.45
			203	0.35	0.44
			222	0.33	0.38
			239	0.30	0.36
			276	0.30	0.35
			303	0.28	0.33
CH_4Ar	ν_3	295	281	0.33	0.35

[a] Estimated error in value of τ_J is ± 0.05 psec.

[b] No satisfactory fit with M-diffusion model.

cularly in the wings of the spectrum is better than the agreement between the observed ν_3 band contours and those calculated with the semiclassical model of Chapter II (see Fig. 5 and 20). This is due, in large part, to the inclusion of all lines arising from rotational manifolds with J = 0 to J = 25 in the calculations reported in the present work, while computational efficiency demanded that our previous calculations included only those transitions arising from the J = 0 to J = 12 manifolds.

We have also compared the correlation functions calculated by Fourier transforming the observed band contours [39] with the correlation functions calculated from the M- and J-diffusion models. In making such comparisons, one must be careful to choose the zero of frequency for the Fourier transformation of the spectral densities in a consistent manner, since the correlation functions are complex functions and the relative magnitudes of the real and imaginary parts will depend on the choice the zero of frequency. In numerical Fourier transformation of experimental band shapes, it is most convenient to choose the frequency at maximum spectral intensity as the zero of frequency. However, in calculating the J-diffusion correlation functions using the memory function technique described in section III-C above, one requires that the correlation function be real and equal to unity at t = 0, and that the time-derivative of the correlation function be zero at t = 0. This implies that the zero of frequency in the calculated spectrum is equal to the first moment, M(1), of the spectrum. It has been shown [76,77,78] that the true band origin ω_o is given by

$$\omega_o = M(1) - 2\bar{B}, \qquad \text{(III-63)}$$

where $\bar{B}$ is the rotation constant of the molecule. This band origin lies closer to the frequency of maximum intensity than does M(1), therefore choosing ω_o as the zero of frequency is more nearly in keeping with choosing the frequency of maximum intensity as zero frequency which is the common practice.[7,10,11,25,38,39] We have chosen therefore to compare the correlation functions obtained by Fourier transformation of observed band contours with ω_o as the zero of frequency with calculated correlation functions rephased to this frequency origin. Since the M-diffusion correlation functions were computed by Fourier transformation of the calculated spectral densities, the choice of the frequency origin was made in the same manner as that for the correlation functions calculated from experimental spectral densities.

The comparison of calculated correlation functions and Fourier transforms of observed ν_3 band contours gave essentially the same values of τ_J as comparisons of calculated and observed band shapes. Unfortunately the points in the digitized ν_4 spectra of CH_4 available [39] were too distantly spaced for computation of meaningful Fourier transforms. We have therefore not attempted to compare calculated and experimental correlation functions for the ν_4 band.

E. DISCUSSION

The semiclassical rotational diffusion models proposed in this chapter are similar to, but not identical to, those proposed in Chapter II which were based on Gordon's semiclassical theory.[2,34] If we form the matrix products indicated in Eq. (II-14) we obtain the reorientational correlation function in the form

$$G(t) = \sum_i W_i \exp[\lambda_i t] \qquad \text{(III-64)}$$

where $\underset{\sim}{\lambda}$ is a diagonal matrix containing the eigenvalues of the matrix $-\underset{\sim}{\Pi} + i\underset{\sim}{\omega}_o$ as defined in Eq. (II-16), the weights, W_i, are given by

$$W_i = \left(\sum_j d_j S_{ji}\right)\left(\sum_\ell (S^{-1})_{i\ell} P_{\ell\ell} d_\ell\right) \qquad \text{(III-65)}$$

and the columns of $\underset{\sim}{S}$ are the eigenvectors of $-\underset{\sim}{\Pi} + i\underset{\sim}{\omega}_{o}$. It is clear from Eq. (III-64) and (II-15) that the reorientational correlation function is a superposition of exponential functions with complex arguments, and that the spectral density is a superposition of Lorentz functions centred at frequencies given by the imaginary part of $\underset{\sim}{\lambda}$, with widths given by the real part of $\underset{\sim}{\lambda}$.[55]

The reorientational correlation functions in the present models appear, at the outset, to be significantly different in form from those of the previous models. However, if one employs the Laplace transform relation in Eq. (III-31) using the free rotor expressions Eqs. (III-38) or (III-46), one can easily show that the Laplace transforms of the correlation functions in the J- and M-diffusion limits are respectively

$$\bar{G}_J(s) = \frac{\sum_{\ell} P_{\ell\ell} d_{\ell}^2 \prod_{\ell' \neq \ell} [(\frac{1}{\tau_J} - i\omega_{\ell'}) + s]}{\sum_{k} P_{kk} d_{k}^2 [-i\omega_k + s] \prod_{k' \neq k} [(\frac{1}{\tau_J} - i\omega_{k'}) + s]} , \tag{III-66}$$

and

$$\bar{G}_M(s) = \sum_{J} \rho_J \frac{\sum_{\ell} P_{\ell\ell}^J (d_{\ell})^2 \prod_{\ell' \neq \ell} [(\frac{1}{\tau_J} - i\omega_{\ell}') + s]}{\sum_{k} P_{kk}^J (d_{k})^2 [-i\omega_k + s] \prod_{k' \neq k} [(\frac{1}{\tau_J} - i\omega_{k'}) + s]} , \tag{III-67}$$

where the indices k and ℓ in Eq. (III-66) represent the collection of labels $\left\{J,K,M,k,f,m\right\}$ in Eq.(III-38), and these indices in Eq. (III-67) represent the collection $\left\{K,M,k,f,m\right\}$ in Eq. (III-46);

$$P_{\ell\ell} = P_{JKM} \quad , \tag{III-68}$$

$$d_{\ell} = \left\langle \Lambda ; JKM \right| \mathcal{D}^{(1)}_{mk} [\Omega(0)] \left| f \right\rangle \quad , \tag{III-69}$$

and

$$P^{J}_{\ell\ell} = P^{J}_{KM} \quad . \tag{III-70}$$

The sums over k and ℓ in Eq. (III-67) are restricted to transitions associated with a particular J-manifold. Since the Laplace transforms given in Eqs. (III-66) and (III-67) are of the form of ratios f(s)/g(s) of polynomials in the Laplace variable s, with the polynomial g(s) in the denominator being of higher degree than the polynomial f(s) in the numerator, the correlation functions themselves must be sums of exponential functions with arguments $\{\Lambda_r t\}$, with the coefficients Λ_r being the solutions to the characteristic equation g(s) = 0.[79] Thus the correlation functions in our previous and present semiclassical representations of the M- and J-diffusion models can be written as superpositions of exponential functions of t.

In order to investigate the similarities of the two models in greater detail, we have compared the exponential parameters in the two approaches to the M-diffusion limit of the extended rotational diffusion model. It was found that both approaches gave identical exponential parameters if the $\underset{\sim}{\Pi}$- matrix of the previous M-diffusion model were specified by

$$\Pi_{ij} = \begin{cases} (1-d_i^2)/\tau_J & i = j \\ -d_i^2/\tau_J & i \neq j \end{cases} \qquad \text{(III-71)}$$

rather than by Eq. (II-13) as in Chapter II. Numerical comparisons of the weights associated with each of the exponential terms in the M-diffusion correlation functions in the two models indicated that, although the previous approach could be modified to give the same exponential parameters as the present model, the weights of the exponential functions were different in the two approaches, and the differences between them varied significantly with τ_J. A comparison of the weights given by the two models, for several values of τ_J, for the three exponential terms in the J = 1 manifold correlation function for the ν_3 band of CH_4 is given in Table 3.

The identity of the characteristic polynomials, whose roots define the exponential parameters in the correlation functions, in the two versions of the semiclassical M-diffusion model for the case of three spectral lines led us to investigate the characteristic polynomi-

TABLE 3

Comparison of Weights of the Exponential Terms in the Correlation Functions in the Two Semiclassical Approaches to M-diffusion for the $J = 1$ Lines in the ν_3 Band of CH_4

Line i	d_i^2	ω_i $(\text{psec}^{-1})^a$
1	0.55556	1.856
2	0.33333	-1.856
3	0.11111	-3.705

τ_J (psec)	λ_k (psec^{-1})	W_k[Eq. (III-65)]	W_k[Eq. (III-79)]
0.01	$-99.991 - 3.366i$	$-.0395 + .00077i$	$-.0001 + .000004i$
	$-99.963 - 0.341i$	$-.0267 + .00066i$	$-.0004 + .000005i$
	$-0.04604 + 0.00105i$	$1.0663 - .00143i$	$1.0005 - .000009i$
0.1	$-9.915 - 3.384i$	$-.0467 + .01169i$	$-.0079 + .0037i$
	$-9.615 - 0.367i$	$-.0701 + .01355i$	$-.0416 + .0060i$
	$-0.4701 + 0.0458i$	$1.1168 - .02525i$	$1.0495 - .0097i$
10.1	$-0.8960 - 3.675i$	$.0865 + .0701i$	$.0900 + .0569i$
	$-0.6615 - 1.824i$	$.3541 + .0667i$	$.3484 + .0687i$
	$-0.4425 + 1.794i$	$.5614 - .1368i$	$.5617 - .1256i$

(continued)

TABLE 3 (continued)

τ_J (psec)	λ_k (psec^{-1})	W_k[Eq. (III-65)]	W_k[Eq. (III-79)]
100.0	$-0.00889 - 3.705i$	$.1111 + .0008i$	$.1111 + .0006i$
	$-0.00667 - 1.856i$	$.3333 + .0006i$	$.3333 + .0006i$
	$-0.00444 + 1.856i$	$.5556 - .0013i$	$.5556 - .0012i$

---

[a] Zero of frequency chosen as the first moment.

als in both M- and J-diffusion limits of the semiclassical rotational diffusional models when a large number of lines were included. The characteristic equation in the present J-diffusion model is

$$\sum_{k} P_{kk} d_k^{\,2} (s - i\omega_k) \prod_{\ell \neq k} (s + \tau_J^{-1} - i\omega_\ell) = 0 \quad ,$$

(III-72)

and can be rewritten in the determinantal form

$$\begin{vmatrix} P_{11} d_1^2 (s - i\omega_1) & -(s+\tau_J^{-1} - i\omega_1) & -(s+\tau_J^{-1} - i\omega_1) & \cdots & -(s+\tau_J^{-1} - i\omega_1) \\ P_{22} d_2^2 (s - i\omega_2) & (s+\tau_J^{-1} - i\omega_2) & 0 & \cdots & 0 \\ P_{33} d_3^2 (s - i\omega_3) & 0 & (s+\tau_J^{-1} - i\omega_3) & \cdots & 0 \\ \vdots & \vdots & \vdots & \ddots & \vdots \\ P_{nn} d_n^2 (s - i\omega_n) & 0 & 0 & \cdots & (s+\tau_J^{-1} - i\omega_n) \end{vmatrix} = 0$$

(III-73)

Since the value of a determinant is unchanged when a linear combination of any number of columns is added to any given column, one can[80] rearrange the determinant in Eq. (III-73) by adding $-P_{22}d_2^{\,2}$ times column 2, $-P_{33}d_3^{\,2}$

times column 3, ... and $-P_{nn}d_n{}^2$ times column n to column 1 to obtain

$$\begin{vmatrix} s+(1-P_{11}d_1^2)/\tau_J-i\omega_1 & -(s+\tau_J^{-1}-i\omega_1) & -(s+\tau_J^{-1}-i\omega_1) & \cdots & -(s+\tau_J^{-1}-i\omega_1) \\ -P_{22}d_2^2/\tau_J & (s+\tau_J^{-1}-i\omega_2) & 0 & \cdots & 0 \\ -P_{33}d_3^2/\tau_J & 0 & (s+\tau_J^{-1}-i\omega_3) & \cdots & 0 \\ \vdots & \vdots & \vdots & \ddots & \vdots \\ -P_{nn}d_n^2/\tau_J & 0 & 0 & \cdots & (s+\tau_J^{-1}-i\omega_n) \end{vmatrix} = 0 \qquad \text{(III-74}$$

In the derivation of Eq. (III-74) from (III-73) it has been noted that

$$\sum_k P_{kk}d_k^2 = 1 \qquad \text{(III-75)}$$

which is implicit in Eqs. (III-66) and (III-67) also. The determinant in Eq. (III-74) can be modified by adding the first column to each of the other columns to obtain

$$\begin{vmatrix} s + (1-P_{11}d_1^2)/\tau_J - i\omega_1 & -P_{11}d_1^2/\tau_J & \cdots & -P_{11}d_1^2/\ {}_J \\ -P_{22}d_2^2/\tau_J & s + (1-P_{22}d_2^2)/\tau_J - i\omega_2 & \cdots & -P_{22}d_2^2/\tau_J \\ \vdots & \vdots & \ddots & \vdots \\ -P_{nn}d_n^2/\tau_J & -P_{nn}d_n^2/\tau_J & \cdots & s+(1-P_{nn}d_n^2)/\tau_J - i\omega_n \end{vmatrix} = 0$$

(III-76)

which can be written in the form

$$|s\underset{\sim}{1} + \underset{\sim}{\Pi} - i\underset{\sim}{\omega}_o| \quad = \quad |(-\underset{\sim}{\Pi} + i\underset{\sim}{\omega}_o) - s\underset{\sim}{1}| = 0$$

(III-77)

where $\underset{\sim}{1}$ is a unit matrix, $\underset{\sim}{\omega}_o$ is a diagonal matrix containing the frequencies of the transitions, and the matrix $\underset{\sim}{\Pi}$ has elements given by

$$\Pi_{ij} = \begin{cases} (1-P_{ii}d_i^2)/\tau_J & i = j\ , \\ -P_{ii}d_i^2/\tau_J & i \neq j\ . \end{cases}$$

(III-78)

The latter form of Eq. (III-77) is precisely the characteristic equation whose roots are determined in the diagonalization of the matrix $(-\underset{\sim}{\Pi} + i\underset{\sim}{\omega}_o)$. Thus, provided we describe the matrix elements of $\underset{\sim}{\Pi}$ by Eq. (III-78), rather than by Eq. (II-12) of the previous chapter, the characteristic equations of the present model [Eq. (III-72)] and the previous model [Eq. (III-77)] are identical. This implies that the two approaches yield correlation functions which are linear combinations of exponential functions of time [Eq. (III-64)] with the exponential parameters of the two approaches being identical. As pointed out above, the weighting factors of the exponential functions in the correlation function are not identical. The weights W_i in Eq. (III-64) are given by Eq. (III-65) for the matrix diagonalization technique employed previously, and by

$$W_i = \frac{\sum_{\ell} P_{\ell\ell} d_{\ell}^{2} \prod_{\ell' \neq \ell} (\lambda_i + \tau_J^{-1} - i\omega_{\ell'})}{\prod_{k \neq i} (\lambda_i - \lambda_k)} \qquad \text{(III-79)}$$

with the present approach. The weighting factors in Eq. (III-79) reduce to those given in Eq. (III-65) only for large values of τ_J where the off-diagonal elements of $\underset{\sim}{\Pi}$ are negligible. It should be noted that for the case when all lines have identical intrinsic line amplitudes $d_i \equiv 1/\sqrt{3}$, the model proposed in Chapter II will have the same $\underset{\sim}{\Pi}$-matrix as the model given in the present work. In the classical limit, (large rotational quantum numbers) this case is indeed realized.

The major differences between the present theory and that given in Chapter II is the method of describing the "collision" process. In this chapter, we have viewed "collisions" as events which result in transfer of molecules between the available rotational states, while in the previous theory, "collisions" were viewed as events wherein line amplitude was transferred between spectral lines. This concept of transfer of line amplitude between lines has some relevance in a classical interpretation of rotational transitions [2,34], but its relation to transfer of molecules between quantum states is obscured by the fact that molecules in a given state can undergo more than a single transition within the rotation-vibration band of interest. The approach in Chapter II is based on the intuitive assumption that molecules within a given quantum state could be subdivided so that equal numbers of molecules were associated with each of the transitions originating in that quantum state. The present theory does not require such assumptions. Gordon [2,34] has pointed out that the line amplitude transfer approach is expected to describe the time dependence of the correlation functions at long times only. However, with the semiclassical approach presented here, no such limitation is apparent in the mathematical development of the model.

The most important improvement in the semiclassical rotational diffusion models presented here is the simplification of the mathematical description of the correlation functions and spectral densities. The treatment in Chapter II was of limited applicability due to its reliance on the diagonalization of the complex non-Hermitian matrix, $-\underset{\sim}{\Pi} + i\underset{\sim}{\omega}_o$, whose order is equal to the number of spectral lines included in the calculations. This diagonalization procedure becomes prohibitively expensive when a very large number of spectral lines (>40) are included. In the application of the theory in Chapter II to the ν_3 band of CH_4, computation costs required us to limit our consideration to the lines arising from the $J = 0$ to $J = 12$ rotational manifolds, which means that ca. 4% of the methane molecules which occupy higher rotational levels were completely neglected. In spite of this deficiency, which led to significant discrepancies between calculated and observed spectral densities in the wings of the band, we were able to obtain satisfactory agreement between theory and experiment. The application of the previous theory to the ν_4 band of CH_4 was impractical since one must include a much larger number of transitions in these calculations. With the present theory, no matrix diagonalization is required since the results are derived from a free rotor memory function which is in turn derived from a free rotor correlation function, or from the Laplace transform of the free rotor correlation function. We have therefore been able to apply the models to the calculation of the ν_4 band of CH_4 where 363 transitions are included for ortho-CH_4, 120 for para-CH_4 and 121 for meta-CH_4.

The angular momentum correlation times, τ_J, obtained from comparisons of calculated J-diffusion and observed ν_3 and ν_4 band shapes of CH_4 in dense gas mixtures, given in Table 2, are plotted against gas density in Fig. 22. The values obtained from analysis of the ν_3 and ν_4 bands do not differ significantly, and as was the case in Chapter II (see Fig. 6), the values are comparable to those obtained by analysis of nuclear relaxation times in high pressure gaseous methane.[56] It is felt therefore that the parameter τ_J is indeed a measure of the time interval during which the rotational state of the molecules remains fixed. The τ_J^{-1} vs. ρ plots in Fig. 22 appear to have non-zero intercepts. This can be attributed to our neglect of instrumental broadening since the values of τ_J which we obtained by comparing calculated and observed band shapes would be lower than the "true" τ_J values in the low density mixtures where instrumental effects could contribute significantly to the band shape.

It has been found in the analysis of spectral band shapes [7,22-28] and nuclear relaxation times, [28-33] that the classical extended rotational diffusion models account for a very large number of observations and are of

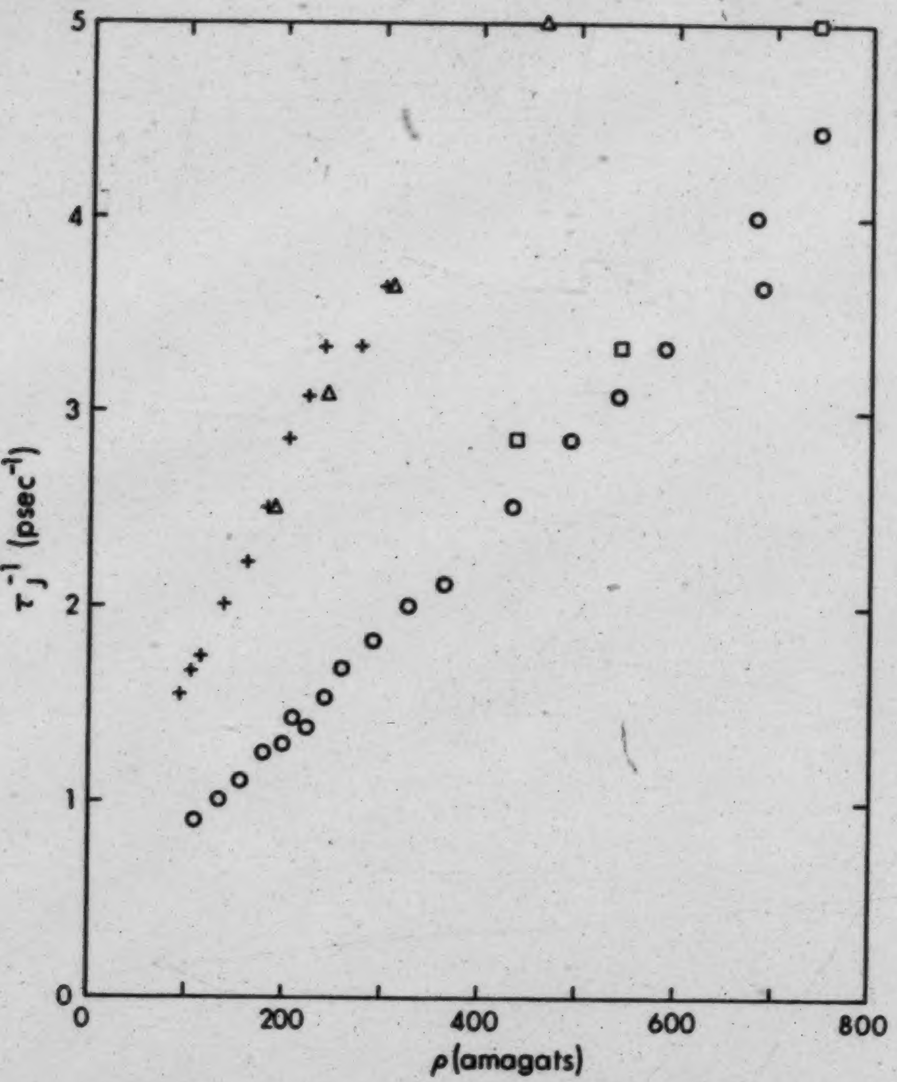

FIGURE 22. Density dependence of τ_J^{-1}. □ - CH_4/He at 295K from ν_3, O - CH_4/He at 297K from ν_4, Δ - CH_4/N_2 at 295K from ν_3, + - CH_4/He at 297K from ν_4. All values of τ_J are taken from comparison of observed band shapes with those calculated with the semiclassical J-diffusion model.

value in interrelating data from different kinds of measurements. The model we have developed in this chapter is a semiclassical version of the extended-rotational diffusion model. This model can be applied efficiently to the study of band shapes composed of a large number of transitions such as the ν_4 mode of methane and should prove useful in the analysis of spectra where the quantum mechanical effects are large and rotational-vibrational coupling is important. The classical model would be invalid and of little value under these conditions.

THE KIVELSON LINEWIDTH THEORY

CHAPTER IV

A. INTRODUCTION

In Chapters II and III, we have developed models for the description of reorientational motion in systems in which the angular momentum correlation time τ_J and the reorientational correlation times τ_θ are of the same order of magnitude. Under these conditions, it is necessary to follow, in detail, the reorientational motion in individual diffusive steps in order to describe the reorientation of a molecule in terms of a rotational diffusion process. In this chapter reorientational motion in liquid systems where τ_J is much shorter than τ_θ will be studied. Under these conditions, molecules reorient by very short rotational steps and they sample a large number of rotational states in the period of time τ_θ. For this reason it is not necessary to follow the rotational process in each individual step and the reorientational motion can be described using a rotational diffusion equation. In the limit where τ_J is much shorter than τ_θ, the extended J-diffusion model reduces to the model described by the diffusion equation approach.[8]

If $W[\Omega_o;t,\Omega]$ defines the conditional probability that a molecule has reoriented from an initial orientational Ω_o to an orientation Ω in time t, the classical rotation diffusion theory [52] leads to a description of the time dependence of $W[\Omega_o;t,\Omega]$ in the form of a rotational diffusion equation

$$-\frac{\partial}{\partial t} W[\Omega_o;t,\Omega] = \sum_{\alpha,\beta} J_\alpha D_{\alpha\beta} J_\beta W[\Omega_o;t,\Omega], \qquad \text{(IV-2)}$$

where J_α is the dimensionless operator for the angular momentum about the α-th axis and $D_{\alpha\beta}$ is the $\alpha\beta$-th component of the diffusion tensor $\underset{\sim}{D}$ given by

$$D_{\alpha\beta} = \lim_{\Delta t \to 0} \frac{1}{2} \int \frac{d\vec{\varepsilon}\,\varepsilon_\alpha \varepsilon_\beta p(\vec{\varepsilon},\Delta t)}{\Delta t}, \qquad \text{(IV-2)}$$

where Δt is a time increment which is much shorter than the times of interest τ_θ, and $p(\vec{\varepsilon},\Delta t)$ gives the probability that the molecule reorients through a solid angle $\vec{\varepsilon}$ in time Δt. In order to obtain Eq. (IV-1), one applies the rotation operator $\exp[-i\vec{\varepsilon}.\vec{J}]$, representing an infinitesimal reorientation ε, to the function $W[\Omega_o;t,\Omega]$, expresses the result as a power series in $\vec{\varepsilon}$ and neglects all terms of order greater than ε^2.

The solutions to the rotational diffusion equation (IV-1) for a molecule with an isotropic diffusion tensor, $D\underset{\sim}{1}$, can be written in the form

$$W[\Omega_o;t,\Omega] = \sum_{\ell,k,m} \frac{(2\ell+1)}{8\pi^2} \mathcal{D}^{(\ell)}_{km}[\Omega_o]\, \mathcal{D}^{(\ell)*}_{km}[\Omega]$$

$$\times \exp\,[-\ell(\ell+1)Dt] \qquad , \qquad \text{(IV-3)}$$

where $\underset{\sim}{\mathcal{D}}^{(\ell)}[\Omega_o]$ is the Wigner $\underset{\sim}{\mathcal{D}}$-matrix [68] which describes the reorientation of a spherical tensor of rank ℓ through the Euler angles Ω_o. The diffusion tensor $\underset{\sim}{D1}$ is usually defined in a coordinate system in which it is diagonal and is generally interpreted in terms of the retarding torques acting on the molecule due to the viscous drag of the solvent using the Stokes-Einstein hydrodynamic relationship.[53] Debye first proposed this type of relationship in his classic treatment [3] of dielectric relaxation in polar liquid [19] and it was later used by Bloembergen, Purcell and Pound [20] to interpret the nuclear spin relaxation times of the molecules in liquid water.

In addition to the study of Raman and infrared band shapes described in Chapters II and III, and the study of dielectric and nuclear relaxation phenomena as noted above, one can also gather information about molecular reorientation in liquids by studying electron spin relaxation of paramagnetic species in dilute liquid solutions. The interpretation of electron spin relaxation times is a particularly useful technique provided that a suitable paramagnetic probe is available.

If the electronic Zeeman and nuclear-electronic hyperfine interactions are anisotropic then the tumbling motion of the molecule modulates the strength of the interactions between the electron spin, nuclear spin and applied magnetic field and gives rise therefore to a time dependent perturbation on the electron spin levels which leads to transitions among them or spin relaxation. For dilute solutions of paramagnetic species, containing a single unpaired electron and one or more magnetic nuclei, the transverse spin relaxation time, T_2, is determined by this rotational modulation of the spin levels. Since T_2 is inversely proportional to the observed spectral linewidths, information about the reorientational motions of the paramagnetic species is easily obtained from experiment provided a suitable description of the effect of the reorientational motion on the anisotropic interactions is available.

The anisotropic electronic Zeeman and electronic-nuclear hyperfine interactions are characterized by second rank spherical tensors, so that the reorientational correlation time which describes the time correlation of these tensors is the correlation time $\tau_\theta^{(2)}$ associated with the correlation function $\left\langle \mathcal{D}^{(2)*}_{km}[\Omega_0]\, \mathcal{D}^{(2)}_{km}[\Omega] \right\rangle$. The rotational diffusion equation theory gives the result

$$\left\langle \mathcal{D}^{(2)*}_{km}[\Omega_o]\mathcal{D}^{(2)}_{km}[\Omega]\right\rangle = \int d\Omega_o \int d\Omega\, \mathcal{D}^{(2)*}_{km}[\Omega_o]$$

$$\times\, \mathcal{D}^{(2)}_{km}[\Omega]\; W\, [\Omega_o;t,\Omega] = \left\langle |\mathcal{D}^{(2)}_{km}[\Omega_o]|^2 \right\rangle$$

$$\times \exp{-6Dt} \qquad \text{(IV-4)}$$

so that

$$\tau_\theta^{(2)} = 1/6D \quad . \qquad \text{(IV-5)}$$

Following the Debye [19] and Bloembergen, Purcell and Pound [20] approach, we assume the Stokes-Einstein [53] relationship

$$D = kT/8\pi r_o^3\eta \qquad \text{(IV-6)}$$

where k is the Boltzmann constant, T the temperature, r_o the hydrodynamic radius of the molecule and η the coefficient of shear viscosity of the solvent: so that

$$\tau_\theta^{(2)} = 4\pi r_o^3\eta/3kT \qquad \text{(IV-7)}$$

The ESR spectrum of a paramagnetic species with one unpaired electron and a single magnetic nucleus of spin I in a dilute liquid solution consists of 2I + 1 lines each with a different linewidth. The widths of these lines ΔH_M, depend on the nuclear spin quantum number, M, and can be expressed by the cubic function

$$\Delta H_M = \alpha' + \alpha'' + \beta M + \gamma M^2 + \delta M^3 \qquad \text{(IV-8)}$$

γ

where the parameters α', α", β, γ, and δ depend on the species, temperature and solvent. Kivelson and Wilson[41] have obtained theoretical expressions for the contribution to the parameters α', β, γ, and δ from the relaxation process due to the rotational modulation of the electronic Zeeman and hyperfine interaction using the Kubo-Tomita formalism for relaxation.[81,82] Other workers [83,84] have verified these expressions by deriving them with Redfield's theory of magnetic relaxation.[85-87] The linewidth parameters are related to the magnetic parameters of the paramagnetic species and the electron resonance frequency by

$$
\begin{aligned}
\alpha' = \frac{2\hbar\tau_{\theta}^{(2)}}{5\sqrt{3}\, g_o\beta_o} \Bigg\{ & \frac{4}{9} B_o^{\,2}(\Delta\gamma^2 + 3\delta\gamma^2) \\
& + I(I+1)\left(\frac{3b^2}{8} + 2C^2 - \frac{\Delta\gamma B_o ba}{6\omega_o} \right) \\
& + u\Bigg(\frac{B_o^{\,2}}{3}\,[\Delta\gamma^2 + 3\delta\gamma^2] \\
& + I(I+1)\left[\frac{7b^2}{8} + \frac{14c^2}{3} - \frac{ba}{\omega_o}\left(\frac{5bf}{8} + \frac{\Delta\gamma B_o}{6} \right)\right]\Bigg) \Bigg\},
\end{aligned}
\tag{IV-9}
$$

$$\begin{aligned}\beta = \frac{2\hbar\tau_\theta^{(2)}}{5\sqrt{3}g_o\beta_o}\Bigg\{ & \frac{4}{3}\, B_o(b\Delta\gamma + 4c\delta\gamma) - \frac{a}{\omega_o}\Bigg(\frac{8}{9} \; (\Delta\gamma B_o)^2 \\ & + \frac{b^2}{8}\Big[3 + 2I(I + 1)\Big]\Bigg) \\ & + u\Bigg(B_o(b\Delta\gamma + 4c\delta\gamma) - \frac{a}{\omega_o}\Bigg[\frac{2}{3}(\Delta\gamma B_o)^2(1 + f) \\ & + \frac{b^2}{4}\Bigg\{ 1 + I(I + 1)[1 + 7f]\Bigg\}\Bigg]\Bigg)\Bigg\}.\end{aligned} \tag{IV-10}$$

$$\begin{aligned}\gamma = \frac{2\hbar\tau_\theta^{(2)}}{5\sqrt{3}\; g_o\beta_o}\Bigg\{ & \frac{5b^2}{8} + \frac{10c^2}{3} - \frac{7}{6}\Delta\gamma B_o b(a/\omega_o) \\ & - u\Bigg(\frac{b^2}{8} + \frac{2}{3}c^2 + \frac{ab}{\omega_o}\Bigg[\frac{\Delta\gamma B_o}{6} \; (5 + 12f) - \frac{5}{8}bf\Bigg]\Bigg)\Bigg\}\end{aligned} \tag{IV-11}$$

and

$$\delta = \frac{\hbar\tau_\theta^{(2)}}{10\sqrt{3}g_o\beta_o}\Bigg\{ b^2(a/\omega_o)[1 + u(1 + f)] \Bigg\} \tag{IV-12}$$

where

$$g_o = \frac{1}{3}(g_x + g_y + g_z) \quad , \tag{IV-13}$$

$$\Delta\gamma = \frac{\beta_o}{2\hbar}\,(2g_z - g_x - g_y) \quad , \qquad \text{(IV-14)}$$

$$\delta\gamma = \frac{\beta_o}{2\hbar}\,(g_x - g_y) \quad , \qquad \text{(IV-15)}$$

$$a = \frac{1}{3}(A_x + A_y + A_z) \quad , \qquad \text{(IV-16)}$$

$$b = \frac{1}{3}(2A_z - A_x - A_y) \; , \qquad \text{(IV-17)}$$

$$c = \frac{1}{4}(A_x - A_y) \; , \qquad \text{(IV-18)}$$

$$u = \left[\, 1 + \omega_o{}^2 \tau_\theta^{(2)2} \,\right]^{-1} \quad , \qquad \text{(IV-19)}$$

and

$$f = \omega_o{}^2 \, \tau_\theta{}^2 u \qquad \text{(IV-20)}$$

g_x, g_y, g_z and A_x, A_y, A_z are the principal values of the electronic Zeeman and hyperfine interaction tensors respectively, β_o is the Bohr magneton, ω_o the frequency of the applied radiation and B_o is the applied magnetic field. All of these parameters, with the exception of $\tau_\theta^{(2)}$, can be determined from the ESR spectra of the species in liquid and solid solutions. Therefore, a study of the linewidth contributions due to motional modulation of anisotropic interactions can yield measurements of $\tau_\theta^{(2)}$.

The residual linewidth, α'', found in Eq. (IV-8) can be determined by subtracting the α' term predicted by the theory of Kivelson and Wilson [41] from the experimentally determined $\alpha' + \alpha''$ if $\tau_\theta^{(2)}$ is known. From a careful investigation of possible relaxation mechanisms, Atkins and Kivelson [43] concluded that the α'' contribution to the linewidth was dominated by motional modulation of the spin-rotational coupling. A theoretical expression for α'' was obtained by a procedure analgous to that used to obtain α, β, γ, δ. The magnitude of the spin-rotational contribution to the linewidth is determined by the magnitude of the components of the spin-rotational coupling tensor and the angular momentum correlation time τ_J. Since the elements of the spin-rotational interaction tensor are not usually available, Kivelson and co-workers [42,43] have used second order perturbation theory to estimate these elements from the elements of the g-tensor. Furthermore, they have used Hubbard's relationship [88]

$$\tau_\theta^{(2)}\tau_J = I/6kT \quad , \qquad \text{(IV-21)}$$

where I is the moment of inertia of the molecule k is the Boltzmann constant, and t the temperature, to estimate τ_J from $\tau_\theta^{(2)}$. With these assumptions, the spin-rotational contribution to the linewidth is

$$\alpha'' = \frac{2\hbar}{9\sqrt{3}g_o\beta}(\partial g)^2 \tau_\theta^{-1} \qquad \text{(IV-22)}$$

where δg is defined by

$$\partial g = [(g_x - g_e)^2 + (g_y - g_e)^2 + (g_z - g_e)^2]^{\frac{1}{2}} \qquad \text{(IV-23)}$$

and g_e is the free electron g-value (2.00231).

Kivelson *et al.*[41,89] applied the linewidth theory described above to interpret the observed ESR linewidths of *bis*(2,4-pentanedionato)oxovanadium(IV) [VOAA] in a series of solvents. They obtained excellent agreement between theory and experiment provided that Eq. (IV-7) was modified to the form

$$\tau_\theta^{(2)} = \frac{4\pi\kappa r_o^3\eta}{3kT} \qquad \text{(IV-24)}$$

here r_o is the hydrodynamic radius of the solute molecule determined from translational diffusion experiments and κ is a dimensionless parameter which they found to be temperature independent, but which varied with the nature of the solvent and solute molecules. After careful consideration of reorientation in a viscous fluid, Kivelson *et al.*[42,90] have defined κ to be a tensor given by

$$\kappa_{ii} = \frac{3}{4r_o^2}\,\frac{\langle T_i^2\rangle}{\langle F_i^2\rangle} \qquad \text{(IV-25)}$$

where T_i and F_i are the i-th components of the torque exerted on the molecule, and the intermolecular force experienced by the molecule respectively. So as not to introduce additional parameters into the model the tensor κ is generally assumed to be a scalar.[17,18,42]

Recent investigations[17,18,44,45] of the ESR linewidths of VOAA and other vanadyl complexes in solutions at low temperatures and also in solutions in hydrogen bonding solvents have indicated apparent weaknesses in the Kivelson linewidth theory. Angerman and Jordan [44] studied the linewidths of VOAA in a number of alcohols and noted that the reorientational correlation time, $\tau_\theta^{(2)}$, assigned from the analysis of the β parameter was different from that determined from the γ parameter. They attributed this discrepancy to the high sensitivity of β to experimental error in the linewidths relative to the sensitivity of γ, rather than to weaknesses in the theory itself. They also observed that the spin-rotational contribution, α'', was much larger than that predicted by Eq. (IV-22) in the region of large η/T. Similar observations were made by Chasteen and Hanna [45] in a study of a series of vanadyl α-hydroxycarboxylate complexes in aqueous solutions, by Huang and Kivelson [17] for tetra-n-butylammonium bis(dimercaptomaleonitrile) nickel(II) $[(n\text{-}C_4H_9)_nN.NiS_4C_4(CN)_4]$ in n-butanol and in $CHCl_3$, and by Hwang, Kivelson and Plachy [18] for VOAA in a number of non-hydrogen bonding solvents at low temperatures and at high pressures.

In order to further investigate the validity of the Kivelson theory, we have studied a series of vanadyl complexes of varying molecular size in toluene, carbon disulfide, chloroform and diphenylmethane (DPM) solutions. The complexes studied were _bis_(3,5-heptanedionato)oxovanadium(IV) [VODE], _bis_(1-phenyl-1,3-butanedionato)oxovanadium(IV) [VOPM], _bis_(2,2,6,6-tetramethyl-3,5-heptanedionato)oxovanadium(IV) [VOTB], and _bis_(1,3-diphenyl-1,3-propanedionato)oxovanadium(IV) [VODP].

In sections B-E of this chapter, the experimental methods employed in obtaining the data are described. In section F, the analysis of the data is presented while in section G the procedures used to interpret the data are assessed and the implications of the results considered.

B. PREPARATION AND CHARACTERIZATION OF VANADYL COMPLEXES

The four vanadyl complexes were prepared using variations of the standard procedures given in _Inorganic Synthesis_ [91] for the preparation of VOAA.

1. Bis(3,5-heptanedionato)oxovanadium(IV) [VODE].

The VODE complex was prepared by refluxing a mixture of 0.5 g vanadium pentoxide (V_2O_5) (Fisher Scientific) and 12.5 g of 3,5-heptanedione (Eastman Organic) for 1.5 hours. The hot reaction mixture was filtered to remove unreacted V_2O_5 and the excess diketone was removed under vacuum. The resulting product was recrystallized twice from acetone and submitted for microanalysis.

Analysis: calculated for $C_{14}H_{22}O_5V$:
C, 52.33 ; H, 6.85
Found: C, 52.08 ; H, 6.78

2. Bis(2,2,6,6-tetramethyl-3,5-heptanedionato)oxovanadium(IV) [VOTB]

The VOTB complex was prepared by refluxing a mixture of 0.5 g V_2O_5 and 18 g of 2,2,6,6-tetramethylheptane-3,5-dione (Pierce Chemical) for 4 hours. The hot reaction mixture was filtered to remove V_2O_5 and the excess diketone was pumped off. The resulting product was recrystallized twice from acetone and submitted for microanalysis.

Analysis: calculated for $C_{22}H_{38}O_5V$:
C, 61.00 ; H, 8.80
Found: C, 61.02 ; H, 8.75

3. Bis(1-phenyl-1,3-butanedionato)oxovanadium(IV) [VOPM]

The VOPM complex was prepared by refluxing a mixture of 0.5 g V_2O_5 and of 1.0 g 1-phenyl-1,3-butanedione (J. T. Baker) in 25 mls of benzene for 1 day. The hot reaction mixture was filtered and the benzene removed under vacuum. The resulting product was recrystallized three times from acetone and submitted for microanalysis.

Analysis: calculated for $C_{20}H_{18}O_5V$:
C, 61.70 ; H, 4.63
Found: C, 61.87 ; H, 4.50.

4. Bis(1,3-diphenyl-1,3-propanedionato)oxovanadium(IV) [VODP]

The VODP complex was prepared by refluxing 0.5 g of V_2O_5 and 0.5 g of 1,3-diphenyl-1,3-propanedione (Eastman Organic) in 5 mls benzene for 1 day. The hot reaction mixture was filtered and the benzene removed under vacuum. The resulting product was recrystallized twice from acetone and submitted for microanalysis.

Analysis: calculated for $C_{30}H_{22}O_5V$:
C, 70.18 ; H, 4.29
Found: C, 70.30 ; H, 4.25.

C. SAMPLE PREPARATION

The solvents toluene (Allied Chemical reagent), carbon disulfide (Matheson, Coleman and Bell), chloroform (Mallinckrodt Analytical reagent), and diphenyl methane (Fisher Scientific) were all purified by vacuum distillation and were stored over molecular sieves (BDH type 4A) under vacuum. Solutions of the vanadyl complexes were prepared by weighing the complex into a vessel with a sidearm fitted with a 4 mm ESR Pyrex sample tube. The solvent was then distilled into the vessel on a grease free portion of a vacuum line. Any traces of oxygen remaining in the samples were removed by pumping on these solutions while they were maintained at -95°C in a toluene slush. The solutions were then poured into the sample tubes and sealed off under vacuum. All solutions were 10^{-3} M.

D. INSTRUMENTATION AND MEASUREMENT TECHNIQUES

The ESR spectra were recorded on a Varian V-4502 spectrometer equipped with a Varian V-4557 temperature control accessory, and the temperature was measured with a copper-constantan thermocouple The magnetic field was calibrated with an Alpha model 3093 digital NMR gaussmeter. The cavity frequency was determined with a Hewlett Packard model X532B frequency meter. The frequency meter was found to be accurate to 0.05% using an aqueous solution of Fremy's salt (g = 2.00550).[92]

The widths of the individual spectral lines were determined by measuring the heights of the lines on a

1 kG sweep and the width of the M = -3/2 line on a narrower sweep (25 - 50 G). The lines were assumed to be of Lorentzian shape so that the height, H, and the width, W, were related through the familiar relationship, $C = HW^2$, where C is constant for a given spectrum and can be determined from the height and width of the M = -3/2 line. Preliminary investigation indicated that the influence of line overlap on the measured linewidths was negligible even at low temperatures and thus no correction was made for overlap. In order to decrease the experimental error in the height the average of four sweeps was used in each calculation. Tables of the observed spectral linewidths are given in Appendix III for each complex/solvent system.

E. ANALYSIS OF THE ESR SPECTRA OF VANADYL COMPLEXES

The spin Hamiltonian, $\hat{\mathcal{H}}$, for a paramagnetic molecule containing a single unpaired electron and a single magnetic nucleus is

$$\hat{\mathcal{H}} = \beta_o \hat{\vec{S}}.\underset{\sim}{g}.\vec{B}_o + \hbar \hat{\vec{I}}.\underset{\sim}{A}.\hat{\vec{S}} \qquad \text{(IV-26)}$$

where $\hat{\vec{S}}$ is the electron spin angular momentum operator, $\hat{\vec{I}}$ the nuclear spin angular momentum operator and $\vec{B}_o$ the applied magnetic field. $\underset{\sim}{g}$ is the electronic Zeeman interaction tensor and $\underset{\sim}{A}$ is the nuclear-electronic hyperfine interaction tensor. Since the magnetic field vector $\vec{B}_o$ is fixed in the laboratory coordinate system and the tensors $\underset{\sim}{g}$ and $\underset{\sim}{A}$ are diagonal in a molecular coordinate system, the interactions are dependent on the orientation of the molecular coordinate system relative to the laboratory coordinate system and thus the ESR transition frequencies are orientation dependent. If we define ω_x, ω_y, ω_z respectively as the ESR transition frequencies when the x, y or z axis of the molecular coordinate system lies along the direction of the applied magnetic field then these frequencies are given by [93]

$$\omega_q = \frac{g_q \beta_o B_o}{\hbar} + A_q M_I + \frac{\hbar C_q^2 [I(I+1) - M_I^2]}{4 g_q \beta_o B_o} \qquad \text{(IV-27)}$$

where

$$C_q^2 = A_x^2 + A_y^2 + A_z^2 - A_q^2 \qquad \text{(IV-28)}$$

and q = x, y or z. In a solid solution the molecules are randomly oriented, however the position of the individual transitions can be identified and these transition frequencies can be used in conjunction with Eq. (IV-27) to determine the individual components of the $\underset{\sim}{g}$ and $\underset{\sim}{A}$ tensors. In Fig. 23, the spectrum of VOTP in a toluene glass is given and some of the transition lines identified.

In a liquid solution where the molecule is tumbl-

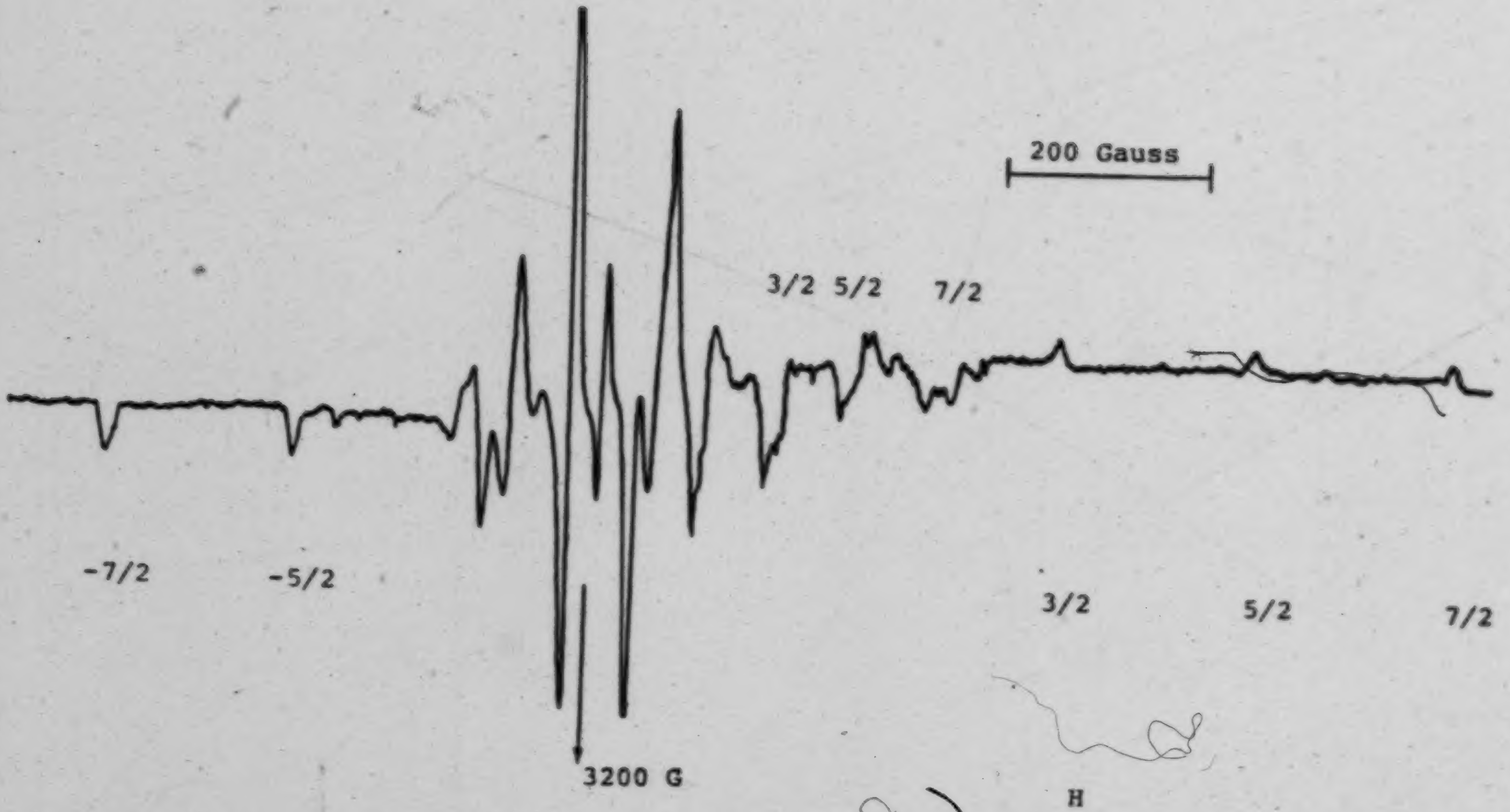

FIGURE 23: ESR spectrum of VOTB in toluene at T = 90 K. The z-transitions are identified below and the x, y-transitions above the spectrum. ω_o = 9.214 GHz.

ing freely, the x, y, z components of each spectral line are averaged to give lines at the frequencies [41]

$$\omega_o = g_o \frac{\beta_o B}{\hbar} + aM + \frac{1}{2} a^2 \; \frac{I(I + 1) - M^2}{g_o \beta_o B/\hbar} \qquad \text{(IV-29)}$$

where β_o is the Bohr magneton, B the magnetic field and g_o and a have been defined in Eqs. (IV-13) and (IV-16) respectively. The liquid spectrum consists of 2I + 1 lines whose positions and widths are determined by the averaging produced by the tumbling motion of the molecule. It is this averaging process which is monitored in studying the reorientational motion of molecules using the linewidth of the ESR spectra. From an iterative procedure. using Eq. (IV-29) and the position of the 8 lines of the liquid spectrum, g_o and a can be calculated. Although the $\underset{\sim}{g}$ and $\underset{\sim}{A}$ tensors could be determined from the glass spectra, Wilson and Kivelson[41] suggest that determining g_o and a from the liquid spectrum, g_z, $g_x - g_y$, A_z, and $A_x - A_y$ from the glass spectrum and combining these data to obtain the remaining parameters is the best approach. g_z can be determined from the positions of the $\pm M_I$ lines in the z-spectra while $g_x - g_y$ and $A_x - A_y$ can be determined from the separation of the x- and y-spectra of a given M_I transition (see Figs. 23,24).

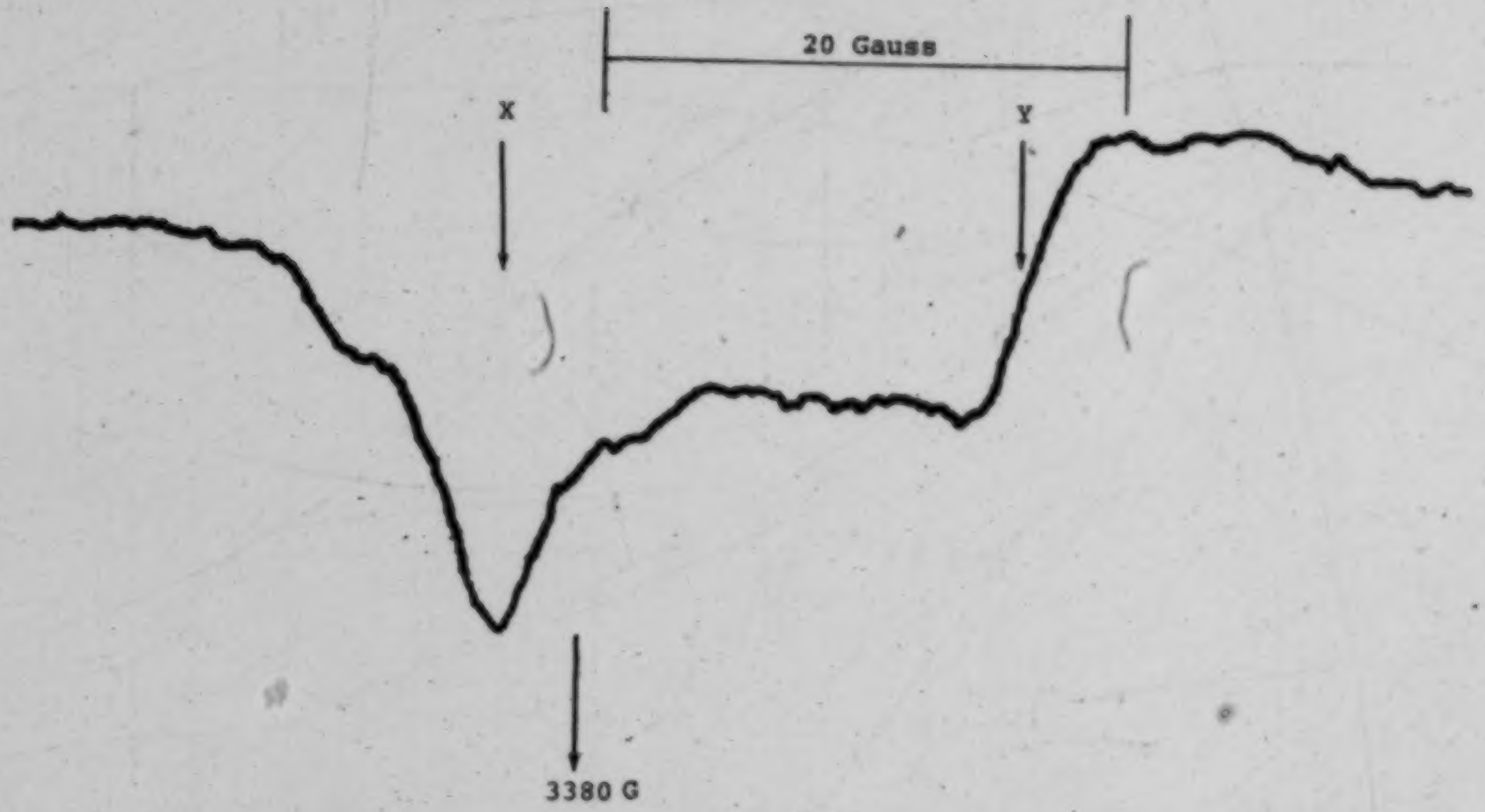

FIGURE 24. ESR spectrum of VOTB in toluene at T = 90°K in the region of the M = 3/2 x, y-transition. The positions of the x and y-transitions are as indicated. ω_o = 9.214 GHz.

In Fig. 24 a section of the VODE/toluene glass spectrum, in the region of the $M_I = 3/2$ x and y transitions, is shown and the positions of the x and y transitions are indicated.

The components of the g and hyperfine interaction tensors determined from the glass and liquid spectra using the procedures outlined above are given in Table 4. These determinations were all carried out on toluene solutions of the complexes.

In Fig. 25, the region of the $M_I = 3/2$ x and y transitions in the VOPM/toluene glass spectrum is shown. Comparing this to the same region of the VODE spectrum shown in Fig. 24, we see that there appears to be an additional transition in the region where the y-transition is expected. We have analysed this spectrum in terms of the two possible y-transitions and obtained two sets of parameters. VOPM can exist as either the cis or trans isomer. X-ray diffraction studies indicate that the cis isomer is the predominant species in the solid state.[94] However ESR studies by Belford et al.[94] on single crystals of bis(1-phenyl-1,3-butanedionato)palladium which has a trans geometry doped with VOPM indicate the possible existence of VOPM as the trans isomer, while the VOPM complex in bis(1-phenyl-1,3-butanedionato)zinc crystals (cis

TABLE 4

Magnetic Parameters of Vanadyl Complexes in Toluene*

Complex / Parameter	VODE	VOPM	VOTB	VODP
g_x	1.983	1.982	1.984	1.988
g_y	1.980	1.982	1.979	1.983
g_z	1.944	1.943	1.945	1.943
A_x (10^9 sec^{-1})	-1.134	-1.117	-1.093	-1.198
A_y (10^9 sec^{-1})	-1.172	-1.202	-1.188	-1.237
A_z (10^9 sec^{-1})	-3.312	-3.289	-3.306	-3.271

---

[*] Estimated error:
g_z ± 0.002
g_x, g_y ± 0.003
A_z ± 1%
A_x, A_y ± 3%

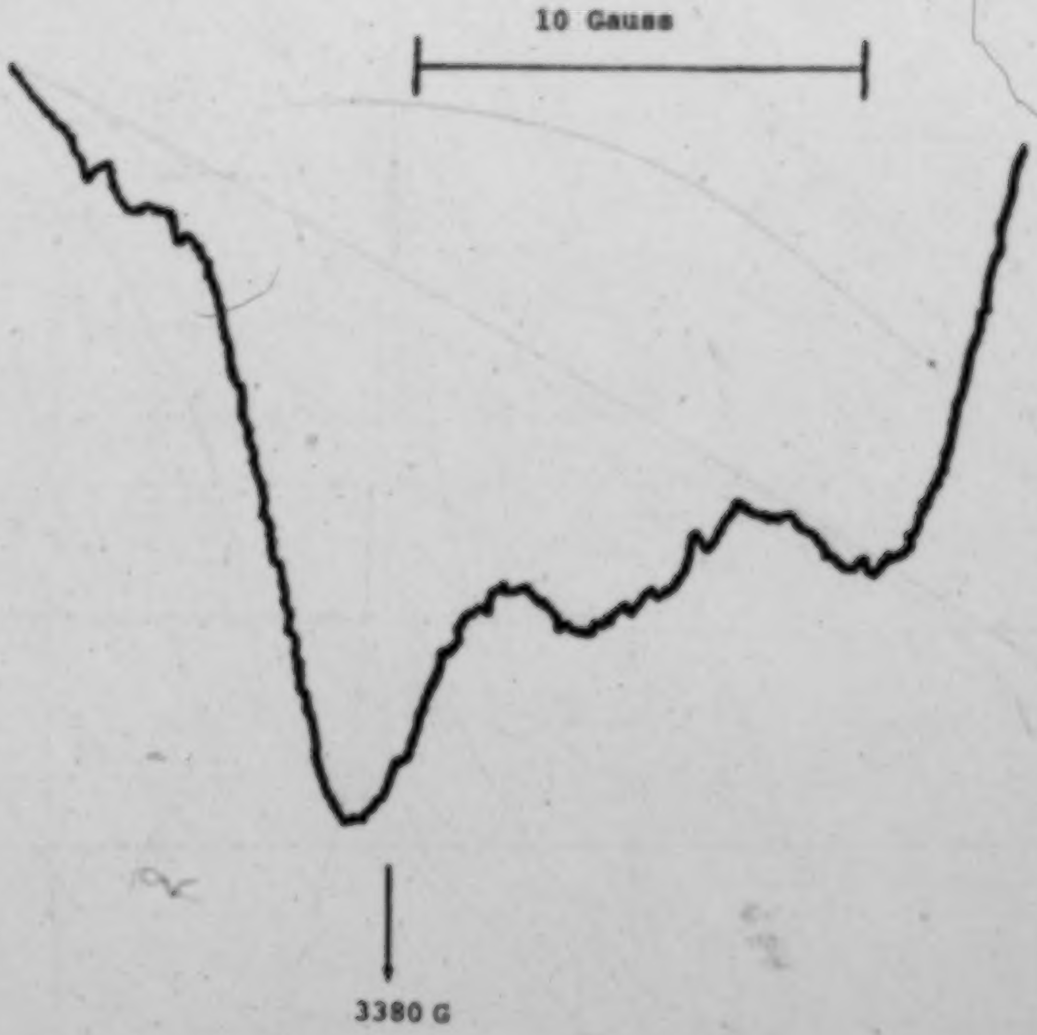

FIGURE 25. ESR spectrum of VOPM in toluene at T = 90°K in the region of M = 3/2 x, y-transition.

geometry) exists as the cis isomer. The g values assigned by Belford et. al.[94] to the cis (Zn matrix) and trans (Pd matrix) isomer of VOPM are similar to those assigned from our analysis of the glass spectra indicating the simultaneous existence of both the cis and trans isomers in the toluene glass. The values reported in Table 4 for VOPM are an average of our two sets of results and are sufficiently accurate for the purpose of our linewidth analysis.

F. ANALYSIS OF ESR LINEWIDTHS

The theoretical expressions for the linewidth parameters [Eqs. (IV-9) - (IV-12)] can be combined with the expression for $\tau_{\theta}^{(2)}$ [Eq. (IV-24)] to obtain expressions for α', β, γ and δ in terms of the ratio η/T and the adjustable parameter κ. Provided η/T is known, κ can be determined from a nonlinear least squares fit of the theoretical linewidth parameters to those determined from experimental linewidths.

In previous applications of the Kivelson linewidth theory,[17,18,41,43-45,89] κ was determined from the η/T dependence of the γ parameter. The procedure had certain advantages, γ is nearly a linear function of η/T, and κ can be determined directly from the slope of a plot of γ vs η/T. The values of γ are usually more precise than the values of β since β is determined essentially from the differences in observed linewidths. Consideration of γ is also more pleasing in that the agreement between theory and experiment is more satisfactory than for β. On the other hand, consideration of only the γ parameter is not a stringent test of the complete theory since only a portion of the theory is being utilized. Secondly, the deviations between experimental and predicted β's cannot be entirely attributed to experimental uncertainties. Finally, fitting one's data for only the parameter which gives the best agreement is a questionable procedure especially in the case of γ, which is less sensitive to changes in η/T than is β. It is for these reasons that we have adopted the procedure of analysing the M-dependent parts of linewidths. We defined the M-dependent part of the linewidths as the experimental linewidths minus the $\alpha' + \alpha''$ contribution obtained by a least squares fit of the experimental linewidths to Eq. (IV-8). It would be more satisfactory to fit the entire linewidth using all the linewidth parameters, however the theory of the residual linewidths is still open to question in view of recently reported results in regions of large η/T.[18,44] A nonlinear least squares routine was used to fit the M-dependent part of the linewidth, obtained at several different temperatures, to the theoretical expression for $\beta M + \gamma M^2 + \delta M^3$ employing Eqs. (IV-10)-(IV-12) and (IV-24). Fortran IV listings of the computer routines used in both the linear and nonlinear least squares analysis are given in Appendix IID. The values of the product κr_o^3 obtained from the analyses of the M-dependent part of the linewidth are given in Table 5. In Table 5, we have also included the values of κr_o^3 obtained from a nonlinear least squares fit of the η/T dependence of experimental β and γ's [determined by fitting the experimental linewidths to Eq. (IV-8)] to Eq. (IV-10) or Eq. (IV-11). A similar analysis was not carried out on δ because of the large experimental errors in this parameter. A study was also made in which the experimental β and γ's were simultaneously fitted to Eq. (IV-10) and Eq. (IV-11). As expected, this latter approach yielded values of κr_o^3 between those obtained from the separate β and γ fits and are not included in Table 5. In these nonlinear least squares analyses convergence was determined by minimizing the relative residuals for the β, γ and $\beta\gamma$ fits and by minimizing the absolute residual for the fit to the M-dependent part of the linewidths. The convergence of the linear least squares routine in fitting Eq. (IV-8) was also determined by minimizing absolute

TABLE 5

Values of κr_0^3 Obtained by Fitting the Kivelson Theory to Experimental β, γ and M-dependent part of Linewidth.*

	VODE				VOPM				VOTB				VODP		
	Toluene	$CHCl_3$	CS_2	DPM	Toluene	$CHCl_3$	CS_2	DPM	Toluene	$CHCl_3$	CS_2	DPM	Toluene	$CHCl_3$	CS_2
β	45.1	52.3	46.1	32.3	74.0	86.7	67.7	52.5	71.6	72.5	70.3	51.0	126	150	120
γ	44.6	56.4	46.4	33.1	70.6	90.2	67.8	52.7	64.2	70.9	66.1	45.4	121	155	123
M-dep	44.4	56.5	46.5	32.9	70.7	90.2	71.3	52.0	64.2	71.2	66.5	45.7	121	153	124

---

* All results in units of $\mathring{A}^3$

residuals. In these least squares analyses several methods of weighting the data based on widths of the spectral lines were examined however, these different weighting procedures had an insignificant effect on the final result. In general, the results obtained by analysis of the γ vs η/T data are similar to those obtained from the analyses of the M-dependent part of the linewidths. The VODP/DPM system was not analysed because the very broad lines in these spectra made the measurement of the spectra difficult since overlap between successive lines was significant.

In Figs. 26-33 the β and γ parameters calculated from Eqs. (IV-10) and (IV-11) using the values of κr_o^3 obtained by fitting the M-dependent part of the linewidths are compared with the experimental values for the complexes in toluene and carbon disulfide. It should be noted that at high temperatures these complexes begin to decompose and that the scatter of points in this region is possibly attributable to this fact. No effort was made to overcome this problem or to try to obtain data at higher temperatures because viscosity data was not available in the region above the standard boiling points of these liquids. Data were not obtained in the very low temperature region because of the lack of viscosity data. The viscosities were calculated from standard formulae.[95,96]

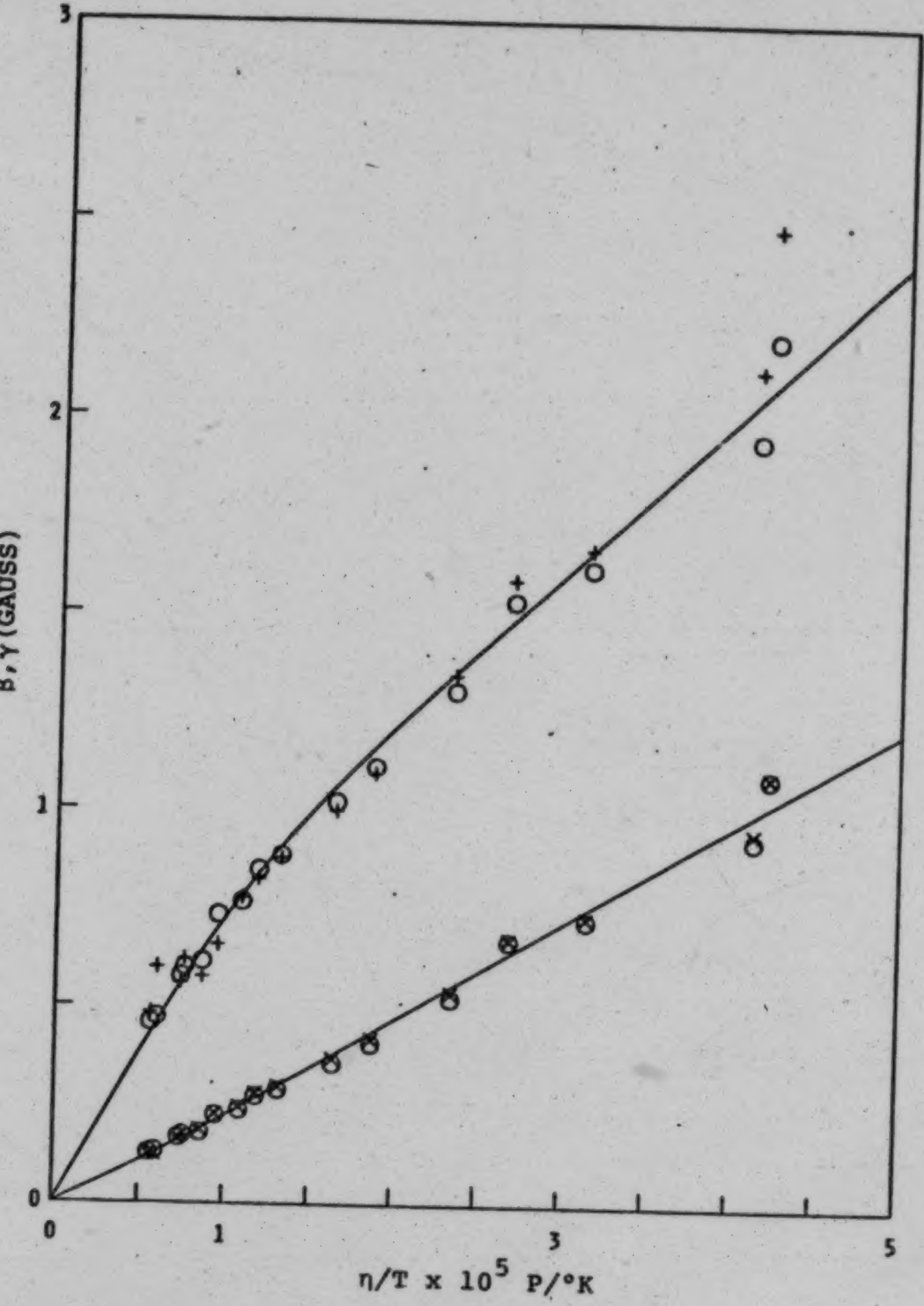

FIGURE 26. β and γ vs η/T for VODE/toluene. Experimental, + - β, x - γ. Predicted by Kivelson theory, ——— - with Stokes-Einstein, O - without Stokes-Einstein.

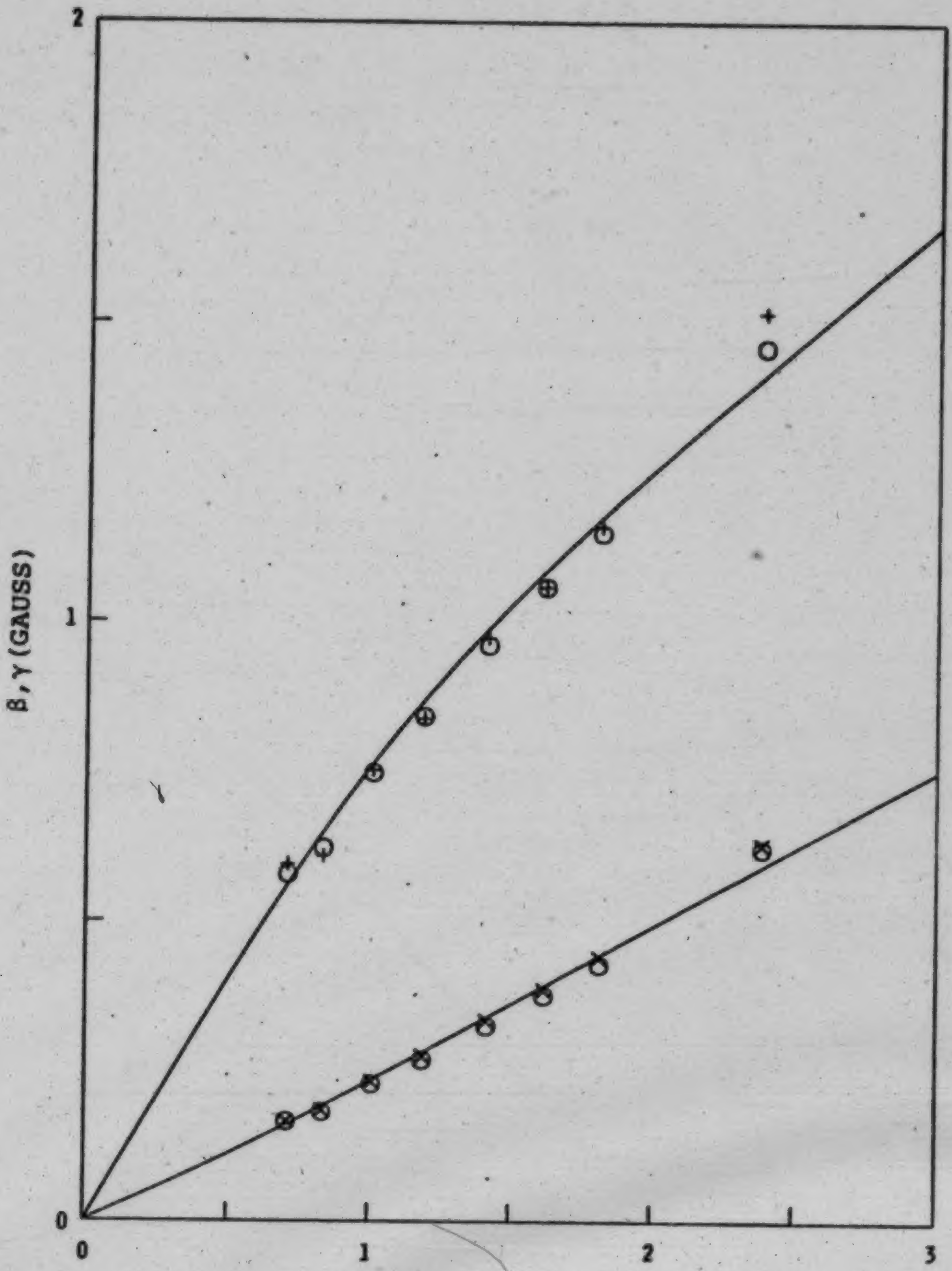

FIGURE 27. β and γ vs η/T for VODE/CS$_2$. Experimental, + - β, x - γ. Predicted by Kivelson theory, ——— - with Stokes-Einstein, O - without Stokes-Einstein.

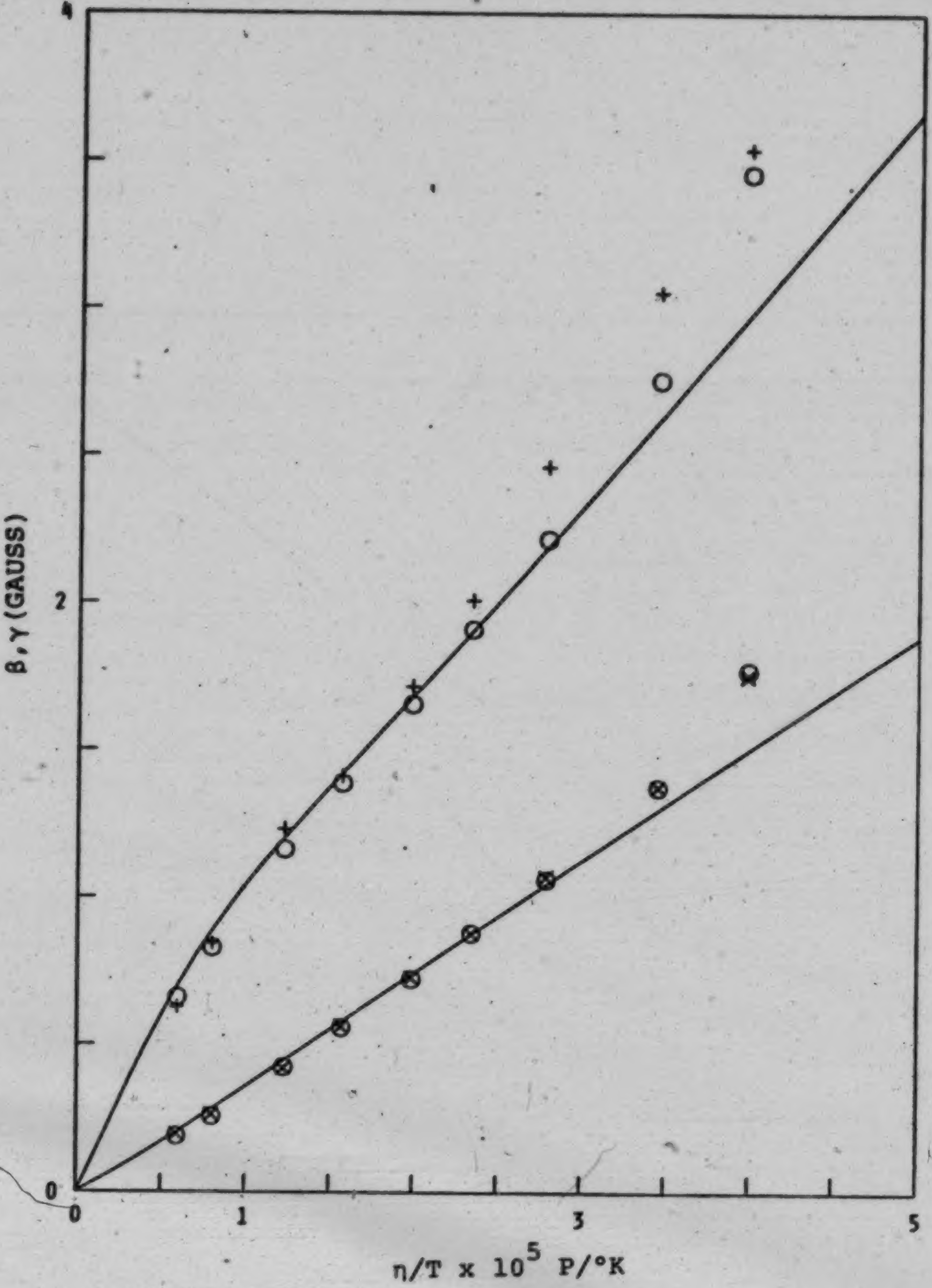

FIGURE 28. β and γ vs η/T for VOPM/toluene. Experimental, + - β, x - γ. Predicted by Kivelson theory, ——— - with Stokes-Einstein, O - without Stokes-Einstein.

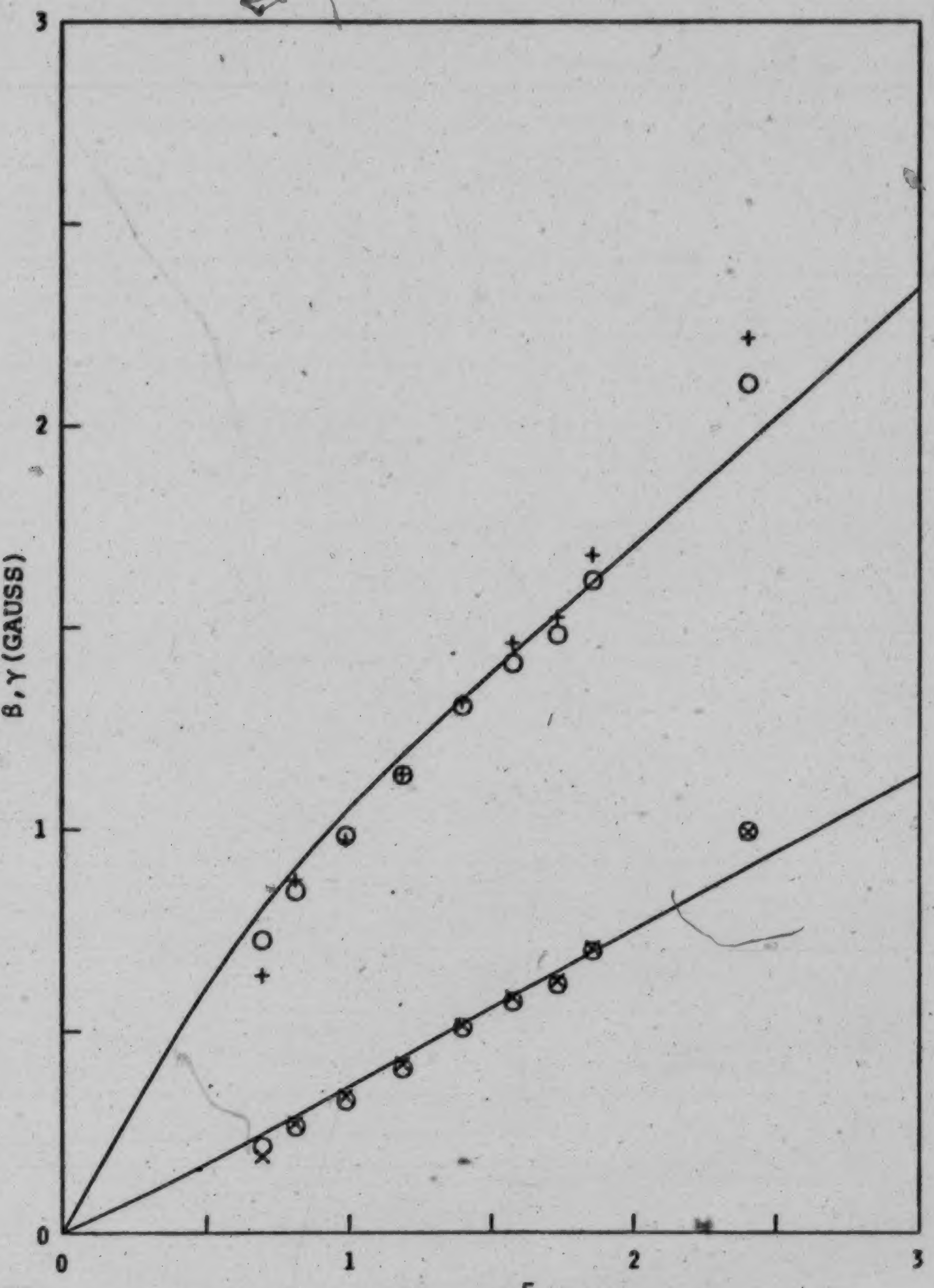

FIGURE 29. β and γ vs η/T for VOPM/CS_2. Experimental, + - β, x - γ. Predicted by Kivelson theory, —— - with Stokes-Einstein, O - without Stokes-Einstein.

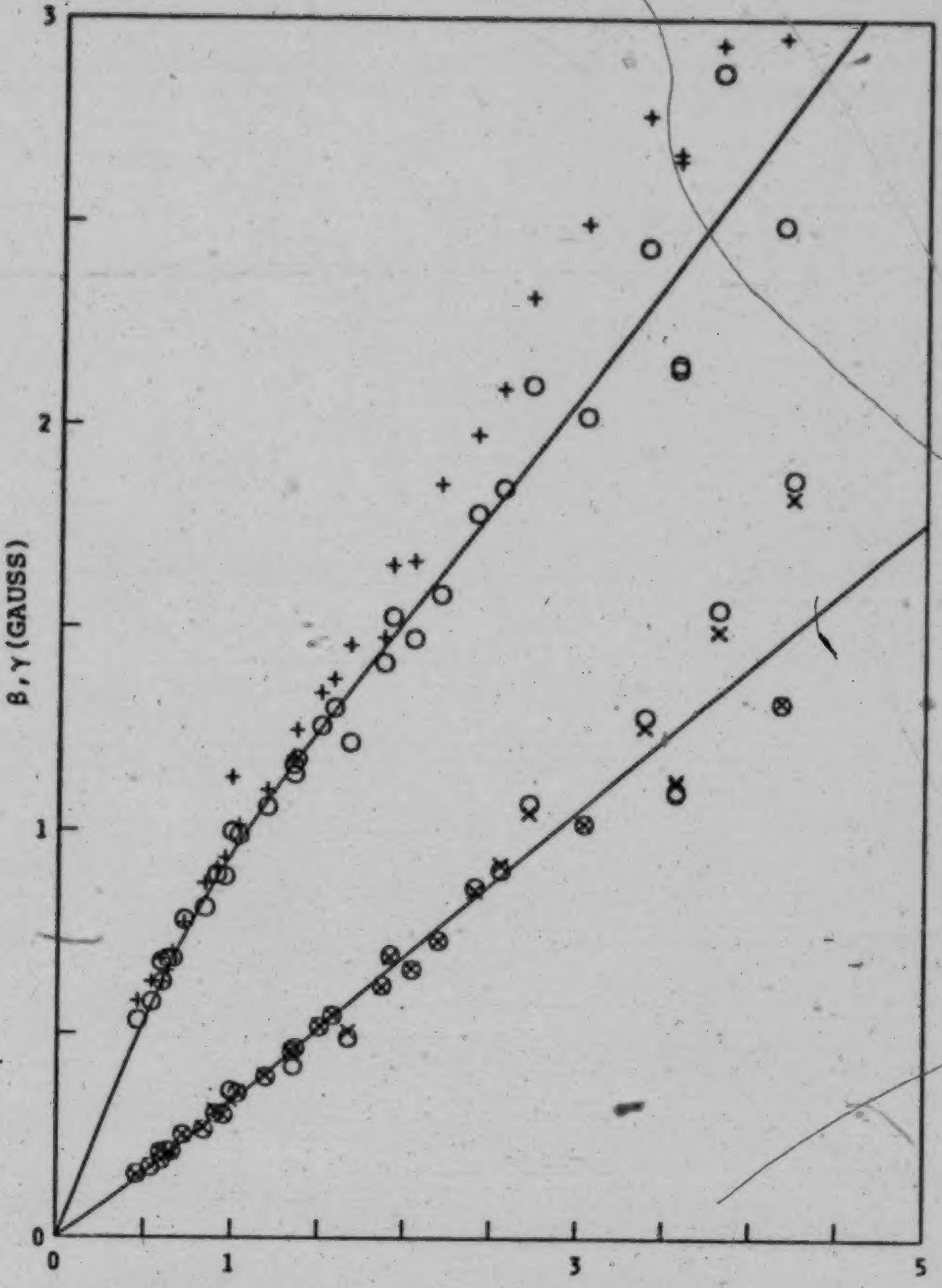

FIGURE 30. β and γ vs η/T for VOTB/toluene. Experimental, + - β, x - γ. Predicted by Kivelson theory, ——— - with Stokes-Einstein, O - without Stokes-Einstein.

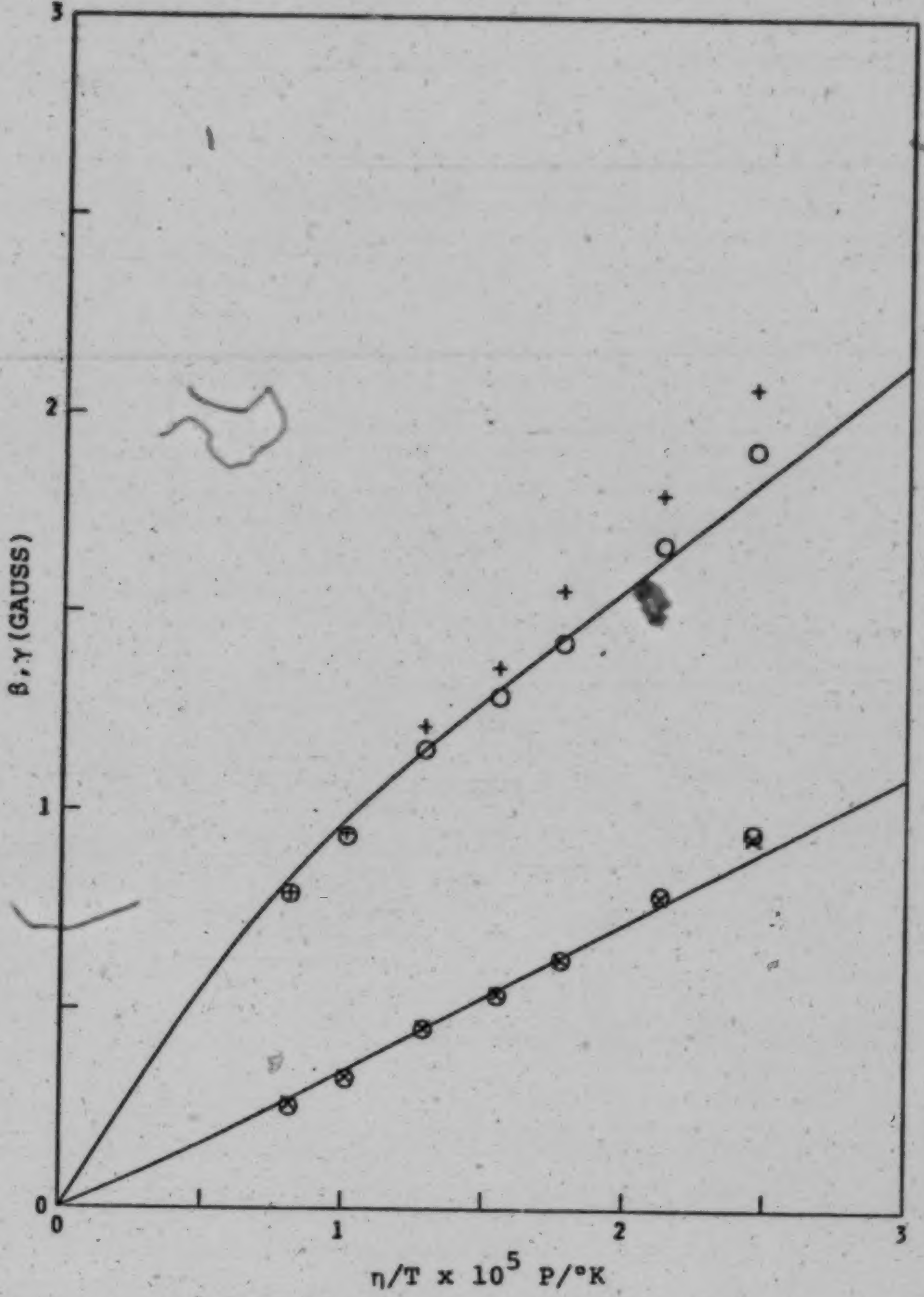

FIGURE 31. β and γ vs η/T for VOTB/CS_2. Experimental, + - β, x - γ. Predicted by Kivelson theory, ——— - with Stokes-Einstein, O - without Stokes-Einstein.

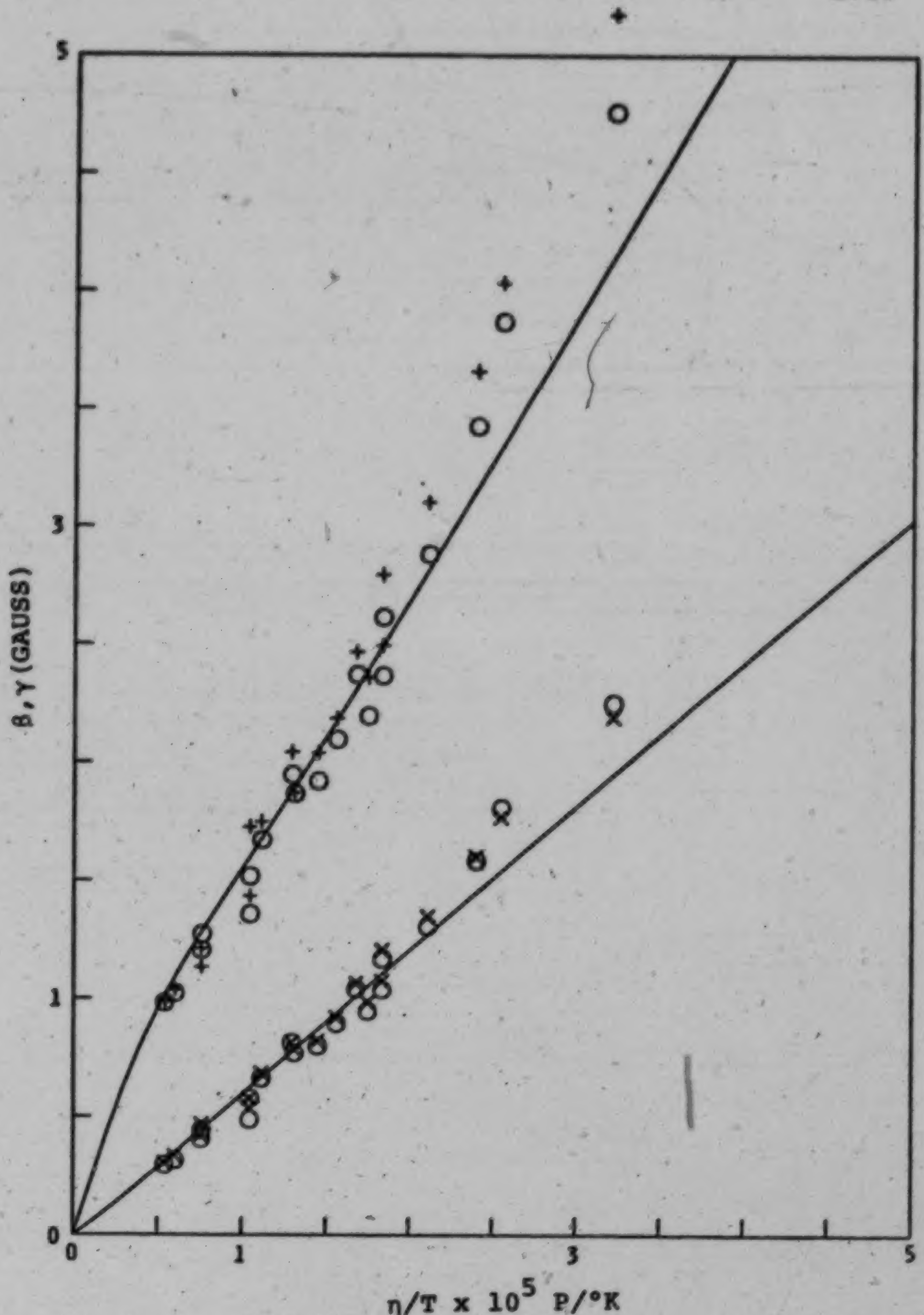

FIGURE 32. β and γ vs η/T for VODP/toluene. Experimental, + - β, x - γ. Predicted by Kivelson theory, —— - with Stokes-Einstein, O - without Stokes-Einstein.

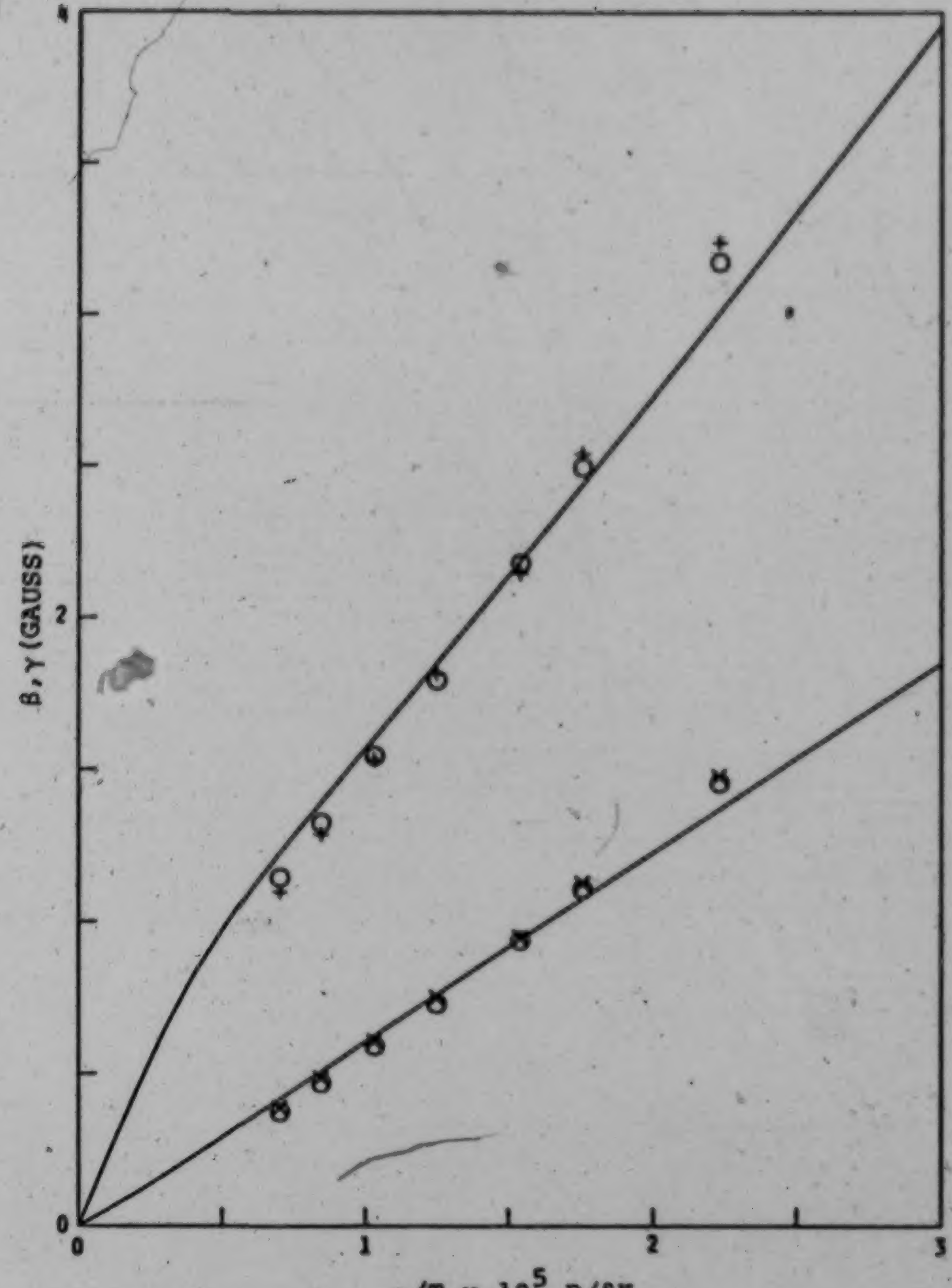

FIGURE 33. β and γ vs η/T for VODP/CS_2.
Experimental, + = β, x - γ. Predicted by Kivelson theory, —— - with Stokes-Einstein, O - without Stokes-Einstein.

The region of temperature and η/T over which the viscosity formulae are valid are given in Table 6.

From a consideration of Figs. 26-33, it is clear that, in general, the agreement between theory and experiment is very good at high temperatures and that it becomes very poor at low temperatures. From examination of Figs. 26-33 and similar figures for the chloroform[89] and DPM solvent systems and the VOAA results of Kivelson _et_ _al_.[18,41] we conclude that in order of decreasing "goodness" of fit the complexes are VOAA, VODE, VOPM, VODP, VOTB. With the exception of VODP and VOTB this order is also the order of increasing molecular weight and increasing molecular size.

The analyses of the experimental data using the Kivelson theory yielded values for the product κr_o^3. Any assignment of the parameter κ is dependent on the magnitude of the effective hydrodynamic radius, r_o. The determination of r_o is somewhat uncertain, however reasonable estimates can be made from translational diffusion experiments interpreted using Stoke's law.[18,42] Such experiments were not performed because we are primarily interested in the relative values of κ for a given complex in different solvents. In order that our κ's bear some resemblance to those already appearing in the literature [42], we have adopted the following procedure. An approximate hydrodynamic radius r_o' for

TABLE 6

Sources of Solvent Viscosities

Solvent	Temperature range (°C)	η/T range (10^{-5} P/°K)	Source
Toluene	0 - 107	2.8 - 0.7	Ref. 95
CS_2	0 - 46	1.8 - 0.8	Ref. 95
$CHCl_3$	-15 - 60	3.2 - 1.2	Ref. 95
DPM	60 - 260	4.5 - 0.5	Ref. 96

each complex/solvent system was calculated from the experimentally determined product κr_o^3 for that system by assuming that the value of κ was equal to the κ for VOAA in that solvent.[42] An average hydrodynamic radius r_o for a given complex was obtained by taking the average of the values of r_o' for that complex. The values of κ determined from the average hydrodynamic radii and the values of κr_o^3 obtained from the analysis of the M-dependent part of the linewidths, along with the values for VOAA in the same solvents are reported in Table 7. We see that the κ's for the different complexes in a given solvent are similar - a result which is indeed expected in view of the interpretation of κ given by Eq. (IV-20) and the similar nature of the complexes studied.

In the vanadyl systems studied here, the spin-rotational contribution to the linewidth, α'', cannot be calculated independently of the larger contribution α' from the modulation of the g and hyperfine interaction tensors. An "experimental" α'' is calculated by subtracting the value of α' predicted by the Kivelson theory from the $\alpha' + \alpha''$ term obtained by fitting Eq. (IV-8) to the experimental linewidths. Unfortunately this procedure results in the inclusion of all the experimental error in $\alpha' + \alpha''$ into the much smaller α'' term. Secondly, any deficiency in α' predicted by

TABLE 7

Values of κ Assigned to Complex-Solvent Systems[*]

Complex \ Solvent	Toluene	$CHCl_3$	CS_2	DPM
VODE	0.647	0.822	0.678	0.479
VOPM	0.654	0.834	0.659	0.480
VOTB	0.677	0.751	0.702	0.482
VODP	0.652	0.823	0.664	-
VOAA[**]	0.642	0.818	0.679	0.484

---

[*] Values indicate best fit but probably significant to 10%.

[**] From references 41,42,89.

the Kivelson theory is included in the experimental α" term. These two possible sources of error must be considered when comparing experimental and predicted values of α".

α" predicted by Eq. (IV-17) is compared with the experimental α" in Figs. 34-35 for the CS_2 and toluene systems. As was the case for β and γ for these systems there is excellent agreement between predicted and experimental values in the region of small η/T (high temperature) and the agreement becomes very poor in the region of large η/T (low temperature). We noted that the deviation between predicted and experimental values occurred at larger values of η/T for the small complexes and for solvents with small κ's as was the case for the β and γ parameters. This consistency suggests the possibility that part of the discrepancies between predicted and experimental values of α" may be due to the failure of the Kivelson theory to correctly predict α' at low temperature. We will have more to say about this point in the next section.

G. DISCUSSION

In the previous sections we have suggested that a fit of the M-dependent part of the linewidths to the corresponding theoretical expression is a more repre-

FIGURE 34

α'' vs η/T for toluene systems

Experimental - +, predicted by Eq. (IV-22) - ——.

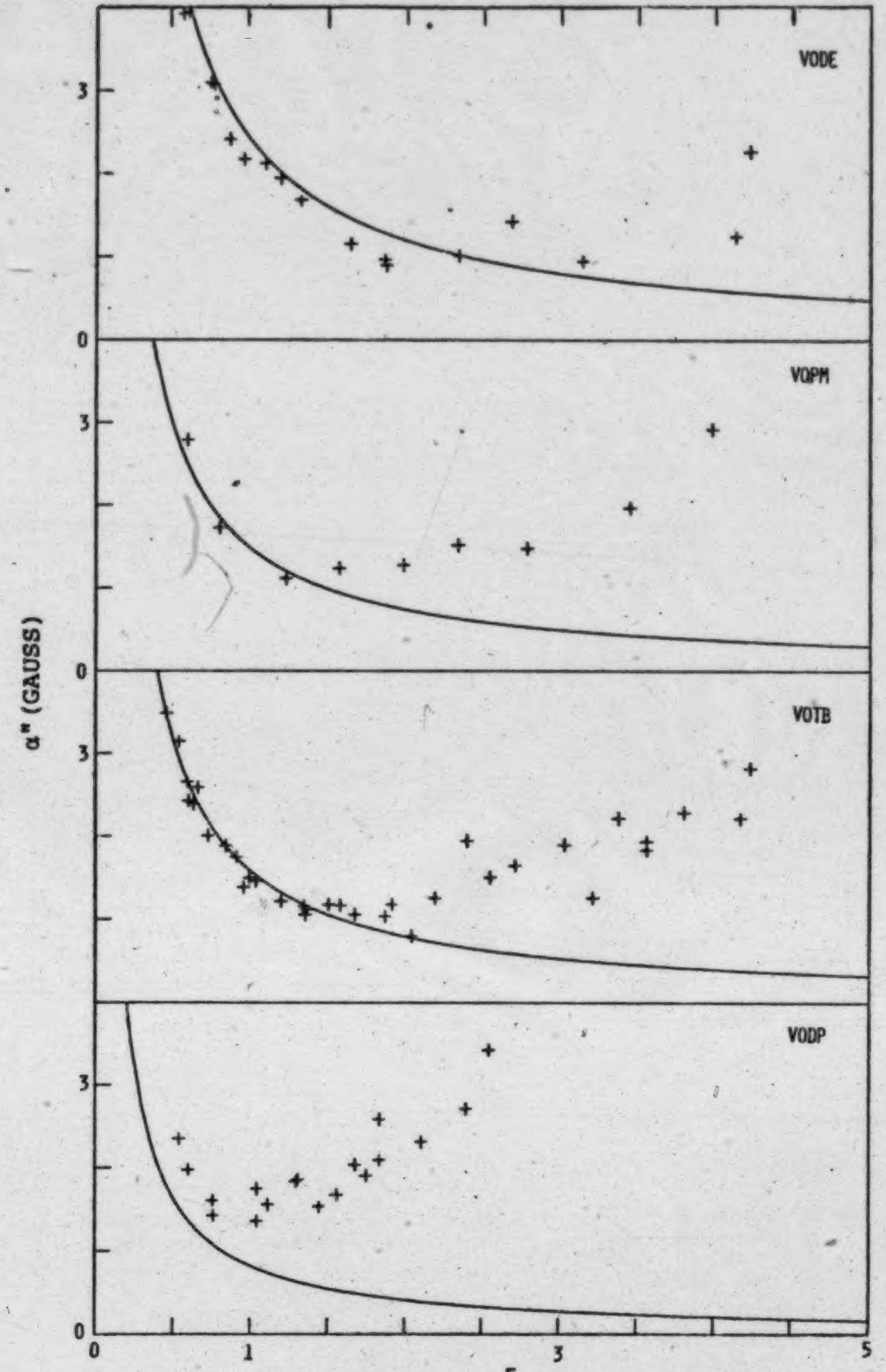
VODE
VOPM
VOTB
VODP
3
0
α" (GAUSS)
0
1
3
5
η/T x 10^5 P/°K

FIGURE 35

α'' vs η/T for carbon disulfide systems

Experimental - +, predicted by Eq. (IV-22) - ——.

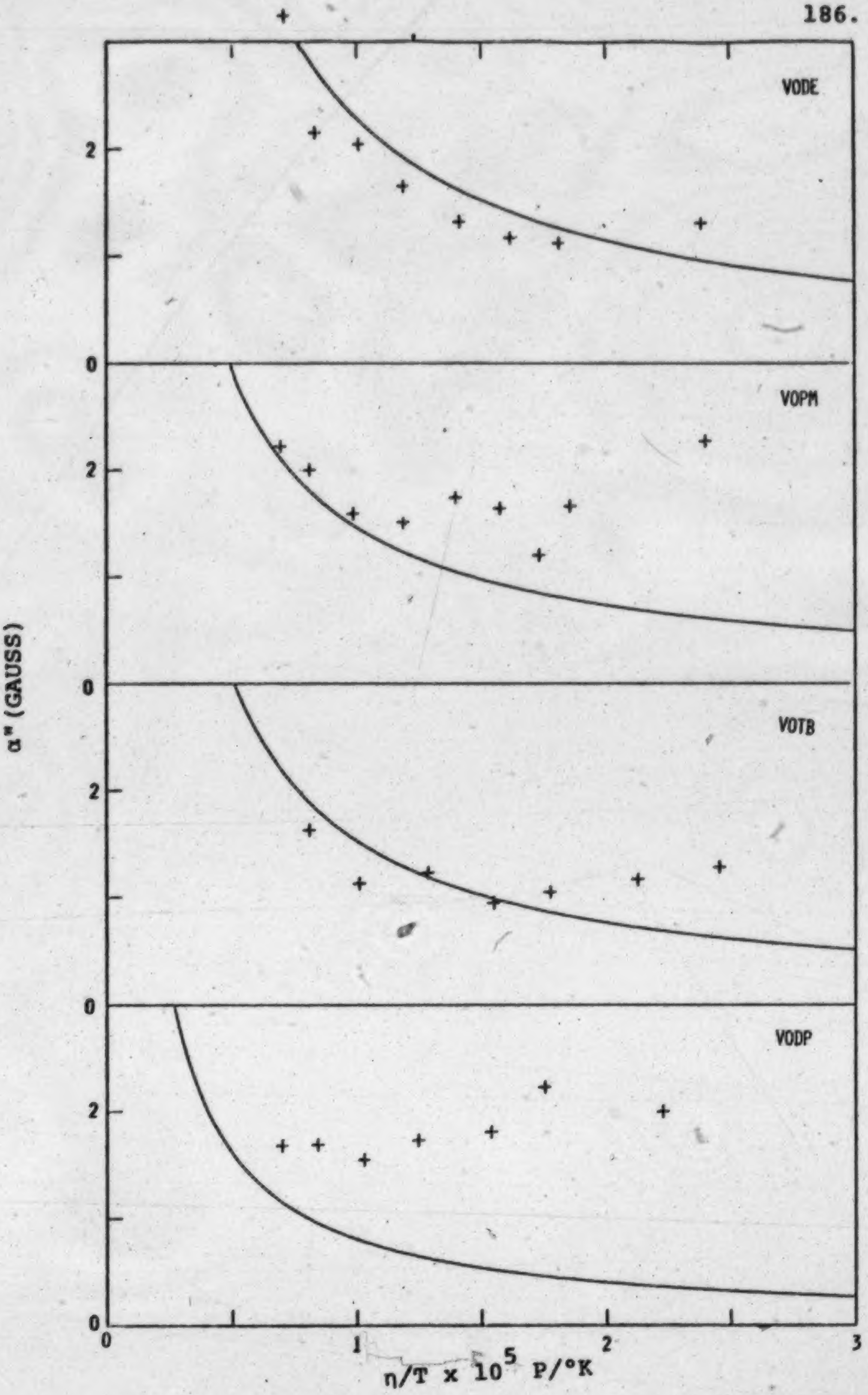
VODE
VOPM
VOTB
VODP
2
0
α" (GAUSS)
0
1
2
3
η/T x 10^5 P/°K

sentative test of the theory than is the previous method of fitting only the parameter γ. Previous workers have justified the neglect of the β parameter in terms of the sensitivity of β to experimental error. We have performed the following computer experiments in order to evaluate the sensitivity of each parameter to experimental error. Eq. (IV-8) was used to generate a set of linewidths from a given set of parameters. An error of ± 10% was then added to these linewidths and these modified linewidths were fit to Eq. (IV-8). The sign of the error added to each linewidth was determined from a table of random numbers.[97] The first 8 digits of the table were associated with the 8 lines of the first spectrum, the next 8 with the lines of the second spectrum and so on. When a digit in the range 0-4 was encountered, an increment of -10% was added to the width of the line associated with this random digit, while an increment of +10% was added if the digit encountered was in the range 5-9. The results of the least squares analyses of the modified linewidths are shown in Table 8. The three sets of parameters selected are representative of the parameters in the low temperature region. Also included in Table 8 are the results for systems in which the 10% increments were all assigned the same sign and the cases where the sign of the error was determined by the sign

TABLE 8

The Effect of a Randomly Assigned Linewidth Error on the Linewidth Parameters[†]

Error (±10%)	A			B			C		
	α	β	γ	α	β	γ	α	β	γ
+ + + + + + + +	9	9	11	9	9	9	10	8	10
- - - - - - - -	11	13	10	11	11	11	10	8	10
- - - - + + + +	1	31	5	2	28	4	2	42	8
+ + + + - - - -	1	82	5	2	66	5	2	42	8
+ - - + + + - -	5	26	15	5	24	16	5	29	26
- + + + - - + -	5	25	15	5	19	17	4	21	25
- - - + + + + -	11	38	26	11	36	31	10	35	61
+ - - - + - - +	13	13	21	14	14	16	11	13	23
+ + - + - + - -	1	5	6	1	5	7	1	4	14
- - - - + + - +	2	7	2	3	4	2	2	9	4
+ + + - - - + -	3	1	4	3	2	3	3	2	6
- - + + + - - +	0	105	2	0	90	0	1	82	2
+ - + + - - + -	0	120	3	0	12	4	0	6	6
- - - - + - - +	10	32	8	10	32	7	9	25	12
- - + + + + - +	6	25	7	6	23	6	6	19	13
- + - + - - + +	4	32	12	5	28	11	4	25	18

A[*] α = 13(53), β = 2.5(20), γ = 1.25(27). δ = 0.005(.3)

B α = 18(49), β = 4(22), γ = 2(29) δ = 0.005(.2)

C α = 13(60), β = 2.5(23), γ = .7(17) δ = 0.005(.4)

(continued......)

TABLE 8 (continued)

[*] Numbers in brackets indicate the percent contribution of the parameter to the sum defined by

$$\sum_{M} \left\{ \alpha + \beta|M| + \gamma M^2 + \delta|M|^3 \right\}$$

[†] Numbers in the table represent the percent relative error in the parameter resulting from the application of the indicated random error.

of M. The system in which the sign of the error was assigned according to the sign of M gave relatively large errors in β and relatively small errors in γ compared to those systems in which the sign of the error was determined randomly. Although the results in Table 8 represent only a few of the very large number of possible assignments of error it is clear from an examination of the results that no binding generalization can be made about the significance of experimental error in β and γ. Although γ certainly appears to be less sensitive to error than β, the errors in β are not sufficient to warrant ignoring the parameter completely. It is interesting to note the apparent stability of α and also that parameters which make larger contributions to the linewidth appear to be less sensitive to the error than those that make smaller contributions. The stability of α is particularly gratifying since the procedure of subtracting α from the linewidths to obtain the M-dependent component adds any error in α to the error in the M-dependent component. Thus it would appear that the procedure of fitting the M-dependent part of linewidths provides the best compromise between a β or γ fit in that the importance of each term is considered.

In order to study the correctness of Kivelson and Wilson's expressions [Eqs. (IV-10) - (IV-12)] independdently of Eq. (IV-24), we have fit the M-dependent parts of the linewidths from each spectrum to the corresponding theoretical expressions to obtain a value for $\tau_\theta^{(2)}$. This procedure is equivalent to allowing κ to be temperature dependent. The $\tau_\theta^{(2)}$'s determined by this procedure are plotted against η/T in Fig. 36 for three of the complexes in carbon disulfide, also included in this figure are the values of $\tau_\theta^{(2)}$ predicted by Eq. (IV-24) using the appropriate κ from Table 7. These plots are very similar in appearance to the γ vs η/T plots given in Figs. 26-33. We see that Eq. (IV-24) is compatible with the observed results at high temperatures, but, at lower temperatures, marked deviations occur. The fact that the values of $\tau_\theta^{(2)}$ determined directly from a fit of the M-dependent part of the linewidths for a given spectrum to the theoretical expressions differ from the value of $\tau_\theta^{(2)}$ obtained when Eq. (IV-24) is employed suggests that the requirement that the validity of Eq. (IV-24) be assumed throughout gives rise to a discrepancy between predicted and experimental values of the parameters. The values of β and γ obtained from these $\tau_\theta^{(2)}$ have also been plotted in Figs. 26-33. From Figs. 26-33 we see that the quality of the fit has been improved by neglecting the Stokes-Einstein relationship. This

FIGURE 36

$\tau_\theta^{(2)}$ vs /T for carbon disulfide systems

Predicted by Kivelson theory with the Stoke-Einstein relations - ———, predicted by Kivelson theory without Stokes-Einstein relation, □ -VODP, x - VOPM, + - VODE.

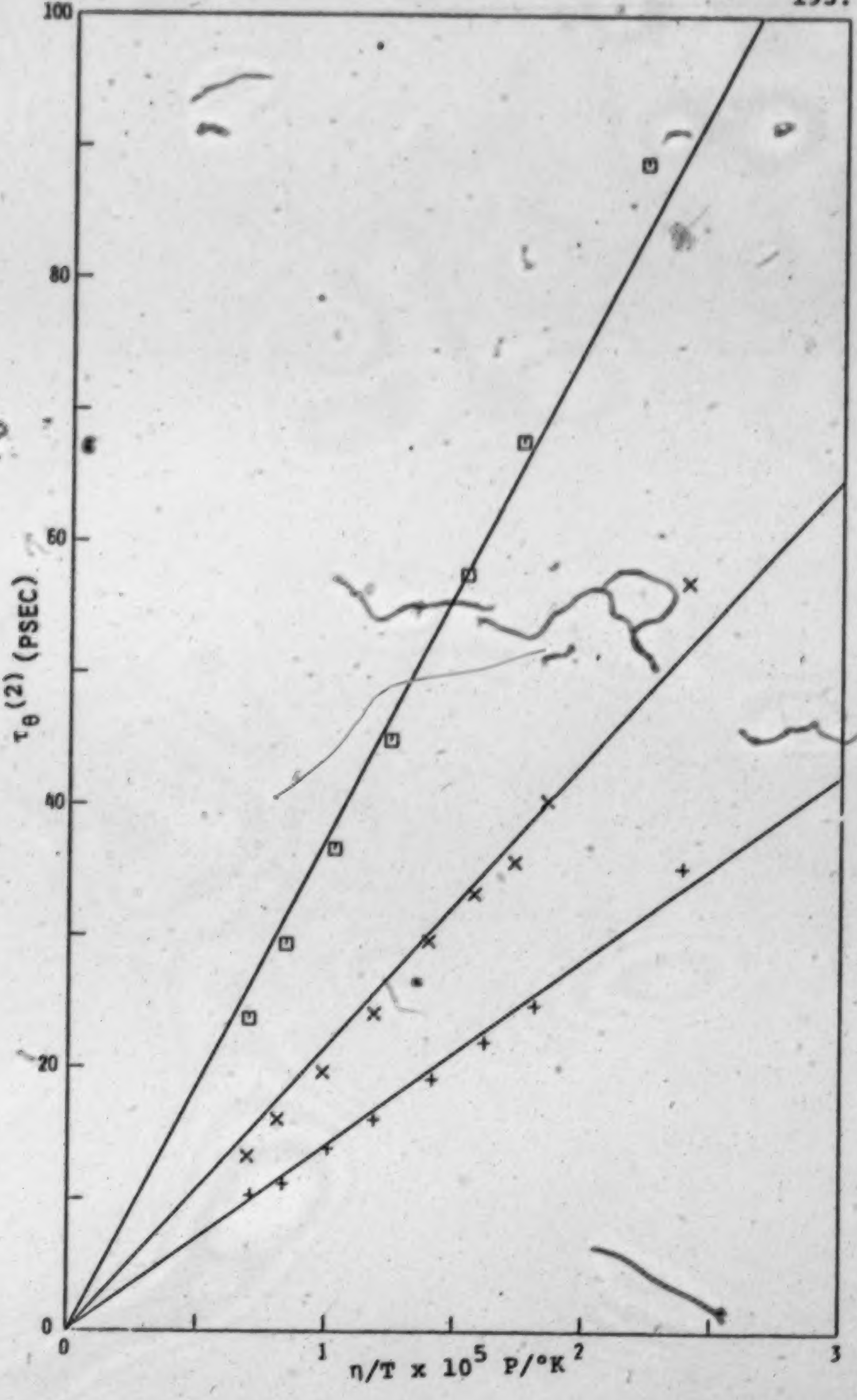
100
80
60
40
20
0
0
1
2
3
$\tau_\theta^{(2)}$ (PSEC)
$\eta/T \times 10^5$ P/°K

observation could be accounted for in one of two ways: either Eq. (IV-24) is not correct over the whole range of η/T or that the temperature and viscosity data is in error. Since the deviations generally occur in the regions outside the region where the viscosity formulae are valid the viscosity data is certainly open to question, however errors in the viscosity data would not account for the dependence of this deviation on the complex itself. For example consider the toluene systems shown in Figs. 26,28,30,32. For the VOTB and VODP systems the theory appears to break down at $\eta/T \cong 1.4 - 1.8 \times 10^{-5}$ poise/°K while for the VODE and VOPM systems the theory appears to be valid as far out as $\eta/T \cong 2.2\text{-}2.4 \times 10^{-5}$ poise/°K. Similarly for the carbon disulfide systems, the VODP and VOTB results are compatible with the theory up to $\eta/T \cong 1.3 - 1.7 \times 10^{-5}$ poise/°K while the VODE and VOPM are good out to $\eta/T \cong 1.7 - 1.9 \times 10^{-5}$ poise/°K. Note that the upper limits for a good fit nearly coincide with the upper limit of the viscosity formulae (see Table 6), this was also the case for the chloroform and DPM systems. This is possibly pure coincidence since the VOAA/toluene data already appearing in the literature [18,41,89] produce good fits in regions outside these limits.

The values of $\tau_\theta^{(2)}$ determined by analysing the data independent of Eq. (IV-24) were used with Eq. (IV-22) to predict new values of α''. The overall agreement between these α'''s and the experimental α'''s obtained using the α' predicted by Eq. IV-9 and the new $\tau_\theta^{(2)}$ is not significantly better than the agreement between predicted and "experimental" values when $\tau_\theta^{(2)}$ was restricted by the Stokes-Einstein relationship.

Kivelson _et al._[18] have considered anisotropic rotational diffusion as a possible explanation of the discrepancy between predicted and experimental values of α''. However, for complexes such as VOAA and those considered in this study the value of $\tau_\theta^{(2)}$ for reorientation about the V-O axis should not differ by more than a factor of 3 or 4 [18] from that about axes perpendicular to the V-O axis, and, since the contributions to the linewidths from rotation about the V-O axis involve only quadratic and bilinear terms in the very small parameters $\delta\gamma$ and c, it is very unlikely that anisotropic diffusion could account for the observed discrepancies.

In this study we have attempted to pinpoint the source of discrepancy between experimental linewidths and those calculated from the Kivelson linewidth theory assuming a modified Stokes-Einstein relationship. Our results indicate that the Stokes-Einstein relationship is the main source of the discrepancy between the predicted and experimental parameters β and γ. However, this observation does not account for the failure of the theory to predict the spin-rotational contribution to the linewidth, α''. Thus we conclude that for large values of η/T, the Stokes-Einstein relationship is not correct and that the simple description of the spin-rotational contributions to the linewidths given in Eq. (IV-20) is inadequate.

CONCLUSIONS

CHAPTER V

Spectral band shapes contain a great deal of information about molecular dynamics and intermolecular interactions.[2,4-10] In order to extract this information from the band shape, one must predict the influence of these factors on the observed spectral band shape. In this thesis, we have considered two different sources of information about molecular reorientation. Chapters II and III have been concerned with the extraction of reorientational information from infrared band shapes, while Chapter IV has been concerned with the extraction of this information from electron spin resonance spectra.

The Fourier transform of the infrared band shape is the reorientational correlation function of the transition dipole moment of the molecule.[2,4] This correlation function contains information about how the orientation of the molecule changes in time. The angular momentum of a molecule is changed by strong torques exerted on the molecule due to the strong intermolecular interactions of the colliding species, during a collision. In principle, if the intermolecular potential for the molecule in a fluid is known, then the average rotational motion of the molecules and thus the reorientational correlation function can be predicted. This predicted correlation function can then be compared to the corresponding experimental correlation function and the accuracy of the intermolecular potential assessed.[34-37]

The aim of the work considered in Chapters II and III was to introduce a model of reorientational motion which could predict the infrared band shape of a reorienting molecule when that band shape was distorted by quantum mechanical interactions. The previously existing theories [2,5,6,8,34-36] were either only applicable to systems in which the band shapes were nearly symmetrical or were highly mathematical theories, which were not easily applied. We have developed two semiclassical models: the first a modification of Gordon's more sophisticated semiclassical theory [2,34,35], the second a semiclassical extended rotational diffusion theory.[5,6,8]

Gordon's semiclassical band shape theory [2,34,35] required explicit knowledge of the intermolecular potential of the molecule in order to predict the outcome of a collisional event using semiclassical scattering theory. In Chapter II, Gordon's semiclassical theory was modified by describing collisional events in terms of the M- and J-diffusion limits of extended rotational diffusion theory. This model was successfully used to interpret the ν_3 infrared band shapes of methane in gaseous and liquid mixtures. This model is practical only for band shapes which could be represented by a small number of individual transitions (<40) and for this reason could not be applied to band shapes of larger molecules where a significant number of rotational states were populated, nor could it be applied to the ν_4 infrared band of methane in which Coriolis coupling caused significant splitting of the transition lines.

In Chapter III we developed a "true" semiclassical extended rotational diffusion model. This model is not severely restricted by the number of individual transitions which could be included and was applied to the ν_4 infrared band shape of methane in gaseous mixtures.

The angular momentum correlation times obtained from the analyses of the ν_3 and ν_4 band shapes [39] and those obtained from an independent NMR-T_1 study [56] show a similar density dependence (see Figs. 6,12), which indicates that the values of τ_J determined from these studies are indeed a measure of the time between strong collisional events. Recently Maryott et al. [30] have compared τ_J's, predicted from NMR-T_1 studies for several liquids including methane, with τ_{cal} the time between collisions predicted using either a cell like or gas like liquid model. They reported that the ratio τ_J/τ_{cal} varied between 1 and 2 for both models indicating that τ_J is a reasonable measure of the time between collisions, not a meaningless adjustable parameter of the theory. In introducing the extended J-diffusion picture of a collision we have ignored the details of the intermolecular potential in the liquid, however the agreement between experimental and predicted band shapes for the CO/He system obtained by Gordon and McGinnis [36], employing an assumed intermolecular potential in their molecular dynamics calculations, is no better than ours using the simpler J-diffusion picture. Thus we must conclude that until more accurate intermolecular potentials become available our simple theory is adequate for the interpretation of band shapes in terms of intermolecular interactions.

Because we have relied on the picture of a collision proposed by classical extended rotational diffusion in Chapters II and III, it is relevant at this time to very briefly mention some of the experimental evidence which supports the J-diffusion model as a reasonable interpretation of reorientational motions. Campbell, Seymour and Jonas [28] have investigated the relationship between $\tau_\theta^{(2)}$ and τ_J predicted by the classical J-diffusion model. They studied the CF_4 in the gas phase (density range 9-120 amagats) and determined τ_J from F^{19} nuclear relaxation times and measured $\tau_\theta^{(2)}$ independently from the Raman band shape. They found that the classical J-diffusion theory correctly related these two correlation times throughout the entire density range studied. Gillen *et al.*[98] have obtained similar results in the liquid region using CCl_4. The spin lattice relaxation time of ^{13}C is dominated by spin-rotational relaxation and τ_J can be calculated from the ^{13}C relaxation times. The transverse relaxation time of the ^{35}Cl nucleus is dominated by quadrupole relaxation which depends on $\tau_\theta^{(2)}$ so that values of $\tau_\theta^{(2)}$ were determined from the ^{35}Cl relaxation times. They found that classical-extended J-diffusion correctly predicted the relationship between $\tau_\theta^{(2)}$ and τ_J throughout the entire liquid region of CCl_4. Similar results for less symmetrical molecules have been obtained in the liquid region.[28,31,32] In addition, several researchers have obtained excellent agreement between experimental and predicted infrared and Raman band shapes using the classical rotational diffusion model.[7,22-28]

The energy levels of the spin states of the paramagnetic species considered in Chapter IV are dependent on the orientation of the molecule relative to the magnetic field, thus the reorientational motion of the molecule modulates the energies of these spin states and the observed ESR spectral linewidths can be interpreted in terms of the tumbling time $\tau_\theta^{(2)}$ of the molecule. The spin magnetic moment of the molecule is also weakly coupled to the rotational magnetic moment of the molecule and this spin-rotational interaction is modulated rapidly in the liquid systems considered here since the rotational state of the molecule is rapidly changed by intermolecular interactions. This gives rise to a linewidth contribution (α'') governed by the angular momentum correlation time τ_J.

The ESR linewidth approach does not yield information about the intermolecular potentials directly although Kivelson et al.[90] have indicated that the parameter κ does contain information about the anisotropy of the intermolecular potential. The reorientational correlation time $\tau_\theta^{(2)}$, which can be obtained from the linewidths, is of direct interest since it indicates the nature of the reorientational motion. $\tau_\theta^{(2)}$'s determined from ESR are often used to obtain information about the active sites of enzymes.[99] A spin label (a molecule containing a paramagnetic center) is allowed to bind to the active site. From the $\tau_\theta^{(2)}$'s of the bound and free spin label and from other changes in the observed spectra, information about the nature of the binding to the active site and about the active site itself may be obtained. For example it is possible to distinguish a binding site that firmly binds the spin label to the larger molecule from a binding site in which the bound spin label is allowed considerable freedom for independent motion.

The aim of the ESR work described in Chapter IV was to further evaluate the Kivelson linewidth theory[41-43] which interprets the linewidths of an observed ESR spectrum in terms of the modulation of the anisotropic electronic Zeeman, nuclear-electronic hyperfine and spin-rotational interactions by molecular motion. Several workers [17,18,44,45] have noted discrepancies between experimental linewidths and those predicted by the Kivelson theory. We have introduced the procedure of analyzing the M-dependent part of the linewidths in terms of the Kivelson theory rather than simply considering the contribution to the linewidth quadratic in M which was the previous practice. We have justified this procedure using computer experiments on test cases and feel that the results from studying the M-dependent part of the linewidth are much more representative of the theory because each parameter is considered in terms of its contribution to the linewidth. We have also analyzed single spectra and obtained values of $\tau_\theta^{(2)}$ independent of the Stokes-Einstein hydrodynamic relationship.[81] These results indicate that if the Stokes-Einstein relationship is ignored, then the agreement between predicted and experimental results is improved. Thus it appears that the assumption of the Stokes-Einstein relationship is the main cause of the discrepancy between predicted and experimental results, however it does not explain the discrepancy between the predicted and experimental α'' which is much greater than that expected from experimental error. Therefore, we conclude that although the deficiency in the β and γ parameters could be accounted for in terms of the assumptions of the Stokes-Einstein relationship, the simple theory predicting the linewidth contribution due to the spin-rotational coupling must be reconsidered.

It would be interesting to study the ^{63}Cu diketonate complexes corresponding to those studied in Chapter IV. The spin-rotational coupling for copper is much larger than for vanadium and thus the α'' contribution to the linewidth would be proportionately larger for the copper complexes. The α'''s determined from such a study, being larger, would have a smaller relative experimental error and thus would provide a more stringent test of the validity of the expressions used to predict α''.

REFERENCES

1. L. J. Marabella, in Spectroscopy of Solvent Systems, edited by D. Burow (Marcel Dekker, New York, 1973) p.313ff.
2. R. G. Gordon, Adv. Magn. Reson. 3, 1 (1968).
3. A. Messiah, Quantum Mechanics, (North-Holland Publishing Company, Amsterdam, 1961) Vol. 1 Chapter VIII.
4. R. G. Gordon, J. Chem. Phys. 42, 3658 (1965).
5. R. G. Gordon, J. Chem. Phys. 44, 1830 (1966).
6. R. E. D. McClung, J. Chem. Phys. 51, 3842 (1969); J. Chem. Phys. 54, 3248 (1971); R. E. D. McClung and H. Versmold, J. Chem. Phys. 57, 2596 (1972).
7. R. E. D. McClung, J. Chem. Phys. 55, 3459 (1971).
8. R. E. D. McClung, J. Chem. Phys. 57, 5478 (1972).
9. F. J. Bartoli and T. A. Litovitz, J. Chem. Phys. 56, 404 (1972).
10. F. J. Bartoli and T. A. Litovitz, J. Chem. Phys. 56, 413 (1972).
11. L. Pauling and E. B. Wilson, Jr., Introduction to Quantum Mechanics (McGraw-Hill, New York, 1935), Chapter XI; E. B. Wilson, Jr., J. C. Decius and P. C. Cross, Molecular Vibrations (McGraw-Hill, New York, 1955), Chapter 7.
12. D. E. O'Reilly, J. Chem. Phys. 49, 5416 (1968).
13. D. E. O'Reilly and E. M. Peterson, J. Chem. Phys. 55, 2155 (1971).
14. D. E. O'Reilly, J. Chem. Phys. 56, 2924 (1972).

15. D. E. O'Reilly, E. M. Peterson and C. E. Scheie, J. Chem. Phys. 60, 1603 (1974).

16. R. T. C. Brown, H. S. Gutowski and K. Shimomura, J. Chem. Phys. 38, 76 (1963).

17. R. Huang and D. Kivelson, Pure Appl. Chem. 32, 207 (1972).

18. J. Hwang, D. Kivelson and W. Plachy, J. Chem. Phys. 58, 1753 (1973).

19. P. Debye, Polar Molecules (Reinhold Publ. Corp., New York, 1929), (also reprinted by Dover Publications, Inc., New York).

20. N. Bloembergen, E. M. Purcell and P. V. Pound, Phys. Rev. 73, 679 (1948).

21. M. Bloom, F. Bridges and W. N. Hardy, Can. J. Phys. 45, 3533 (1967).

22. G. Lévi, M. Chalaye and E. Dayan, Compt. Rend. Acad. Sci. (Paris) 274B, 50 (1972).

23. G. Lévi and M. Chalaye, Chem. Phys. Letters 19, 263 (1973).

24. G. Lévi, M. Chalaye, F. Marsault-Herail and J. P. Marsault, Mol. Phys. 24, 1217 (1972).

25. J. P. Marsault, F. Marasault-Herail and G. Lévi, Mol. Phys. 26, 997 (1973).

26. S. Sunder and R. E. D. McClung, Chem. Phys. 2, 467 (1973).

27. S. Sunder and R. E. D. McClung, Can. J. Phys. in press (1974).

28. J. H. Campbell, S. J. Seymour and J. Jonas, J. Chem. Phys. 59, 4151 (1973).

29. K. T. Gillen, D. C. Douglass, M. S. Malmberg and A. A. Maryott, J. Chem. Phys. 57, 5170 (1972).

30. A. A. Maryott, M. S. Malmberg and K. T. Gillen, Chem. Phys. Letters, 25, 169 (1974).

31. R. A. Assink and J. Jonas, J. Chem. Phys. 57, 3329 (1972).

32. A. A. Maryott, T. C. Farrar and M. S. Malmberg, J. Chem. Phys. 54, 64 (1971).

33. R. E. D. McClung, Chem. Phys. Letters, 19, 304 (1973).

34. R. G. Gordon, J. Chem. Phys. 45, 1649 (1966).

35. W. A. Neilsen and R. G. Gordon, J. Chem. Phys. 58, 4131 (1973).

36. R. G. Gordon and R. P. McGinnis, J. Chem. Phys. 55, 4898 (1971).

37. W. B. Neilsen and R. G. Gordon, J. Chem. Phys. 58, 4149 (1973).

38. A. Cabana, R. Bardoux and A. Chamberland, Can. J. Chem. 47, 2915 (1969).

39. R. L. Armstrong, S. M. Blumenfield and C. G. Gray, Can. J. Phys. 46, 1331 (1968).

40. G. Herzberg, Molecular Spectroscopy. II Infrared and Raman Spectra of Polyatomic Molecules, (van

Nostrand, Princeton, N.J., 1945), p.447ff.

41. R. Wilson and D. Kivelson, J. Chem. Phys. 44, 154 (1966).

42. R. E. D. McClung and D. Kivelson, J. Chem. Phys. 49, 3380 (1968).

43. P. W. Atkins and D. Kivelson, J. Chem. Phys. 44, 169 (1966).

44. N. S. Angerman and R. B. Jordan, J. Chem. Phys. 54, 837 (1971).

45. N. D. Chasteen and M. W. Hanna, J. Phys. Chem. 76, 3951 (1972).

46. R. G. Gordon, J. Chem. Phys. 43, 1307 (1965).

47. M. Fixman and K. Rider, J. Chem. Phys. 51, 2425 (1969).

48. A. G. St. Pierre and W. A. Steele, Phys. Rev. 184, 172 (1969).

49. A. G. St. Pierre and W. A. Steele, J. Chem. Phys. 57, 4638 (1972).

50. F. Perrin, J. Phys. Radium 5, 497 (1934).

51. W. H. Furry, Phys. Rev. 107, 7 (1957).

52. L. D. Favro, Phys. Rev. 119, 53 (1960).

53. A. Einstein, Theory of Brownian Movement, edited by R. Furth, translated by A. D. Cowper (Dover Publications, New York, 1956).

54. P. Rigny and J. Virlet, J. Chem. Phys. 47, 4645 (1967).

55. C. S. Johnson, Jr., Adv. Magn. Reson. 1, 33 (1965).

56. C. J. Gerritsma, P. H. Oosting and N. J. Trappeniers, Physica (Utr.) 51, 381 (1971); P. H. Oosting and N. J. Trappeniers, Physica (Utr.) 51, 395 (1971); Physica (Utr.) 51, 418 (1971).

57. R. F. Curl, Jr., J. V. V. Kasper, K. S. Pitzer and K. Sathianandan, J. Chem. Phys. 44, 4636 (1966); R. F. Curl, J. V. V. Kasper and K. S. Pitzer, J. Chem. Phys. 46, 3220 (1967).

58. H. A. Jahn, Proc. R. Soc. Lond. 168, 469, 495 (1938).

59. E. K. Plyler, E. D. Tidwell and L. R. Blaine, J. Res. Natl. Bur. Stand. (U.S.) 64A, 201 (1960).

60. W. H. J. Childs and H. A. Jahn, Proc. R. Soc. Lond. 169, 451 (1939).

61. E. B. Wilson, Jr., J. Chem. Phys. 3, 276 (1935).

62. R. G. Gordon and R. P. McGinnis, J. Chem. Phys. 49, 2455 (1968).

63. A. Ben-Reuven, S. Kimel, M. A. Hirshfeld and J. H. Jaffe, J. Chem. Phys. 35, 955 (1961).

64. H. L. Welsh, P. E. Pashler and A. F. Dunn, J. Chem. Phys. 19, 340 (1951).

65. F. Bliot, C. Abbar and E. Constant, Mol. Phys. 24, 241 (1972).

66. F. Bliot and E. Constant, Chem. Phys. Letters 18, 253 (1973).

67. D. J. Berne and G. D. Harp, Adv. Chem. Phys. 17, 63 (1970).

68. M. E. Rose, Elementary Theory of Angular Momentum (Wiley, New York, 1957).

69. D. L. Kreider, R. G. Kuller, D. R. Ostberg and F. W. Perkins, An Introduction to Linear Analysis (Addison-Wesley, Don Mills, Ontario, 1966) p.206ff.

70. S. G. Mikhlin and K. L. Smolitskiy, Approximate Methods for Solution of Differential and Integral Equations, (American Elsevier, New York, 1967) p.285.

71 J. Moret-Bailly, J. Molec. Spectry. 15, 344 (1965).

72. M. Migeotte, L. Neven and J. S. Swensson, An Atlas of Nitrous Oxide, Methane and Ozone Infrared Absorption Bands, (Louvain, Univ. of Liege, 1958).

73. J. Moret-Bailly, Cahiers Phys. 15, 237 (1961).

74. T. E. Eagles and R. E. D. McClung, Chem. Phys. Letters, 22, 414 (1973).

75. J. Moret-Bailly, L. Gautier and J. Montagutelli, J. Molec. Spectry. 15, 355 (1965).

76. M. Chalaye, E. Dayan and G. Lévi, Chem. Phys. Letters, 8, 337 (1971).

77. G. Lévi, M. Chalaye and E. Dayan, Chem. Phys. Letters, 12, 462 (1972).

78. R. G. Gordon, J. Chem. Phys. 39, 2788 (1963).

79. J. C. Jaeger, Introduction to Laplace Transformation (Methuen, London 1949), p.7.

80. H. Margenau and G. M. Murphy, Mathematics of Physics and Chemistry, (Van Nostrand, Princeton, N.J. (1956).

81. R. Kubo and K. Tomita, J. Phys. Soc. Japan 9, 888 (1954).

82. D. Kivelson, J. Chem. Phys. 27, 1087 (1957); J. Chem. Phys. 33, 1094 (1960).

83. J. H. Freed and G. K. Fraenkel, J. Chem. Phys. 39, 326 (1963).

84. A. Hudson and G. R. Luckhurst, Chem. Rev. 69, 191 (1969).

85. A. G. Redfield, Adv. Magn. Reson. 1, 1 (1965).

86. C. P. Slitchter, Principles of Magnetic Resonance, (Harper and Row Publishers, New York, 1963).

87. A. Abragam, The Principles of Nuclear Magnetism (Oxford University Press, Oxford, 1961).

88. P. S. Hubbard, Phys. Rev. 131, 1155 (1963).

89. R. Wilson and D. Kivelson, J. Chem. Phys. 44, 4440 (1966).

90. D. Kivelson, M. G. Kivelson and I. Oppenheim, J. Chem. Phys. 52, 1810 (1970); J. Phys. Soc. Japan 26, 288 (1969).

91. Inorganic Synthesis, edited by T. Moeller (McGraw-Hill, New York, 1957) Vol. V, p.113ff.

92. S. H.Glarum and J. H. Marshall, J. Chem. Phys. 41, 2182 (1964).

93. R. E. D. McClung, Can. J. Phys. 46, 2271 (1968).

94. M. A. Hitchman and R. L. Belford, Inorg. Chem. 8, 958 (1969).

95. International Critical Tables (Kynoch Press, Birmingham, England,1930), Vol. 7, p.213; (1929), Vol. 5, p.11.

96. J. N. Friend and W. D. Hargreaves, Phil. Mag. 35, 136 (1944).

97. Handbook of Mathematical Functions, edited by M. Abramowitz and I. A. Segun (Dover Publications, New York, 1964).

98. K. T. Gillen, J. H. Noggel and T. K. Leipert, Chem. Phys. Letters 17, 505 (1972).

99. Molecular Biology, edited by A. Rich and N. Davidson (W. H. Freeman and Co., San Francisco, 1968), p.113ff.

100. Reference 68, Section 13.

101. Reference 68, Section 16.

102. Wigner (Gruppentheorie, Friendrich Vieweg une Sohn, Braunschweig, 1931) p.231.

103. Reference 68, Section 14.

104. Reference 68, Chapter V.

APPENDIX I

THE WIGNER $\mathcal{D}$ MATRIX AND ANGULAR MOMENTUM THEORY

In order to describe the effects of rotational motion of molecules on the interactions between the molecule and an external field, it is often necessary to define a tensor in a given coordinate system in terms of its components in another coordinate system. For example we are often interested in defining an electric field in a molecular coordinate system in terms of its components in the laboratory coordinate system. Throughout this thesis, rotations have been described using the conventions of Rose.[68] In this convention, the coordinate systems are rotated and not the functions. The sense of a rotation follows the right-hand screw rule i.e. roations of a right-handed coordinate system +90° about the z-axis rotates the x-axis onto the original positive y-axis. The rotation of a coordinate system by an amount α is equivalent to the rotation of a function by an amount $-\alpha$ thus if the operator $\hat{R}_z(\alpha)$ represents the rotation of the coordinate system by an angle α about the z-axis then

$$\hat{R}_z(\alpha)f(\phi) = f(\phi-\alpha) \qquad \text{(A-1)}$$

where $f(\phi)$ is the function and ϕ is the azimuthal angle of polar coordinates. Performing a Taylor series expansion of the function $f(\phi-\alpha)$ we obtain

$$f(\phi-\alpha) = \sum_{n=0}^{\infty} \frac{1}{n!} \left(-\alpha \frac{\partial}{\partial\phi}\right)^n f(\phi) \tag{A-2}$$

$$= \exp\left(-\alpha \frac{\partial}{\partial\phi}\right) f(\phi),$$

thus the rotation operator $\hat{R}_z(\alpha)$ is given by $\exp\left(-\alpha \frac{\partial}{\partial\phi}\right)$. In spherical polar coordinates, the reduced angular momentum operator $\hat{J}_z$ is given by

$$\hat{J}_z = -i \frac{\partial}{\partial\phi},$$

thus the rotation operator is

$$\hat{R}_z(\alpha) = \exp(-i\alpha\hat{J}_z) . \tag{A-3}$$

Similar considerations yield

$$\hat{R}_x(\alpha) = \exp(-i\alpha\hat{J}_x) , \tag{A-4}$$

and

$$\hat{R}_y(\alpha) = \exp(-i\alpha\hat{J}_y) , \tag{A-5}$$

where $\hat{J}_x$ and $\hat{J}_y$ are the reduced angular momentum operators for the x and y components of the angular momentum.

Any general transformation between two coordinate systems can be represented by three successive rotations. The Eulerian transformation is a most useful way of carrying out such a coordinate transformation. It is defined in terms of the following three rotations: (1) the coordinate system (x, y, z) is rotated through an angle α about the z-axis to become (x', y', z'), (2) the coordinate system (x', y', z') is then rotated through an angle β about the y'-axis to become (x", y", z"), (3) the coordinate system (x", y", z") is then rotated through an angle γ about the z"-axis to yield the desired coordinate systems (x‴, y‴, z‴). The angles α, β, $\gamma \equiv \Omega$ are referred to as the Euler angles of the transformation. In terms of the rotation operators defined in Eqs. (A-3) - (A-5) the Eulerian transformation is

$$\begin{aligned}\hat{R}(\alpha,\beta,\gamma) &= \hat{R}_{z''}(\gamma)\hat{R}_{y'}(\beta)\hat{R}_{z}(\alpha)\\ &= \exp(-i\gamma\hat{J}_{z''})\exp(-i\beta\hat{J}_{y'})\exp(-i\alpha\hat{J}_{z}).\end{aligned} \tag{A-6}$$

It can be shown [100] that the rotations, described in Eq. (A-6) about axes in different coordinate systems, can be expressed as rotations about axes in the initial coordinate system, provided that the rotations are done in the reverse order. Thus,

$$\hat{R}(\alpha,\beta,\gamma) = \exp(-i\alpha\hat{J}_{z})\exp(-i\beta\hat{J}_{y})\exp(-i\gamma\hat{J}_{z}). \tag{A-7}$$

The Wigner rotation matrix or $\mathcal{D}$-matrix is the matrix representation of the rotation operator in angular momentum space and is defined by

$$\hat{R}(\alpha,\beta,\gamma)\left|J,M\right\rangle = \sum_{M'} \left|J,M'\right\rangle \mathcal{D}^{(J)}_{M'M}(\alpha,\beta,\gamma). \quad \text{(A-8)}$$

where $\left|J,M\right\rangle$ is an angular momentum wavefunction. Substituting Eq. (A-7) into Eq. (A-8) and premultiplying by $\left\langle J,M'\right|$, we obtain

$$\mathcal{D}^{(J)}_{M'M}(\alpha,\beta,\gamma) = \left\langle J,M'\right|\hat{R}(\alpha,\beta,\gamma)\left|J,M\right\rangle$$

$$= \exp(-i\alpha M')\left\langle J,M'\right|\exp(-i\beta\hat{J}_y)\left|J,M\right\rangle \exp(-i\gamma M), \quad \text{(A-9)}$$

where the operator $\hat{J}_z$ has been applied to $\left\langle J,M'\right|$ and $\left|J,M\right\rangle$.

From Eqs. (A-6) - (A-9) the relationships [Eqs. (III-18) and (III-19)] used in Chapter III can be obtained:

$$\mathcal{D}^{(J)}_{M'M}(\alpha,0,0) = \exp(-i\alpha)\,\delta_{M,M'} \quad \text{(A-10)}$$

and

$$\mathcal{D}^{(J)}_{M'M}(\alpha,\beta,\gamma)^{-1} = \mathcal{D}^{(J)}_{M',M}(-\alpha,\,-\beta,\,-\gamma)$$

$$= \mathcal{D}^{(J)*}_{M,M'}(\alpha,\beta,\gamma)\ , \quad \text{(A-11)}$$

also it can be shown[100] that

$$\mathcal{D}^{(J)*}_{M'M}(\alpha,\beta,\gamma) = (-1)^{M'-M}\,\mathcal{D}^{(J)}_{-M',-M}(\alpha,\beta,\gamma) \quad \text{(A-12)}$$

The orthogonality relationships [Eq. (III-20) - (III-21)] are developed in detail by Rose[101] and will not be given here since the development is extensive. Wigner[102] has shown that the $\mathcal{D}$-matrices are proportional to the rotational wavefunction for a symmetric top, Ψ_{JKM}. This relationship is given by

$$\Psi_{JKM}(\alpha,\beta,\gamma) = \left(\frac{2J+1}{8\pi^2}\right)^{\frac{1}{2}} \mathcal{D}^{(J)}_{-K-M}(\alpha,\beta,\gamma) \quad \text{(A-13)}$$

where the multiplicative term is a normalizing constant.

The coupling of two angular moments is described by the Clebsch-Gordon series defined by,

$$|J,M\rangle = \sum_{M_1} C(J_1J_2J;M_1,M-M_1)\,|J_1,M_1\rangle\,|J_2,M-M_1\rangle \quad \text{(A-14)}$$

where

$$J_1 + J_2 \geq J \geq |J_1 - J_2| \quad \text{(A-15)}$$

and C is the Clebsch-Gordon coefficient. The function $|J,M\rangle$ is the angular momentum wavefunction of the coupled representation while $|J_1,M_1\rangle$ and $|J_2,M-M_1\rangle$

are wavefunctions of the uncoupled representation. Using Eqs. (A-8) and (A-14) one can obtain[103]

$$\mathcal{D}^{(J_1)}_{K,M}(\Omega)\ \mathcal{D}^{(J_2)}_{K_2M_2}(\Omega) = \sum_J C(J_1J_2J;K_1K_2)C(J_1J_2J;M_1M_2)\ \mathcal{D}^{(J)}_{K_1+K_2,M_1+M_2}(\Omega)\ . \qquad \text{(A-16)}$$

This relationship is often useful in simplifying expressions containing products of $\mathcal{D}$-matrices.

If we define tensors so that they transform under rotations in the same way as the angular momentum wavefunctions do, then all the relationships derived to manipulate angular momentum wavefunctions using the $\mathcal{D}$-matrix can be used to manipulate these tensors. Tensors defined in this way are referred to as spherical tensors. The components of a tensor operator $\hat{T}_\ell$ of rank ℓ satisfy the following comutator relationships,[104]

$$\left[\hat{J}_z, \hat{T}_{\ell u}\right] = u\hat{T}_{\ell u} \qquad \text{(A-17)}$$

$$\left[\hat{J}_+, \hat{T}_{\ell u}\right] = \sqrt{\ell(\ell+1)-u(u+1)}\ \ T_{\ell,u+1}. \qquad \text{(A-18)}$$

$$\left[\hat{J}_-, \hat{T}_{m}\right] = \sqrt{\ell(\ell+1)-u(u-1)}\ \ T_{\ell,u-1}\ . \qquad \text{(A-19)}$$

where J_+ and J_- are the raising and lowering operators, A first rank spherical tensor operator has components

$$\hat{T}_{10} = \hat{T}_z \tag{A-20}$$

$$\hat{T}_{1\pm1} = \mp \frac{1}{\sqrt{2}} \left(\hat{T}_x \pm i\hat{T}_y \right) \tag{A-21}$$

where $\hat{T}_q$, $q = x,y,z$ are the components of the corresponding cartesian tensor operator. The angular momentum operators used in Eqs. (A-17) - (A-19) can also be defined in terms of the cartesian components.

In obtaining Eq. (III-6) in Chapter III, we have assumed that the mixed products of $\mathcal{D}$-matrices in Eq. (III-5) vanished when ensemble averages were performed. This will now be demonstrated using the relationships given above and the orthogonality relationships given by Rose.[101] The expression of interest is the integral over all orientations,

$$K = \int d\Omega \left\langle JKM \middle| \mathcal{D}^{(\ell)*}_{km}[\Omega] \middle| J'K'M' \right\rangle \left\langle J'K'M' \middle| \mathcal{D}^{(\ell)}_{k'm'}[\Omega] \middle| JKM \right\rangle . \tag{A-22}$$

Henceforth the argument Ω of the $\mathcal{D}$-matrices will not be shown explicitly since it is Ω in all cases. Substituting Eq. (A-13) into Eq. (A-22) and using Eq. (A-12) we obtain

$$K = \int d\Omega \, \frac{(2J+1)(2J'+1)}{(8\pi^2)^2} (-1)^{M'-K'} \mathfrak{D}^{(J)*}_{-K-M} \mathfrak{D}^{(\ell)*}_{km}$$

$$\mathfrak{D}^{(J')}_{K'M'} \mathfrak{D}^{(J')}_{-K'-M'} \mathfrak{D}^{(\ell)}_{k'm'} \mathfrak{D}^{(J)}_{-K-M} \, . \qquad \text{(A-23)}$$

After applying the coupling expression [Eq. (A-16)] we obtain

$$K = \frac{(2J+1)(2J'+1)}{(8\pi^2)^2} (-1)^{M'-K'} \sum_{\mathcal{J},\mathcal{J}',\mathcal{J}''} C(J\ell\mathcal{J};-Kk)^{*} C(J\ell\mathcal{J};-Mm)^{*}$$

$$\times\, C(J'J'\mathcal{J}';K',-k')C(J'J'\mathcal{J}';M'-M')C(\ell J\mathcal{J}'';K',-K)C(\ell J\mathcal{J}'';m',-M)$$

$$\int d\Omega \, \mathfrak{D}^{(\mathcal{J})}_{\mathcal{K}\mathcal{M}} \mathfrak{D}^{(\mathcal{J}')}_{00} \mathfrak{D}^{(\mathcal{J}'')}_{\mathcal{K}''\mathcal{M}''} \qquad \text{(A-24)}$$

where $\mathcal{K} = -K+k \qquad \mathcal{K}'' = -K+k'$

$\mathcal{M} = -M+m \qquad \mathcal{M}'' = -M+m'$. (A-25)

The orthogonality relation for a triple product of $\mathfrak{D}$-matrix components given by Rose[101] reduces the integral in Eq. (A-18) to

$$\frac{8\pi^2}{2\mathcal{J}+1} C(\mathcal{J}\mathcal{J}'\mathcal{J}'';\mathcal{K}'0)C(\mathcal{J}\mathcal{J}'\mathcal{J}'';\mathcal{M}'0)\delta_{\mathcal{K}'+0,\mathcal{K}}\delta_{\mathcal{M}'+0,\mathcal{M}} \, .$$

Thus the integral vanishes unless $K' = K$ and $M' = M$. Combining these conditions with (Eq. (A-25) we find the integral vanishes unless k = k' and m = m' which is the required condition assumed in Chapter III.

APPENDIX II

This Appendix gives the FORTRAN computer programs used in the course of this work.

A. Semiclassical Band Shape Program (Gordon method).

B. Program to calculate the free rotor memory function from the free rotor correlation function.

C. Program to calculate the correlation function from the free rotor memory function.

D. Linear and non-linear least squares programs used in Chapter IV.

1. Program to fit linewidths to a cubic function in M.

2. Program to fit M-dependent part of the linewidth.

```
C
C    THIS PROGRAM CALCULATES SPECTRAL DENSITIES AND REORIENTATIONAL
C    CORRELATION FUNCTIONS USING EITHER M OR J DIFFUSION
C
C    CARD #1 : TEMPERATURE; TAUJ; HEIGHT OF HEIGHT NORMALIZED
C              SPECTRA; MAXIMUM J QUANTUM NUMBER (DEFAULT=9
C                       : MAX=12);
C              IPLOT( CONTROL PARAMETER); FM M OR J ?
C              TEMP <0.0   STOP.
C
C    FM=1 100% M-DIF
C    FM=0  100% J-DIF
C    IPLOT 0--YES;  1-- NO
C    1. HEIGHT ?
C    2. G(T) ?
C    3. AREA   PLOTS ?
C
C    CARD #2: TITLE TO APPEAR ON PLOTS AND OUTPUT
      COMPLEX*8 SM(3,3),MLAM(3),DUMP3(3,3)
      REAL OMO(37),D(37),P(37),RI(345),OMOW(345),WW(191),BUFFER(1024),
     #  TITLE(22),XX(191)
      COMPLEX*8 S(37,37),SINV(37,37),LAM(37),C1,SUMA,SUMB,A(37),B(37),
     #  RC(345),DUMMY(37,37)
      REAL NORM,DEG(13),XD(2)
      LOGICAL INTH(37)
      INTEGER INT(37),IPLOT(3)
      DATA OMO/3028.740,3038.500,3048.180,3057.720,3067.240,3076.650,
     #  3086.410,3095.190,3104.450,3113.430,3018.810,3018.640,3018.380,
     #  3018.620,3017.470,3016.940,3016.510,3016.070,3015.610,3009.000,
     #  2999.010,2988.920,2978.880,2968.630,2958.340,2948.060,2937.830,
     #  2927.200,3122.75,3014.13,2916.72,3131.87,3013.29,2906.20,
     #  3140.311,3012.44,2895.62/
      DATA TITLE/'INTE','NSIT','Y   ','FREQ','UENC','Y   ',16*'    '/
      DATA D/1.0000000,0.7453560,0.6831300,0.6546536,0.6382847,
     #  0.6276459,0.6201736,0.6146362,0.6103679,0.6069769,0.5773502,
     #  0.5773502,0.5773502,0.5773502,0.5773502,0.5773502,.5773502,
     #  0.5773502,0.5773502,0.3333333,0.4472135,0.4879500,0.5091750,
     #  0.5222329,0.5310850,0.5374838,0.5423261,0.5461186,0.6042180,
     #  0.5773503,0.5491696,0.6019293,0.5773503,0.5516773,0.6,0.5773503,
     #  0.5537749/
      DATA DEG/5.0,9.0,25.0,77.0,117.0,121.0,273.0,285.0,357.0,513.0,
     #  609.0,621.0,925.0/
      DATA NORM/'NORM'/
C
C     INITIATION OF PLOTS
C
      REAL YD(2)/0.0,2.0/
      IC=0
      YORIG=-10.0
      XORIG=17.0
      XSIZE=14.9606
      YSIZE=7.874
      CALL PLOTS(BUFFER,4096)
      CALL PLOT(2.0,2.0,-3)
    1 READ (5,901,END=29) TEMP,TAUJ,HEIGHT,J,(IPLOT(I),I=1,3),FM
      IF (TEMP.LT.0.0) GO TO 29
      READ (5,902) (TITLE(I),I=7,22)
      N=28
      IF (J.NE.0) N=J+J+J+1
      JJJ=J
C
C    CALCULATION OF POPULATIONS
C    DEG=((2J+1)**2) (NUC.SPIN.FACTOR)
C    P=DEG*EXP(-E/KT)
C    -E/KT=-7.51702*J*(J+1)/TEMP
C
      EFAC=-7.51702/TEMP
      P(1)=DEG(1)
      SUM=DEG(1)
      DO 2 J=2,10
      TERM=DEG(J)*EXP(EFAC*FLOAT((J-1)*J))
      K=J+9
      M=J+18
      P(J)=TERM
      P(K)=TERM
      P(M)=TERM
    2 SUM=SUM+TERM
      IF (N.EQ.28) GO TO 4
      NJ=N/3
      KKK=NJ+1
      K2=28
      DO 3 J=11,KKK
      K=K2+1
      K1=K+1
      K2=K+2
      TERM=DEG(J)*EXP(EFAC*FLOAT((J-1)*J))
      P(K)=TERM
      P(K1)=TERM
      P(K2)=TERM
    3 SUM=SUM+TERM
    4 CONTINUE
      DO 5 J=1,N
    5 P(J)=P(J)/SUM
C
C     SETTING UP S-MATRIX
C
      DEN=(1.88496E11)*TAUJ
      P(1)=3.0*P(1)
      DO 6 I=1,N
      DO 6 J=1,N
      DEL=0.0
      IF (I.EQ.J) DEL=1.0
      REALS=((DEL-0.3333333*P(J)*D(J)/D(I))/DEN)*(FM-1.0)
      IF (P(J).EQ.P(I)) REALS=REALS-FM*(DEL-(D(J)/(3.0*D(I))))/DEN
      COMPS=DEL*OMO(I)
    6 S(J,I)=CMPLX(REALS,COMPS)
      P(1)=P(1)/3.0
C
C     DIAGONALIZATION
C
      IF (FM.NE.1.0) GO TO 15
C
C     M-DIFFUSION
C
      DO 10 IDIG=1,9
      KK=IDIG+1
      DO 7 I=1,3
      K=KK+9*(I-1)
      SM(I,1)=S(K,KK)
      SM(I,2)=S(K,KK+9)
    7 SM(I,3)=S(K,KK+18)
      CALL ALLMAT(SM,MLAM,3,3,NCAL,DUMP3,DUMMY,A,B,INTH,INT)
      WRITE (6,903) NCAL
C
C     PLACING INFORMATION BACK INTO S-MATRIX
C
      DO 8 I=1,3
      K=KK+9*(I-1)
      S(K,KK)=SM(I,1)
      S(K,KK+9)=SM(I,2)
      S(K,KK+18)=SM(I,3)
    8 LAM(K)=MLAM(I)
      CALL CMINVS(SM,3,3)
      DO 9 I=1,3
      K=KK+9*(I-1)
      SINV(K,KK)=SM(I,1)
      SINV(K,KK+9)=SM(I,2)
    9 SINV(K,KK+18)=SM(I,3)
   10 CONTINUE
```

```
      LAM(1)=S(1,1)
      S(1,1)=(1.0,0.0)
      SINV(1,1)=(1.0,0.0)
      IF (N.EQ.28) GO TO 17
      KK=26
      K=28
      DO 14 IDIG=10,JJJ
      KK=KK+3
      DO 11 I=1,3
      K=K+1
      SM(I,1)=S(K,KK)
      SM(I,2)=S(K,KK+1)
   11 SM(I,3)=S(K,KK+2)
      CALL ALLMAT(SM,MLAM,3,3,NCAL,DUMP3,DUMMY,A,B,INTN,INT)
      WRITE (6,903) NCAL
      K=K-3
      DO 12 I=1,3
      K=K+1
      S(K,KK)=SM(I,1)
      S(K,KK+1)=SM(I,2)
      S(K,KK+2)=SM(I,3)
   12 LAM(K)=MLAM(I)
      CALL CMINVS(SM,3,3)
      K=K-3
      DO 13 I=1,3
      K=K+1
      SINV(K,KK)=SM(I,1)
      SINV(K,KK+1)=SM(I,2)
   13 SINV(K,KK+2)=SM(I,3)
   14 CONTINUE
      GO TO 17
   15 CONTINUE
C
C     J-DIFFUSION
C
      CALL ALLMAT(S,LAM,N,37,NCAL,SINV,DUMMY,A,B,INTN,INT)
      WRITE (6,903) NCAL
C
C    THIS SECTION INVERTS THE S-MATRIX
C
      DO 16 I=1,N
      DO 16 J=1,N
   16 SINV(I,J)=S(I,J)
      CALL CMINVS(SINV,N,37)
   17 CONTINUE
C
C    CALCULATION OF LINE SHAPES
C
      C1=(0.0,1.0)
C
C    DOT PRODUCTS
C
      DO 19 J=1,N
      SUMA=(0.0,0.0)
      SUMB=(0.0,0.0)
      LAM(J)=LAM(J)*C1
      DO 18 I=1,N
      SUMA=SUMA+D(I)*S(I,J)
   18 SUMB=SUMB+SINV(J,I)*P(I)*D(I)
      A(J)=SUMA
   19 B(J)=SUMB
C
C    ACTUAL CALCULATION OF BANDSHAPE
C
      OM=2844.0
      DO 21 I=1,345
      OM=OM+1.0
      SUMA=(0.0,0.0)
      DO 20 J=1,N
   20 SUMA=SUMA+A(J)*B(J)/(OM+LAM(J))
```

```
      SUMA=SUMA/(5.92176E11)
      RI(I)=AIMAG(SUMA)
      RC(I)=SUMA
   21 ONOW(I)=OM
      WRITE (6,904)  (TITLE(I),I=7,22)
      WRITE (6,905)  FM
      WRITE (6,906)  TAUJ,TEMP
      WRITE (6,907)  (ONOW(I),RC(I),I=1,345)
      RMAX=RI(69)
      DO 22 I=100,250
      IF (RMAX.GT.RI(I)) GO TO 22
      RMAX=RI(I)
      WMAX=ONOW(I)
   22 CONTINUE
      RAT=HEIGHT/RMAX
      DO 23 J=1,345
   23 RI(J)=RI(J)*RAT
      WRITE (6,908)  HEIGHT
      WRITE (6,909)  (ONOW(I),RI(I),I=1,345)
C
C    PLOTS
C
      DO 24 J=1,191
      K=J+83
      WW(J)=ONOW(K)
   24 XX(J)=RI(K)
      XD(1)=WW(1)
      XD(2)=WW(191)
      IF (IPLOT(1).EQ.1) GO TO 25
      CALL PLOTME(XSIZE,YSIZE,2,XD,YD,TITLE,.FALSE.,0.0,4)
      CALL PLOTME(XSIZE,YSIZE,191,WW,XX,TITLE,.TRUE.,0.0,4)
      CALL RDORIG(IC,YORIG,XORIG)
   25 CONTINUE
      RATNOR=RAT
      CALL DPCOR(ONOW,RI,WMAX,TITLE,TEMP,RAT,IPLOT)
      ARAT=31.41593/RAT
      REALA=RAT/RATNOR
      TP=ARAT/(HEIGHT*1.884956E12)
      WRITE (6,910)  REALA,RAT,TP
      DO 26 J=1,191
   26 XX(J)=XX(J)*ARAT
      WRITE (6,911)
      WRITE (6,909)  (WW(I),XX(I),I=1,191)
      IF (IPLOT(2).EQ.1)  GO TO 27
      CALL RDORIG(IC,YORIG,XORIG)
   27 CONTINUE
      TITLE(22)=NORM
      IF (IPLOT(3).EQ.1)  GO TO 28
      CALL PLOTME(XSIZE,YSIZE,2,XD,YD,TITLE,.FALSE.,0.0,4)
      CALL PLOTME(XSIZE,YSIZE,191,WW,XX,TITLE,.TRUE.,0.0,4)
      CALL RDORIG(IC,YORIG,XORIG)
   28 CONTINUE
      GO TO 1
   29 CALL PLOT(0.0,0.0,999)
      STOP
  901 FORMAT (F10.0,E10.3,F10.0,I3,5I1,F10.0)
  902 FORMAT (' ',16A4)
  903 FORMAT (' NUMBER OF EIGENVALUES FOUND=',I3)
  904 FORMAT ('       ',16A4)
  905 FORMAT (' FRACTION OF M-DIFFUSION=',F5.2)
  906 FORMAT ('  CALCULATED INTENSITIES ','J-DIFFUSION TAUJ=',E13.3,
     #'SECONDS,TEMP=',F6.1//'FREQUENCY INTENSITIES (REAL,IMAGINARY)')
  907 FORMAT (2(F10.1,2E20.6))
  908 FORMAT ('1SPECTRA NORMALIZED TO MAXIMUM HEIGHT OF',F10.5)
  909 FORMAT (5(F10.1,F10.3))
  910 FORMAT ('AREA UNDER ORIGINAL SPECTRAL DENSITY',E20.6/'AREA UNDER N
     #ORMALIZED(HEIGHT) SPECTRAL DENSITY',E20.6/'REORIENTATION CORRELATI
     #ON TIME',E20.6,'/SEC')
  911 FORMAT ('1 SPECTRA NORMALIZED TO AREA OF 10 PI')
      END
      SUBROUTINE DPCOR(W,INT,WMAX,TITLE,TEMP,RAT,IPLOT)
C
C    CALCULATION OF DIPOLE CORRELATION FUNCTIONS
C
C    WB=(K*T/I)**0.5 = ((0.2565E24)*TEMP)**0.5
C    K = 1.38E16 GRAM(CM/SEC)**2
C    I = 5.38E-40 GRAM(CM)**2
C
      REAL INT(345),W(345),G(101),TT(101)
      REAL SCALE(22),TITLE(22)
      REAL SG(101)
      DATA SCALE/'    ','G(T)','    ','    ','TIME',17*'    '/
      REAL XD(2)/0.0,7.6/
      REAL YD(2)/0.0,1.0/
      INTEGER IPLOT(5)
      WB=SQRT((0.2565E24)*TEMP)
      DO 1 I=7,22
    1 SCALE(I)=TITLE(I)
      DO 3 IT=1,101
      RT=0.1*FLOAT(IT-1)
      TT(IT)=RT
      RT=RT/WB
      SUM=0.0
      SSUM=0.0
      FRT=1.884956E11*RT
      DO 2 IW=1,345
      SSUM=SSUM+INT(IW)*SIN(FRT*(W(IW)-WMAX))
    2 SUM=SUM+INT(IW)*COS(FRT*(W(IW)-WMAX))
C
C    2 PI*SPEED LIGHT = 1.884955592E11
C
      IF (IT.EQ.1) RAT=SUM
      SG(IT)=SSUM/RAT
    3 G(IT)=SUM/RAT
      WRITE (6,901) WMAX,WB
      WRITE (6,902) (TT(I),G(I),SG(I),I=1,101)
      IF (IPLOT(2).EQ.1) RETURN
      XSIZE=38.0*0.3937
      YSIZE=20.0*0.3937
      CALL PLOTME(XSIZE,YSIZE,2,XD,YD,SCALE,.FALSE.,0.0,4)
      CALL PLOTME(XSIZE,YSIZE,77,TT,G,TITLE,.TRUE.,0.0,4)
      CALL PLOTME(XSIZE,YSIZE,77,TT,SG,TITLE,.TRUE.,0.0,4)
      RETURN
  901 FORMAT ('1 DIPOLAR CORRELATION FUNCTION CALCULATED
     #  ABOUT',F10.1,' CM-1'/'  TIME IN REDUCED UNITS OF 1/OMEGABAR,
     # OMEGABAR=',E16.6)
  902 FORMAT (4(F5.1,2F7.4))
      END
```

SECTION B

```
C     THIS PROGRAM READS THE TIME(REDUCED UNITS) AND
C     THE FREE ROTOR CORRELATION FUNCTION AND ITS FIRST
C     DERIVATIVE ON 3. IT WRITES TIME AND THE ASSOCIATED
C     MEMORY FUNCTION ON 4.
C     NUCLEAR SPIN SYMMETRY ORDER A,E,F
C
C     TIME(502)=OMEGABAR
C     TIME(503)=TEMP
C     G(502)=AVERAGE FREQUENCY
C     GP(502)=K(0)
C
C     ON 5
C     CARD #1 : NT; NUMBER OF INCREMENTS OF DEL T TO
C                BE CONSIDERED
C
      COMPLEX*8 KA(502),KE(502),KF(502),G(502),GP(502)
      REAL TIME(503)
      READ (5,901) NT
      READ (3) TIME
      WRITE (4) TIME
      DELT=TIME(2)
C
C     A
C
      READ (3) G
      READ (3) GP
      CALL GPKP(G,GP,NT,KA,DELT)
      KA(502)=G(502)
      WRITE (4) KA
C
C     E
C
      READ (3) G
      READ (3) GP
      CALL GPKP(G,GP,NT,KE,DELT)
      KE(502)=G(502)
      WRITE (4) KE
C
C     F
C
      READ (3) G
      READ (3) GP
      CALL GPKP(G,GP,NT,KF,DELT)
      KF(502)=G(502)
      WRITE (4) KF
      RAW=REAL(KA(502))
      REW=REAL(KE(502))
      RFW=REAL(KF(502))
      WRITE (6,902) TIME(503),RAW,REW,RFW
      WRITE (6,903) (TIME(I),KA(I),KE(I),KF(I),I=1,NT)
      STOP
  901 FORMAT (I4)
  902 FORMAT ('1  FREE ROTOR MEMORY FUNCTIONS FOR NU-4 IR BAND OF',
     #' METHANE : TEMP=',F10.1,' DEG K'/'-   CALCULATED ABOUT ','AVERAGE
     # FREQUENCY OF THE STICK SPECTRA'/'  A  ',F10.3/'  E  ',F10.3/
     #'  F  ',F10.3)
  903 FORMAT ('-  TIME(RED)',10X,'A-SYMMETRY',19X,'E-SYMMETRY',19X,
     #'F-SYMMETRY'/(F8.2,3X,3(2E13.4,3X)))
      END
```

```
C
C     THIS SUBROUTINE CALCULATES THE FREE ROTOR
C     MEMORY FUNCTION FROM THE FREE ROTOR FUNCTIONS
C
      SUBROUTINE GPKF(GT,GP,ITIME,K,DELT)
      COMPLEX*8 GT(502),GP(502),K(502),C1
      K(1)=-GP(502)
      DELT2=DELT/2.0
      K(2)=-(GP(2)-GP(1))/DELT2-GT(2)*K(1)
      DO 2 N=3,ITIME
      NM1=N-1
      C1=0.0
      NP1=N+1
      DO 1 M=2,NM1
      C1=C1+GT(NP1-M)*K(M)
    1 CONTINUE
      K(N)=-C1-C1-(GP(N)-GP(1))/DELT2-GT(N)*K(1)
    2 CONTINUE
      RETURN
      END
```

```
C
C     CALCULATION OF REORIENTATIONAL CORRELATION FUNCTION FROM FREE
C     ROTOR MEMORY FUNCTION AND THE MEMORY FUNCTION EQUATION
C     K(T)=K(T)FR*EXP(-T/TAUJ)
C     FREE POTOR MEMORY FUNCTION READ IN ON 4
C     K(502)=AVERAGE FREQUENCY OF STICK SPECTRA
C     TIME(502)=OMEGABAR; TIME(503)=TEMP
      COMPLEX*8 CPHASE(501),CEXP,CMPLX,CA,CE,CF,CPHA(501),CPHF(501),
     #  KAT(501),KET(501),KFT(501),GA(501),GE(501),GF(501)
      COMPLEX*8 K(502),C1,GT(501),KP(501),C3,KA(502),KE(502),KF(502)
      REAL TIME(503),BUFFER(1024),KR(501),KI(501),TITLE(22),TITLEK(22)
C
C     INITIATION OF PLOT ROUTINES
C
      CALL PLOTS(BUFFER,4096)
      DATA TITLEK/'  K(','T)/K','(0) ',' TI','ME(R','ED) ',16*'    '/
      DATA TITLE/'    ','G(T)','    ',' TI','ME(R','ED) ',16*'    '/
      REAL YD(2)/0.0,1.0/
      REAL YDK(2)/-0.5,1.0/
      REAL XD(2)/0.0,7.6/
      REAL XC(3)/0.0,4.0,7.6/
      REAL YC(3)/0.0,0.0,0.0/
      IC=0
      YORIG=-10.0
      XORIG=17.0
      XSIZE=14.9606
      YSIZE=7.874
      CALL PLOT(2.0,2.0,-3)
      READ (4) TIME
      READ (4) KA
      READ (4) KE
      READ (4) KF
      WB=TIME(502)
      WA=REAL(KA(502))
      WE=REAL(KE(502))
      WF=REAL(KF(502))
      WPB= (5.0*WA+2.0*WE+3.0*WF)/10.0
      WA=WPB-WA
      WE=WPB-WE
      WF=WPB-WF
      TEMP=TIME(503)
      DELT=TIME(2)
      B1=5.194
      CPHASE(1)=1.0
      CPHA(1)=1.0
      CPHF(1)=1.0
      CA=CEXP(CMPLX(0.0,(B1+B1+WA)*DELT*1.885E11/WB))
      CE=CEXP(CMPLX(0.0,(B1+B1+WE)*DELT*1.885E11/WB))
      CF=CEXP(CMPLX(0.0,(B1+B1+WF)*DELT*1.885E11/WB))
      DO 1 I=2,501
      CPHA(I)=CPHA(I-1)*CA
      CPHASE(I)=CPHASE(I-1)*CE
      CPHF(I)=CPHF(I-1)*CF
    1 CONTINUE
      DO 2 I=1,501
      CPHA(I)=CPHA(I)*5.0
      CPHASE(I)=CPHASE(I)*2.0
      CPHF(I)=CPHF(I)*3.0
    2 CONTINUE
C
C     TAUJ (SEC)
C     TMAX (RED) MAXIMUM TIME TO BE CONSIDERED
C
C     IPLTK     PLOT K(T) ?
C     IG        G(T) ?
C     IPLTG     PLOT G(T) ?
C     PAR=0     YES
C     PAR=1     NO
C
```

```
    3 READ (5,901) TAUJ,ITMAX,IPLTK,IG,IPLTG
      IF (TAUJ.LT.0.0) GO TO 8
      TMAX=TIME(ITMAX)
      READ (5,902) (TITLE(I),I=7,22)
      DO 4 I=7,22
      TITLEK(I)=TITLE(I)
    4 CONTINUE
      TJRED=TAUJ*WB
C
C     MULTIPLYING K(T)-FR BY EXP(-T/TAUJ)
C
      RATK=REAL(K(1))
      R1=EXP(-DELT/TJRED)
      R2=1.0
      KAT(1)=KA(1)
      KET(1)=KE(1)
      KFT(1)=KF(1)
      DO 5 I=2,501
      R2=R2*R1
      KAT(I)=KA(I)*R2
      KET(I)=KE(I)*R2
      KFT(I)=KF(I)*R2
    5 CONTINUE
      IF (IG.EQ.1) GO TO 3
      WRITE (6,903) (TITLE(I),I=7,22)
      WRITE (6,904) TEMP,TAUJ,TJRED
      WRITE (6,905)
C
C     A
C
      WRITE (6,906)
      CALL KG(KAT,GA,DELT,ITMAX,TIME)
C
C     E
C
      WRITE (6,907)
      CALL KG(KET,GE,DELT,ITMAX,TIME)
C
C     F
C
      WRITE (6,908)
      CALL KG(KFT,GF,DELT,ITMAX,TIME)
      GT(1)=5.0*GA(1)+2.0*GE(1)+3.0*GF(1)
C
C     NORMALIZING G(T) AND PHASING SO FIRST MOMENT
C     OF THE SPECTRAL DENSITY = 2 B1
C
      RRR=REAL(GT(1))
      GT(1)=GT(1)/RRR
      C3=0.5
      DO 6 I=2,ITMAX
      C1=(CPHA(I)*GA(I)+CPHASE(I)*GE(I)+CPHF(I)*GF(I))/RRR
      GT(I)=C1
      C3=C3+C1
    6 CONTINUE
      TAUTHA=REAL(DELT*(C3-GT(ITMAX)/2.0))/(1.-REAL(GT(ITMAX)))
      TWB=TAUTHA/WB
      WRITE (6,909)
      WRITE (6,910) (TIME(I),GT(I),I=1,ITMAX)
      WRITE (6,911) TAUTHA,TWB
      IF (IPLTG.EQ.1) GO TO 3
      J=IFIX(7.6/DELT)
      IF (TMAX.LT.7.6) J=ITMAX
      CALL PLOTME(XSIZE,YSIZE,2,XD,YD,TITLE,.FALSE.,0.0,4)
      IJ=J+1
      DO 7 I=1,IJ
      KR(I)=REAL(GT(I))
      KI(I)=AIMAG(GT(I))
    7 CONTINUE
```

```
      CALL PLOTME(XSIZE,YSIZE,J,TIME,KR,TITLE,.TRUE.,0.0,4)
      CALL PLOTME(XSIZE,YSIZE,J,TIME,KI,TITLE,.TRUE.,0.05,4)
      CALL RDORIG(IC,YORIG,XORIG)
      GO TO 3
    8 CALL PLOT(0.0,0.0,999)
      STOP
  901 FORMAT (E10.0,I4,3I1)
  902 FORMAT (16A4)
  903 FORMAT ('1',16A4)
  904 FORMAT ('-',
     $'REORIENTATIONAL CORRELATION FUNCTION CALCULATED FROM',' FREE ROTO
     $R MEMORY FUNCTION'/' TEMP=',F8.2,' DEG K; TAUJ=',E10.3,' SEC, =',
     $E10.4,' (RED)')
  905 FORMAT (' CORRELATION FUNCTION CALCULATED FROM MEMORY',' FUNCTION
     $BY TRAPEZOIDAL RULE  SQRT(G(T)*G(T)) & G(T)*G(T)')
  906 FORMAT ('-    A-SYMMETRY')
  907 FORMAT ('1    E-SYMMETRY')
  908 FORMAT ('1    F-SYMMETRY')
  909 FORMAT ('1 GA,GE,GF: WEIGHTED SUM(5:2:3);PHASE SUCH THAT THE',
     $' AVERAGE FREQUENCY IS WEIGHTED SUM OF WPA,WPE,WPF')
  910 FORMAT ('- REORIENTATIONAL CORRELATION FUNCTIONS ADJUSTED SO',
     $' FIRST MOMENT=2B1=10.388 CM-1'/(2(F10.2,5X,2E15.7,10X)))
  911 FORMAT ('-REORIENTATIONAL CORRELATION TIME= ',E11.3,'(RED) = ',
     $E11.3,' SEC')
      END

C
C     THIS SUBROUTINE CALCULATES G(T) FROM K(T)
C
      SUBROUTINE KG(KP,GT,DELT,ITMAX,TIME)
      COMPLEX*8 KP(501),GT(501),C3,KSUM(501),C1
      REAL TIME(503)
      WB=TIME(502)
      RC1=DELT*DELT/2.
      RC2=REAL(1.0+RC1*KP(1)/2.)
      C3=(-1.0+RC1*(KP(2)+KP(1)/2.))/RC2
      RC4=RC1/RC2
      KSUM(1)=C3
      ITM1=ITMAX-1
      DO 1 I=2,ITM1
      KSUM(I)=RC4*(KP(I+1)+KP(I))
    1 CONTINUE
      GT(1)=1.0
      GT(2)=(1.0-RC1*KP(2)/2.0)/RC2
      WRITE (6,901)  TIME(1),GT(1)
      WRITE (6,901)  TIME(2),GT(2)
      C3=GT(1)/2.0+GT(2)
      DO 3 N=3,ITMAX
      IF (TIME(N).LE.7.6) IJ=N
      C1=-KSUM(N-1)/2.
      NN2=N-2
      DO 2 J=1,NN2
      C1=C1-GT(N-J)*KSUM(J)
    2 CONTINUE
      GT(N)=C1
      C3=C3+C1
      AAAA=CABS(GT(N))
      AAAAA=AAAA*AAAA
      WRITE (6,901) TIME(N),C1,AAAA,AAAAA
    3 CONTINUE
      TAUTHA=REAL(DELT*(C3-GT(ITMAX)/2.0))/(1.-REAL(GT(ITMAX)))
      TWB=TAUTHA/WB
      WRITE (6,902) TAUTHA,TWB
      RETURN
  901 FORMAT (F10.4,4E16.7)
  902 FORMAT ('-REORIENTATIONAL CORRELATION TIME= ',E11.3,'(RED) = ',
     $E11.3,' SEC')
      END
```

```
       INTEGER ISKIP(8),NWT(8)
C
C     THIS PROGRAM FITS OBSERVED EXPERIMENTAL ESR
C     LINEWIDTHS TO A CUBIC FUNCTION IN M.
C
C     USES DR. HIRSS'S LEAST SQUARES ROUTINE MODIFIED
C     TO WEIGHT POINTS.
C
C     INPUT ON 5
C
C     CARD #1 : IMOD,IWT
C               IMOD=1 READS ISKIP ON 3
C               IWT=1 WEIGHTS POINTS AS 1/(WIDTH**3)
C                  =0 NO WEIGHTING
C     CARD #2 : TITLE UP TO 40 CHARACTERS
C     CARD #3 : PPW,TC,ETA
C               PPW, PEAK TO PEAK WIDTHS IN GAUSS
C               PPW(1)=0.0   STOP
C               PPW(1)=100.0  READS NEW TITLE CARD
C               TC=TEMPERATURE IN DEGREE C.
C               ETA=VISCOSITY IN CENTIPOISE
C
C     INPUT ON 3
C              ISKIP, INTEGER VECTOR
C              IF ISKIP(I)=1 I-TH LINE NOT CONSIDERED IN FIT
C     OUTPUT ON 9 SUMMARY OF PARAMETERS
C     OUTPUT ON 6 LSQ OUTPUT
C
       REAL D(11),A(10),PPM(8),PPW(8)
       REAL TITLE(10)
       REAL INC(11)/'    ',' MIC',9*'    '/
       REAL M(8)/-3.5,-2.5,-1.5,-0.5,0.5,1.5,2.5,3.5/
       REAL MM(8)/12.25,6.25,2.25,0.25,0.25,2.25,6.25,12.25/
       REAL MMM(8)/-42.875,-15.625,-3.375,-.125,.125,3.375,15.625,42.875/
       DATA ISKIP/0,0,0,0,0,0,0,0/
       IW(A)=IFIX(0.25E6/(A**3))
       WRITE (9,901)
       D(1)=1.0
       READ (5,902) IMOD,IWT
       GO TO 2
     1 READ (5,903) (PPW(I),I=1,8),TC,ETA
       IF (PPW(1).EQ.0.0) GO TO 11
       IF (PPW(1).NE.100.0) GO TO 3
     2 READ (5,904) ISOL,TITLE
       WRITE (9,905) TITLE
       GO TO 1
     3 CONTINUE
       WRITE (6,906) TITLE
       IF (IMOD.EQ.0) GO TO 5
     4 READ (3,907) (ISKIP(I),I=1,8)
       GO TO 6
     5 ISKIP(8)=0
       IF (PPW(8).EQ.0.0) ISKIP(8)=1
     6 CONTINUE
       DO 7 I=1,8
       IF (ISKIP(I).EQ.1) GO TO 7
       D(2)=M(I)
       D(3)=MM(I)
       D(4)=MMM(I)
       D(5)=PPW(I)
       NWT(I)=IW(PPW(I))
       IF (IWT.EQ.0) NWT(I)=0
       CALL LSQSM(4,D,NWT(I))
     7 CONTINUE
```

```
      CALL LSQSV(N)
C
C     A(1)=ALPHA
C     A(2)=BETA
C     A(3)=GAMMA
C     A(4)=DELTA
C
      TK=TC+273.15
      GOB=A(3)/A(2)
      EOT=ETA/TK
      WRITE (6,908) GOB,EOT,ETA,TC,TK
C
C    THEORETICAL WIDTHS AND STD(FROM EXPERIMENT)
C
      DO 8 I=1,8
    8 PPH(I)=A(1)+A(2)*H(I)+A(3)*HH(I)+A(4)*HHH(I)
      WRITE (6,909)
      SUM=0.0
      COUNT=0.0
      DO 10 J=1,8
      CAL=PPW(J)
      THE=PPH(J)
      DIF=CAL-THE
      IF (PPW(J).EQ.0.0) GO TO 9
      SUM=SUM+DIF*DIF
      COUNT=COUNT+1.0
      GO TO 10
    9 DIF=1.0E20
      CAL=1.0E20
   10 WRITE (6,910) CAL,THE,DIF,INC(ISKIP(J)+1)
      SUM=(SUM/COUNT)**0.5
      WRITE (6,911) SUM
      WRITE (9,912) TK,EOT,(A(JJ),JJ=1,4),GOB,ETA
      IF (IMOD.EQ.0) GO TO 1
      GO TO 4
   11 WRITE (9,913)
      STOP
  901 FORMAT (' TEMP DEG K   ETA*/TEMP',6X,'ALPHA',9X,'BETA',10X,
     $'GAMMA',9X,'DELTA',4X,'GAMMA/BETA ',4X,'ETA')
  902 FORMAT (2I3)
  903 FORMAT (10F7.0)
  904 FORMAT (10A4)
  905 FORMAT (' ',10A4)
  906 FORMAT ('0',10A4)
  907 FORMAT (8I1)
  908 FORMAT (' GAMMA/BETA',E16.8/' ETA/TEMP',E18.8/' ETA(CP) ',E18.8/
     $' TEMP(C) ',F18.2/' TEMP(K) ',F18.2)
  909 FORMAT ('-   CALCULATED  THEORETICAL  DIFFERENCE')
  910 FORMAT (' ',F10.3,2F13.3,A4)
  911 FORMAT ('-RMS DIFFERENCE=',F10.5)
  912 FORMAT (' ',F8.2,E12.3,F13.3,2F14.4,F15.4,2F11.4)
  913 FORMAT (' ALL VALUES OF ETA IN 10 TO -3 CENTIPOISE')
      END
```

SECTION D-2

```
C
C     THIS PROGRAM DOES A NONLINEAR LEAST SQUARES FIT TO THE
C     N-DEPENDENT PART OF THE LINEWIDTH TO KIVELSON'S EXPRESSIONS
C     WITH STOKES-EINSTEIN.
C     VARIABLE PARAMETER KAPA*R**3
C
C     USES KARL HALLINS'S DRIVER ROUTINE FOR BIRSS'S LINEAR PROGRAM.
C
C     ABSOLUTE RESIDUALS
C
C     INPUT
C
C      CARD #1 : AX,AY,AZ,GX,GY,GZ (A'S AND WO IN (1/SEC)*E-9)
C      CARD #2 : WO,BO (BO IN GAUSS)
C      CARD #3 : TITLE (ENDFILE STOP)
C      CARD #4 : PPW,ETA,TEMP,ALPHA(EXPERIMENTAL)
C                PPW(1)<0 STOPS READING DADA
C                ( THERE WILL BE ONE OF THESE CARDS FOR EACH SPECTRUM)
C
       IMPLICIT REAL*8(D)
       REAL*4 TITLE(10),TEMPV(301)
       REAL*8 D(11),DM(301),DA(10),DX(301),DY(301),DPY
       REAL*8 F,U,TR,WTR2,PPW(8),ALPHA,DEOT
       DIMENSION NWT(301)
       COMMON /NAME/ NT,NB,NPT,NPAR
       COMMON /PARDPY/ F,U,TR,WTR2
       DATA DS/0.0D0/,DOT/0.0D0/,NP/0/
       REAL*8 MVEC(8)/-3.5D0,-2.5D0,-1.5D0,-.5D0,.5D0,1.5D0,2.5D0,3.5D0/
       EXTERNAL DPY
       NT=0
       NPT=0
       CALL COMPUT
     1 READ (5,901,END=8) TITLE
       NIT=0
       NPT=0
       NPAR=1
       DA(1)=64.0D0
       WRITE (6,902) TITLE
       DO 3 I=1,100
       READ (5,903) PPW,ETA,TEMP,ALPHA
       IF (PPW(1).LT.0.0D0) GO TO 4
       DEOT=DBLE(ETA/(TEMP+273.15))
       DO 2 J=1,8
       IF (PPW(J).EQ.0.0D0) GO TO 2
       NPT=NPT+1
       DY(NPT)=PPW(J)-ALPHA
       DX(NPT)=DEOT
       DM(NPT)=MVEC(J)
       NWT(NPT)=1
       TEMPV(NPT)=TEMP
     2 CONTINUE
     3 CONTINUE
     4 WRITE (6,904)  (I,DA(I),I=1,NPAR)
     5 CALL DERIV(D,DA,DX,DM,DY,NWT)
       DO 6 IB=1,NPAR
     6 DA(IB)=DA(IB)+D(IB)
       WRITE (6,905) NT
       WRITE (6,906)  (I,DA(I),I=1,NPAR)
       DDDD=DA(1)**.3333333
       WRITE (6,907) DDDD
       IF ((NIT.GT.0).AND.(NT.LE.NIT)) GO TO 5
       IF (NB.EQ.1) GO TO 5
       WRITE (6,908)
       DO 7 IC=1,NPT
       DPR=DPY(DX(IC),DM(IC),DA,NPAR)
       DEL=DY(IC)-DPR
       DS=DS+DEL*DEL
       DOT=DOT+DEL
     7 WRITE (6,909) DX(IC),DY(IC),DPR,DEL,NWT(IC),DM(IC),TEMPV(IC),TR
```

```
      DS=DSQRT(DS/DFLOAT(NPT-NPAR))
      WRITE (6,910) DS,DOT
      WRITE (2,901) TITLE
      WRITE (2,911) DDDD,DS,DOT
      DS=0.0D0
      DOT=0.0D0
      NT=0
      NF=0
      NPT=0
      GO TO 1
    8 WRITE (6,912)
      STOP 0
  901 FORMAT (10A4)
  902 FORMAT ('1',10A4)
  903 FORMAT (11F5.0)
  904 FORMAT (' LSQSM FIT : INITIAL GUESSES'/('ODA(',I2,') = ',1PD12.5))
  905 FORMAT ('OAFTER ',I2,' ITERATIONS THE PARAMETERS NOW ARE :')
  906 FORMAT ('ODA(',I2,') = ',1PD18.8)
  907 FORMAT ('     R(ANGSTROMS)= ',F10.3)
  908 FORMAT ('-EOT,Y(EXP),Y(THE),E-T,WT,M,TEMP,TR')
  909 FORMAT (D11.3,3F10.2,I5,2F6.1,D12.4)
  910 FORMAT ('OOBSERVED-CALCULATED STANDARD DEVIATION = ',1PD18.8/
     *'OSUMMED DIFFERENCES = ',D18.8)
  911 FORMAT (3D20.7)
  912 FORMAT ('ODATA EXHAUSTED ; ENDFILE ENCOUNTERED ON READ')
      END


      REAL FUNCTION DPY*8(DX,DM,DA,NPAR)
      IMPLICIT REAL*8(A-H,O-Z)
      REAL*8 DA(1)
      COMMON /LWP/ BS,B1T,B2T,GS,G1T,G2T,DS,WO
      COMMON /PARDPY/ F,U,TR,WTR2
      TR=3.03439D-10*DX*DA(1)
      WTR2=(TR*WO)**2
      U=1.0/(1.0+WTR2)
      F=U*WTR2
      DPY=(BS+U*(B1T-F*B2T)+(GS+U*(G1T+F*G2T)+DS*DM*(1.+U*(1.+F)))*DM)*
     *  DM*TR
      RETURN
      END
      SUBROUTINE DERIV(D,DA,DX,DM,DY,MWT)
      IMPLICIT REAL*8(A-H,O-Z)
      REAL*8 DA(1),D(1),DX(1),DM(1),DY(1)
      INTEGER MWT(1)
      COMMON /NAME/ NT,MB,NPT,NPAR
      COMMON /LWP/ BS,B1T,B2T,GS,G1T,G2T,DS,WO
      COMMON /PARDPY/ F,U,TR,WTR2
      EXTERNAL DPY
      DO 1 IA=1,NPT
      DMM=DM(IA)
      DSDM=DS*DMM
      DXX=DX(IA)
      DPR=DPY(DXX,DMM,DA,NPAR)
      A=(BS+(GS+DSDM)*DMM)
      B=(B1T+(G1T+DSDM)*DMM)
      C=(-B2T+(G2T+DSDM)*DMM)
      D(1)=DMM*3.03439D-10*DXX*(A+U*(B*(1.-F-F)+C*F*(3.-4.*F)))
      D(2)=(DY(IA)-DPR)
    1 CALL LSQSM(0,NPAR,D,MWT(IA),MA)
      CALL LSQSM(1,NPAR,D,MA,MB)
      NT=NT+1
      RETURN
      END
      SUBROUTINE COMPUT
      IMPLICIT REAL*8(A-H,O-Z)
      COMMON /LWP/ BS,B1T,B2T,GS,G1T,G2T,DS,WO
      READ (5,901) AX,AY,AZ,GX,GY,GZ
      READ (5,901) WO,BO
      STOG=3.9390D-7/(GX+GY+GZ)
      AX=AX*1.0D9
      AY=1.0D9*AY
      AZ=AZ*1.0D9
      WO=WO*6.28319D9
      WRITE (6,902) AX,AY,AZ,GX,GY,GZ,WO,BO
      B=.6666667*(AZ-.5*(AX+AY))
      C=.25*(AX-AY)
      DDG=(GZ-.5*(GX+GY))*8.7944D6*BO
      DG=.5*(GX-GY)*8.7944D6*BO*C
      BDDG=B*DDG
      DDG2=DDG*DDG
      BS=B*B
      CS=C*C
      AOWO=(AX+AY+AZ)/(3.*WO)
      B1T=(.2*BDDG-.13333333*DDG2*AOWO+.8*DG-.8375*BS*AOWO)*STOG
      B2T=(AOWO*(.1333333*DDG2+5.5125*BS))*STOG
C
C     BETA(NS)=U*(B1T-FB2T)
C
      GS=(.125*BS+.66666667*CS-.2333333*AOWO*BDDG)*STOG
      G1T=(-.025*BS-.1666667*BDDG*AOWO-.13333333*CS)*STOG
      G2T=((.125*BS-.4*BDDG)*AOWO)*STOG
C
C     GAMMA(NS)=U*(G1T+F*G2T)
C
      DS=(.05*BS*AOWO)*STOG
      BS=(.2666667*BDDG+1.066667*DG-AOWO*(.17777778*DDG2+.8625*BS))*STOG
      RETURN
  901 FORMAT (6F10.0)
  902 FORMAT ('1AX=',D12.4/' AY=',D12.4/' AZ=',D12.4/' GX=',F12.3/
     #' GY=',F12.3/' GZ=',F12.3/' WO=',E12.4/' BO=',F12.2)
      END
```

APPENDIX III

The tables in the Appendix give the peak to peak widths of the lines of the ESR spectrum. The temperature is given in °C and the viscosities are in poise. The peak to peak widths were calculated from the peak to peak heights of the observed ESR lines and the width of the M = -3/2 line.[a,b]

---

[a] Linewidths which could not be determined due to the noise in the spectrum are indicated by a.

[b] Temperature quoted are accurate to ± 0.5°C.

TABLE 9

EXPERIMENTAL LINEWIDTHS FOR THE VODE SYSTEMS

T(°C)	η/T 10^5P/°K	-7/2	-5/2	-3/2	-1/2	1/2	3/2	5/2	7/2
TOLUENE									
-20.4	4.226	20.4	15.5	12.9	13.0	15.5	20.2	26.4	34.1
-19.4	4.134	18.8	14.1	12.0	12.0	14.0	18.2	23.4	29.9
-5.9	3.143	14.8	11.4	9.9	10.0	11.7	14.8	18.9	24.5
2.6	2.684	13.9	10.9	9.5	9.7	11.3	14.1	18.4	23.2
10.4	2.342	12.2	9.8	8.6	8.8	10.1	12.5	15.8	19.6
24.4	1.869	10.3	8.6	7.8	8.0	9.1	11.0	13.6	16.8
24.8	1.859	10.4	8.6	7.8	8.0	9.1	10.9	13.6	16.7
33.3	1.638	9.8	8.3	7.7	7.9	8.9	10.6	12.9	15.7
49.0	1.316	9.2	8.0	7.5	7.8	8.6	10.1	12.1	14.4
57.1	1.184	9.0	7.9	7.5	7.8	8.6	9.9	11.7	14.1
63.7	1.090	8.7	7.8	7.4	7.7	8.4	9.7	11.4	13.3
75.1	0.950	8.1	7.4	7.1	7.4	8.1	9.2	10.6	12.8
83.9	0.860	8.0	7.3	7.1	7.3	7.9	8.8	10.1	11.7
95.7	0.756	8.0	7.4	7.3	7.6	8.1	9.1	10.3	11.8
98.3	0.735	8.0	7.4	7.3	7.6	8.1	8.9	10.1	11.6
119.8	0.593	7.9	7.4	7.3	7.8	8.1	9.0	10.0	10.9
126.1	0.559	7.8	7.3	7.3	7.5	7.9	8.7	9.6	10.7
CHLOROFORM									
-24.4	3.799	23.6	17.6	14.4	14.2	16.8	21.8	28.7	37.0
-19.7	3.504	21.5	16.1	13.2	13.3	15.6	20.2	26.5	34.9
-10.0	2.987	18.3	13.8	11.6	11.5	13.5	17.3	22.6	28.9
-5.3	2.770	17.2	12.9	10.9	10.9	12.8	16.2	21.3	27.1
-0.4	2.574	15.4	11.8	10.1	10.3	11.8	14.8	19.3	25.1
8.5	2.255	14.1	11.0	9.5	9.5	11.1	13.8	17.7	22.6
13.7	2.095	13.4	10.6	9.2	9.3	10.8	13.2	16.7	21.5
22.0	1.870	12.3	9.7	8.6	8.7	9.9	12.2	15.5	19.4
27.3	1.741	12.0	9.7	8.5	8.6	9.7	11.8	14.9	18.6
32.5	1.629	11.2	9.1	8.2	8.3	9.5	11.5	14.3	17.8

EXPERIMENTAL LINEWIDTHS FOR THE VODE SYSTEMS

T(°C)	η/T 10^5P/°K	-7/2	-5/2	-3/2	-1/2	1/2	3/2	5/2	7/2
44.9	1.396	10.6	8.9	8.1	8.3	9.3	11.1	13.7	16.8
46.6	1.367	11.6	9.4	8.5	8.5	9.4	11.3	13.9	17.2
46.9	1.362	10.2	8.6	7.8	8.0	8.9	10.7	12.9	16.0
63.3	1.126	9.4	8.1	7.6	7.8	8.6	10.2	12.2	14.7
85.7	0.886	8.9	7.9	7.6	7.8	8.5	9.7	11.4	13.4
DIPHENYLMETHANE									
31.3	7.673	22.6	16.4	13.5	13.5	16.2	21.3	28.0	36.0
36.6	6.909	22.5	16.9	13.5	13.6	16.4	21.7	29.7	a
43.7	6.034	20.5	15.3	12.8	12.9	15.4	20.0	26.1	34.1
46.8	5.698	18.8	14.3	11.9	11.9	14.3	17.9	23.6	0.0
60.5	4.475	15.8	12.1	10.4	10.5	12.3	15.8	20.1	23.6
78.9	3.321	12.4	9.8	8.9	8.9	10.2	12.4	16.4	21.2
88.4	2.879	11.2	9.1	8.3	8.5	9.8	11.9	14.9	18.7
98.9	2.478	10.4	8.6	7.9	8.1	9.2	11.1	13.6	16.9
101.1	2.402	10.5	8.8	8.0	8.2	9.2	11.1	13.6	17.0
112.2	2.071	9.3	7.9	7.3	7.6	8.4	9.8	11.9	14.4
119.1	1.894	9.6	8.3	7.9	8.0	8.9	10.6	12.8	15.6
126.6	1.726	9.5	8.2	7.6	7.8	8.6	10.2	12.1	14.5
139.2	1.484	9.4	8.2	7.8	7.9	8.6	10.0	11.9	14.3
141.5	1.447	9.1	8.3	7.8	7.8	8.7	10.8	13.9	17.6
161.6	1.159	8.3	7.6	7.3	7.4	8.1	9.1	10.4	12.1
CARBON DISULFIDE									
-32.5	2.385	13.3	10.4	9.1	9.3	10.8	13.5	17.3	22.0
-11.7	1.813	10.8	8.8	8.0	8.2	9.4	11.4	14.1	17.4
-2.3	1.617	10.1	8.4	7.7	8.0	9.0	10.8	13.1	16.3
9.0	1.414	9.4	8.0	7.4	7.7	8.7	10.3	12.5	15.0
24.9	1.188	8.8	7.7	7.3	7.6	8.4	9.7	11.6	13.8
40.9	1.009	8.4	7.5	7.2	7.5	8.2	9.4	11.0	13.0
60.5	0.833	7.7	7.0	6.8	7.1	7.7	8.6	9.9	11.6
78.9	0.707	8.1	7.6	7.4	7.6	8.2	9.1	10.3	11.7

TABLE 10

EXPERIMENTAL LINEWIDTHS FOR THE VOPM SYSTEMS

T(°C)	η/T 10^5P/°K	-7/2	-5/2	-3/2	-1/2	1/2	3/2	5/2	7/2
TOLUENE									
-17.7	3.985	28.9	21.1	17.4	17.2	21.0	27.6	37.8	51.6
-10.7	3.452	24.1	17.7	14.6	14.7	17.8	23.5	31.5	41.2
0.5	2.788	20.3	14.6	12.3	12.5	14.8	19.1	25.5	32.9
10.4	2.342	16.8	12.9	11.1	11.2	13.3	16.9	22.1	28.8
20.6	1.985	14.7	11.4	9.9	10.1	11.8	14.9	19.2	24.8
36.3	1.567	12.3	9.8	8.8	9.0	10.4	13.0	16.4	20.7
54.5	1.224	9.9	8.3	7.7	8.0	9.3	11.4	14.2	17.4
90.7	0.797	8.6	7.6	7.2	7.6	8.4	9.7	11.4	13.7
120.1	0.590	8.4	7.8	7.6	7.8	8.4	9.4	10.8	12.5
CHLOROFORM									
-19.8	3.509	32.3	23.2	19.0	18.7	22.4	29.4	40.6	54.7
-8.7	2.927	26.5	19.3	15.9	15.8	18.8	24.8	33.8	44.9
-0.7	2.584	23.8	17.4	14.5	14.4	16.9	22.2	28.8	39.1
12.4	2.133	19.2	14.5	12.2	12.2	14.2	18.4	24.3	32.7
24.0	1.821	16.8	12.9	10.9	11.0	12.8	16.4	21.4	27.8
36.1	1.555	14.4	11.2	9.7	9.8	11.3	13.8	18.4	23.7
56.5	1.216	12.1	9.8	8.7	8.9	10.1	12.4	15.6	19.9
95.5	0.803	10.0	8.6	8.0	8.3	9.2	10.9	13.1	16.0
125.2	0.605	9.2	8.2	7.9	8.2	8.9	10.2	11.9	14.0
DIPHENYLMETHANE									
30.5	7.798	42.1	29.8	24.0	23.4	29.9	39.2	54.5	
39.4	6.546	35.7	25.6	19.8	18.8	22.4	29.4	38.5	52.3
51.6	5.222	25.7	19.2	15.9	15.9	19.3	25.0	34.8	45.2
63.8	4.232	21.1	15.9	13.4	13.4	16.0	20.8	27.2	36.3

EXPERIMENTAL LINEWIDTHS FOR THE VOPM SYSTEMS

T(°C)	η/T 10^5P/°K	-7/2	-5/2	-3/2	-1/2	1/2	3/2	5/2	7/2
76.6	3.442	17.1	12.9	11.1	11.2	13.2	16.8	22.4	28.8
95.1	2.615	14.3	11.3	9.8	10.1	11.7	14.7	18.8	24.6
125.1	1.758	11.0	9.0	8.2	8.4	9.4	11.5	14.3	17.7
154.3	1.254	9.2	7.9	7.4	7.6	8.4	10.1	12.3	14.8
CARBON DISULFIDE									
-32.9	2.402	18.4	13.9	11.8	12.0	14.2	18.3	24.0	31.7
-13.6	1.857	14.4	11.3	9.8	10.1	11.7	14.8	18.9	24.3
-8.1	1.732	13.2	10.4	9.1	9.3	10.8	13.6	17.2	22.0
-0.1	1.575	12.9	10.3	9.1	9.4	10.8	13.4	16.8	21.3
10.1	1.398	12.0	9.8	8.8	9.1	10.4	12.7	15.7	19.9
25.0	1.187	10.6	8.9	8.1	8.3	9.5	11.4	14.1	17.3
42.8	0.987	9.5	8.2	7.7	7.9	8.9	10.5	12.8	15.4
63.4	0.811	9.0	7.9	7.5	7.8	8.7	10.1	11.8	14.0
81.3	0.694	7.3	7.5	7.3	7.6	8.3	9.5	11.0	13.0

TABLE 11

EXPERIMENTAL LINEWIDTHS FOR THE VOTB SYSTEMS

T(°C)	η/T 10^5P/°K	-7/2	-5/2	-3/2	-1/2	1/2	3/2	5/2	7/2
TOLUENE									
-20.5	4.235	29.0	20.9	17.2	17.2	21.0	27.3	39.8	a
-19.8	4.172	25.8	19.8	16.5	16.4	19.4	25.8	31.9	41.4
-15.5	3.807	25.3	18.9	15.7	15.5	18.8	24.3	32.5	45.8
-12.3	3.565	23.3	17.2	14.4	14.4	17.1	21.8	28.1	34.7
-9.7	3.382	22.8	17.0	14.2	14.1	17.3	22.3	28.9	39.1
-4.1	3.033	20.1	15.2	12.8	13.0	15.4	20.2	25.8	32.4
2.0	2.715	19.0	14.1	11.8	12.0	14.3	18.6	24.4	32.8
5.5	2.552	18.0	13.6	11.4	11.4	13.5	17.3	22.8	28.6
8.9	2.404	17.2	13.3	11.3	11.5	13.7	17.0	21.8	28.6
14.3	2.195	15.1	11.6	10.1	10.4	12.1	15.4	20.0	24.6
18.8	2.041	13.9	10.7	9.4	9.5	11.2	14.2	18.0	22.7
22.9	1.915	13.9	10.8	9.4	9.6	11.2	14.3	18.4	23.6
24.4	1.869	13.2	10.4	9.1	9.6	10.8	13.5	17.2	22.1
31.9	1.672	12.4	9.8	8.7	8.9	10.3	12.8	16.1	18.7
35.8	1.580	12.1	9.7	8.7	8.9	10.3	12.7	15.9	20.2
39.2	1.505	11.8	9.5	8.5	8.7	10.1	12.4	15.5	19.4
46.3	1.365	11.0	8.9	8.1	8.4	9.6	11.7	14.7	18.1
46.9	1.353	10.8	8.9	8.1	8.3	9.5	11.4	14.3	17.7
47.3	1.345	10.9	9.0	8.2	8.3	9.6	11.6	14.5	18.1
56.2	1.196	10.2	8.5	7.9	8.1	9.2	11.1	13.4	16.7
68.1	1.034	9.7	8.2	7.7	7.9	8.9	10.6	13.0	15.7
71.4	0.993	8.8	7.6	7.4	7.7	8.9	10.6	13.1	15.9
74.7	0.954	9.0	7.8	7.3	7.7	8.6	10.0	12.1	14.5
79.2	0.908	9.4	8.1	7.6	7.8	8.8	10.3	12.3	14.7
85.9	0.841	9.0	7.9	7.5	7.8	8.7	10.0	11.8	13.9
99.9	0.724	8.4	7.5	7.2	7.5	8.3	9.5	11.1	13.4
109.0	0.659	8.4	7.7	7.5	7.8	8.5	9.6	11.0	12.9
113.4	0.631	8.0	7.4	7.2	7.5	8.1	9.2	10.6	12.6

EXPERIMENTAL LINEWIDTHS FOR THE VOTB SYSTEMS

T(°C)	$\eta/T^{5}10$ P/°K	-7/2	-5/2	-3/2	-1/2	1/2	3/2	5/2	7/2
118.3	0.600	7.9	7.4	7.1	7.4	8.0	9.0	10.2	11.9
119.7	0.593	8.2	7.5	7.3	7.6	8.2	9.3	10.7	12.5
130.2	0.538	8.4	7.7	7.4	7.7	8.3	9.3	10.5	11.8
148.0	0.458	8.0	7.4	7.3	7.6	8.1	9.0	10.1	11.4
CHLOROFORM									
-18.9	3.457	28.6	21.1	17.0	16.8	19.9	26.2	35.4	45.0
-9.5	2.962	24.3	18.2	14.8	14.6	17.2	22.1	29.5	37.9
2.7	2.454	18.3	13.8	11.4	11.5	16.1	17.2	22.0	27.7
3.4	2.430	19.4	14.7	12.2	12.1	14.3	18.1	23.7	30.4
11.4	2.165	17.3	13.2	11.2	11.3	13.1	16.2	21.3	26.8
15.8	2.035	16.1	12.4	10.5	10.5	12.4	15.6	20.2	25.1
22.2	1.862	14.6	11.4	9.9	9.9	11.4	14.2	18.0	23.4
29.7	1.687	13.5	10.6	9.0	9.1	10.3	13.0	16.2	21.1
35.1	1.577	13.2	10.5	9.1	9.2	10.6	13.1	16.6	20.3
38.6	1.508	12.9	10.2	9.1	9.2	10.4	13.0	16.3	20.7
54.9	1.238	11.4	9.3	8.3	8.5	9.6	11.6	14.4	17.8
58.6	1.188	11.4	9.3	8.4	8.6	9.7	11.8	14.5	18.3
61.0	1.155	11.0	9.1	8.2	8.4	9.5	11.4	14.2	17.1
70.4	1.039	10.2	8.6	7.9	8.1	9.0	10.6	12.9	15.8
81.5	0.925	9.7	8.3	7.7	7.9	8.9	10.3	12.4	15.1
84.8	0.894	10.0	8.6	8.0	8.3	9.3	10.8	12.9	15.7
99.2	0.773	9.4	8.2	7.8	8.0	8.9	10.4	12.1	14.5
DIPHENYLMETHANE									
30.4	7.814	42.0	29.6	23.8	23.1	29.6	39.5	55.4	a
37.6	6.777	31.9	23.1	18.9	18.5	23.0	30.5	43.2	a
47.3	5.645	28.8	20.8	17.2	17.2	21.1	27.3	37.4	a
57.7	4.694	23.3	17.1	14.3	14.3	17.4	22.8	30.7	41.1
71.4	3.738	16.7	13.6	11.8	11.5	13.5	17.4	21.9	25.3

EXPERIMENTAL LINEWIDTHS FOR THE VOTB SYSTEMS

T(°C)	η/T 10^5P/°K	-7/2	-5/2	-3/2	-1/2	1/2	3/2	5/2	7/2
71.8	3.714	17.0	12.6	10.8	10.9	12.8	16.2	21.7	27.6
91.1	2.767	13.6	10.9	9.5	9.6	11.2	14.0	18.6	24.1
102.6	2.355	13.2	10.2	9.0	9.4	10.7	13.4	16.7	20.5
105.3	2.270	12.1	9.7	8.8	9.0	10.4	12.6	15.6	19.2
120.5	1.862	11.0	9.3	8.3	8.5	9.8	12.0	15.0	17.5
120.6	1.859	11.1	9.1	8.3	8.6	9.7	11.7	14.4	18.0
128.9	1.676	10.1	8.6	8.0	8.2	9.2	10.9	13.3	15.8
142.4	1.432	10.4	8.6	8.0	8.3	9.4	11.3	13.1	15.6
147.3	1.353	9.3	8.0	7.6	7.8	8.6	10.0	12.0	14.1
157.4	1.212	8.9	7.8	7.4	7.7	8.5	9.7	11.7	13.8
175.0	1.011	8.4	7.7	7.4	7.7	8.3	9.4	10.9	12.6
200.0	0.797	8.6	7.7	7.4	7.6	8.2	9.9	11.4	13.7
CARBON DISULFIDE									
-34.6	2.457	17.3	13.0	11.1	11.2	13.3	17.1	22.6	29.7
-24.0	2.127	15.3	11.8	10.1	10.3	12,1	15.4	19.9	26.0
-10.1	1.775	13.3	10.4	9.1	9.3	10.9	13.6	17.4	21.9
1.2	1.549	12.0	9.5	8.5	8.7	10.1	12.5	15.8	19.8
17.4	1.287	10.9	9.0	8.1	8.4	9.6	11.7	14.6	17.9
40.5	1.011	9.3	7.9	7.4	7.6	8.6	10.1	12.3	14.9
63.7	0.810	8.7	7.7	7.3	7.5	8.3	9.6	11.4	13.4

TABLE 12

EXPERIMENTAL LINEWIDTHS FOR THE VODP SYSTEMS

T(°C)	η/T 10^5P/°K	-7/2	-5/2	-3/2	-1/2	1/2	3/2	5/2	7/2
TOLUENE									
-7.1	3.217	39.1	28.1	22.6	22.6	28.7	37.0	49.2	a
5.6	2.547	30.4	21.7	17.7	17.8	22.0	29.1	39.3	a
9.1	2.399	27.2	19.6	16.3	16.4	20.2	27.0	35.9	48.1
16.8	2.107	24.3	17.6	14.6	14.7	17.8	23.6	31.2	40.5
25.7	1.834	21.9	16.1	13.6	13.5	16.6	21.5	28.7	36.9
25.7	1.834	20.6	15.6	13.1	13.3	15.8	20.3	26.8	34.0
28.9	1.748	19.6	14.7	12.6	12.8	15.0	19.2	25.5	31.5
31.6	1.677	19.5	14.6	12.3	12.4	15.0	19.4	25.7	33.4
36.7	1.559	17.6	13.4	11.4	11.6	13.8	17.8	23.3	29.7
41.9	1.447	16.1	12.4	10.7	11.0	13.0	16.8	21.6	27.3
49.5	1.308	15.6	12.1	10.5	10.7	12.8	15.9	20.4	26.9
50.4	1.292	15.1	11.9	10.1	10.6	12.7	16.1	21.2	27.6
62.0	1.113	13.7	10.7	9.3	9.6	11.3	14.3	18.8	23.3
67.3	1.043	12.6	10.0	9.0	9.4	11.2	14.1	17.6	21.8
95.2	0.760	10.9	8.9	8.0	8.3	9.3	11.2	14.4	17.9
95.5	0.757	10.5	8.7	8.0	8.3	9.5	11.6	14.1	17.5
118.4	0.600	9.7	8.3	7.7	8.0	9.1	10.8	12.8	15.5
129.6	0.539	9.3	8.1	7.8	8.2	9.1	10.7	12.7	15.3
CHLOROFORM									
-20.0	3.524	59.8	40.9	31.0	30.5	39.3	51.5	75.7	a
-7.3	2.863	45.1	30.6	24.0	24.0	29.4	39.1	52.8	a
-7.3	2.863	41.1	29.3	23.6	23.1	28.1	38.2	52.1	68.3
1.0	2.517	34.9	25.0	20.2	19.8	24.1	32.0	43.7	60.5

EXPERIMENTAL LINEWIDTHS FOR THE VODP SYSTEMS

T(°C)	η/T 10^5P/°K	-7/2	-5/2	-3/2	-1/2	1/2	3/2	5/2	7/2
2.2	2.473	34.1	24.1	19.3	19.4	23.2	31.0	43.9	59.8
9.1	2.236	31.6	22.6	18.4	18.1	21.8	28.8	38.8	52.3
12.4	2.133	31.1	22.9	18.3	18.2	21.9	29.4	39.9	53.5
14.0	2.086	30.2	21.9	17.7	16.6	20.5	26.9	36.3	46.3
20.0	1.921	26.4	19.1	15.8	15.7	18.8	24.6	32.6	44.4
26.6	1.758	24.5	18.0	14.8	14.8	17.8	23.3	31.0	40.2
32.1	1.638	22.8	16.8	13.9	13.9	16.6	21.8	28.9	37.4
39.5	1.490	20.1	15.0	12.6	12.6	15.1	19.4	25.7	32.4
44.3	1.405	19.3	14.2	12.0	12.1	14.2	18.4	24.7	32.4
51.1	1.295	18.6	14.0	11.8	11.9	14.0	18.0	23.7	31.3
64.7	1.107	16.3	12.5	10.7	10.7	12.8	16.4	21.6	28.4
70.7	1.038	14.5	11.6	10.1	10.3	12.1	15.4	20.2	26.2
87.1	0.872	13.5	10.7	9.4	9.5	11.0	13.9	17.8	22.2
93.0	0.822	12.7	10.2	9.1	9.4	10.8	13.6	17.5	22.0
119.2	0.640	9.8	8.5	7.9	8.4	9.4	11.1	13.4	16.6

CARBON DISULFIDE

T(°C)	η/T 10^5P/°K	-7/2	-5/2	-3/2	-1/2	1/2	3/2	5/2	7/2
-27.5	2.227	25.1	18.1	15.1	15.2	18.4	24.5	33.2	44.2
-9.0	1.753	20.4	15.4	13.0	13.1	15.9	20.3	27.1	35.5
1.8	1.538	17.9	13.6	11.6	11.8	14.1	17.9	23.1	31.3
20.6	1.246	15.2	11.8	10.2	10.4	12.3	15.6	19.6	25.7
38.9	1.029	12.8	10.2	9.1	9.3	10.9	13.6	17.4	22.0
59.5	0.842	11.5	9.4	8.5	8.8	10.1	12.2	15.3	19.2
80.1	0.699	10.2	8.5	8.0	8.3	9.4	11.1	13.6	16.9